Retrospective Drug Testing: Can the Skin Provide a Record of Drug Taking History?

Jones, Jennifer

Award date:
2017

Awarding institution:
University of Bath

Retrospective Drug Testing: Can the Skin Provide a Record of Drug Taking History?

submitted by

Jennifer Jones

for the degree of Doctor of Philosphy

of the

University of Bath

Department of Mathematical Sciences

January 2017

Acknowledgements

Firstly I would like to sincerely thank my primary supervisor Jane White for conceiving a fascinating research topic, her constant support and her belief in my abilities throughout. My deepest thanks also goes out to my supervisors Begoña Delgado-Charro and Richard Guy who were instrumental to my continued progress and the ultimate success of the research. Thank you also to my examiners Nick Britton and Marcus Tindle for an enjoyable viva and for their helpful advice.

A special thanks to Steve and Rob for their technical help, emotional support and endless patience, and my fellow researchers Amy, Katy, Jack and Chris for making the good days great. Finally thank you to my family and my many other friends who I am sure will be overjoyed to see the back of this!

This research was funded by the Engineering and Physical Sciences Research Council (EPSRC).

Abstract

It has been shown that prolonged systemic presence of a drug can cause a build up of that drug in the skin. This drug 'reservoir', if properly understood, could provide useful and important information about the recent drug-taking history of a patient. In this thesis we create three mathematical models which combine to explore the potential for a drug reservoir to form in the skin and be collected as a method of monitoring compliance. The first model is used to characterise time-dependent drug concentrations in plasma and tissue following a customisable drug regimen. Outputs from this model provide boundary conditions for the second, spatio-temporal model of drug build-up and concentration profile in the skin. This then provides initial conditions for the final model which predicts the extraction. These models are then used to identify the scenarios which have the greatest potential for successfully monitoring patient compliance via the skin.

We focus in particular on drugs that are highly bound as this will restrict their potential to move freely into the skin but which are lipophilic so that, in the unbound form, they would demonstrate an affinity to the outer layers of the skin (which are built around a lipid matrix). We highlight how this study might be used to inform future experimental design and data collection in order to provide relevant parameter estimates for reservoir formation and its potential to contribute to enhanced drug monitoring techniques.

Contents

Chapter 1

Introduction

Worldwide, non-compliance to drug regimens poses a significant challenge to effective treatment strategies. A report by the World Health Organisation estimated that only 50% of patients living with chronic illness in developed countries adhere to prescribed treatment [1]. The level of non-compliance in treatment of addiction is higher still [2]. In order to tackle the issue of non-compliance, an effective method of monitoring occurrence of non-compliance is necessary. There are two approaches to monitoring: 'direct' methods such as blood and urine sampling, which are unable to detect poor long-term compliance and 'indirect' methods such as questionnaires, pill counting, and self reporting, which are easily manipulated by the patient [3]. The need for a more reliable method of monitoring is therefore apparent.

Alternative drug monitoring methods via non-conventional biological fluids and matrices are available, but less widely used due to practical difficulties [4, 5]. Drug monitoring via keratinised matrices, such as hair and nails, are able to provide information about history of medication, compliance, and drug abuse but can usually only provide a binary result (positive/negative) and cannot test for more recent drug use or current levels [5, 6, 7].

In this thesis we are interested in compliance monitoring via the skin. On entry to the systemic circulation, a drug distributes into all of the tissues in the body to varying extents. In general, this process is reversible as the tissue and blood compartments are in dynamic equilibrium. In the case of the skin, differentiation and death of skin cells means that some drug can be trapped in and amongst the cells, potentially providing an archive of drug taking history of a patient.

The reservoir function of the skin is a recognised phenomenon in the field of transdermal absorption [8]. A reservoir of drug in the skin was first identified for the case of topically applied corticosteroids after a prolonged therapeutic effect was

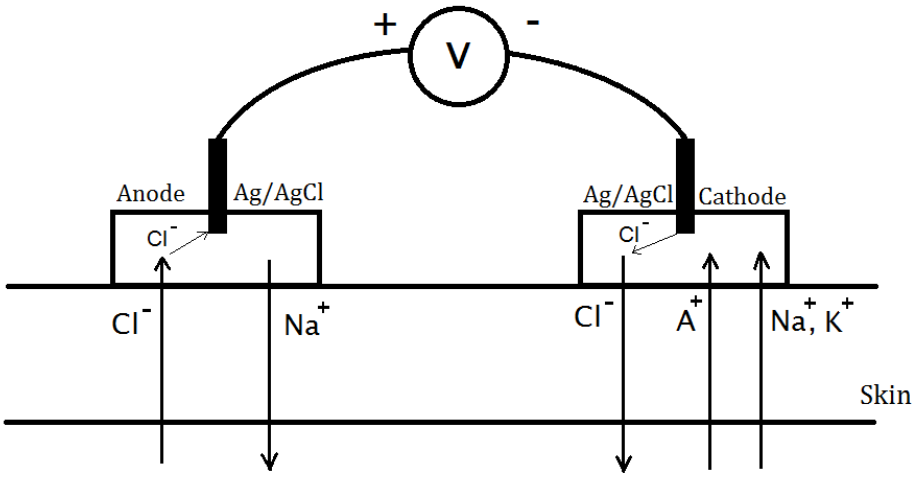

Figure 1-1: Schematic of reverse iontophoresis, where A^+ represents an unspecified positive ion.

observed [9, 10]. Presence of a reservoir in the skin has since been demonstrated for many other drugs [8]. Moreover it has been shown, via tape stripping, that the main site of this skin reservoir is the stratum corneum (SC), the layer of dead cells at the surface of the skin [8, 9, 11].

Research on the presence of a reservoir in the SC is generally focused on formation from an external source, specifically topically applied drugs and chemical exposure [8]; drug that comes into contact with the skin surface enters the body via passive diffusion. As only unbound drug diffuses the cause of a reservoir forming in the SC is thought to be high keratin binding and slow desorption kinetics [12]. Binding within the skin is most typical for lipophilic drugs with high molecular weight [13, 14].

More recently, detection of a 'reservoir' of drug in the skin as a result of its systemic presence has highlighted the potential of skin to act as a site for non-invasive monitoring [15], both to measure systemic drug levels and to estimate historic usage by exploiting the reservoir. The existence of such a reservoir has been demonstrated for a number of molecules (including urea [16, 17], glucose [18], and lithium [15]) by reverse iontophoresis.

Reverse iontophoresis is a blood sampling technique. Two electrodes are placed on the skin of a patient where a small electric current is passed between them. The current encourages the flow of ions and other molecules to the skin's surface where they can be collected and analysed. A schematic of reverse iontophoresis is given in Figure 1-1 and the process is described in detail in Chapter 4. Iontophoresis was developed as a drug delivery technique but due to its non-selective nature, as

drug is delivered at one electrode, molecules are simultaneously pulled from the skin and plasma at the other. It has therefore more recently also been utilised as a sampling technique [19].

Reverse iontophoresis benefits from being non-invasive, resulting in a reduced risk of infection and less associated pain. This offers the potential for increased patient compliance. Moreover, reverse iontophoresis machines do not require trained personnel to operate them and therefore offer the possibility for patients to use them in the home. Indeed, in 2001 the FDA approved the use of the GlucoWatch Biographer, a reverse iontophoresis device worn on the wrist which returned glucose levels every 20 minutes to help with the management of diabetes [20]. However, there were a number of issues with the watch [21] and so in 2006 when Cygnus inc., the company who made the GlucoWatch, closed down, production ceased.

Reverse iontophoresis is still in development and a blood sample is required to calibrate the results to the blood concentration of an individual patient. Research on an internal standard is under way [22, 23]. Another perceived problem with reverse iontophoresis is the initial lag time; the period of time between first starting the machine and readings correlating with plasma concentrations. For this reason it is advised that the electrical current should be applied for a minimum of 2 hours. Drug cannot instantly travel between the plasma and collection pad and so there is an associated delay that is inherent. Studies for certain molecules report "very high" extractions within the first hour of current application which reduce in subsequent readings to reflect plasma concentration. These initial high readings are thought to be the draining of a reservoir that has built up in the SC.

Lag time is still viewed as a hindrance, with information collected about the reservoir often unused. It has been suggested that the initial readings may prove useful in disease diagnosis [17] or compliance monitoring [19, 24] but this potential has yet to be fully explored. If we can create a mechanistic model that predicts reverse iontophoretic extraction resulting from a given dose regimen, then it is possible that we will be able to interpret reverse iontophoretic extraction in the context of compliance. Currently only one such mathematical model exists in a paper by Paulley *et al.* [24] which mathematically models the accumulation and extraction of a lithium reservoir in the SC. This model is based on results from the study by Leboulanger *et al.* [15] in which reverse iontophoresis was performed on bipolar patients chronically dosed with lithium. In this paper the authors describe a two model system to determine the accumulation and extraction of a lithium reservoir in the stratum corneum. The first of the two models is a two compartment (blood serum and stratum corneum) model where drug enters the SC directly from the serum compartment and is lost from the SC compartment through a linear term describing skin renewal. The second model is an extension to the first, incorporating a third compartment which represents the 'collection

pad' for reverse iontophoresis. The paper showed that the amount of lithium collected can be related to the amount of lithium administered and therefore demonstrated the potential for reverse iontophoresis to determine medium term (2 weeks) compliance. Lithium is in some respect the simplest case as it is not metabolised, it doesn't bind in the plasma or skin, and is a small, positively charged ion meaning it is easily extracted via reverse iontophoresis.

The paper by Paulley *et al.* [24], along with evidence from Leboulanger *et al* [25, 15], provided significant motivation for this thesis. Using Paulley *et al.* as a starting point, complexities and other modelling techniques are built in from the literature at each stage to create a more realistic and versatile modelling approach to compliance monitoring via reverse iontophoresis. In particular, we are interested in a drug that is metabolised within the body, is bound to molecules within the body, and which is lipophilic. These choices reflect the properties of many prescription drugs that are metabolised as well as excreted by the body and which bind to proteins and other molecules within both the plasma and the tissue.

The drug buprenorphine which is used to treat opiate addiction where compliance is an essential component of effective treatment, satisfies these three criteria and so acts as a motivation for our choice. Buprenorphine is a semi-synthetic opioid used in the treatment of opioid addiction with additional uses as a treatment for chronic pain at lower doses. Buprenorphine is an ideal candidate for this type of drug monitoring as it is often used for the treatment of heroin addiction as part of a rehabilitation plan enforced by a court order. It is suitable as doses are regular, usually daily, and it is an interesting case as characteristics of this drug such as its metabolism, lipophilicity, and binding with plasma bring added complexities to the modelling of reservoir formation. The chronic administration of buprenorphine allows the reservoir to build up making it an ideal case study.

The ultimate aim of this project is to create a customisable model system that takes a drug regimen and predicts systemic levels of that drug, along with the SC drug reservoir size and resulting extraction reading. The model structure consists of three sub-models: systemic concentration, drug reservoir formation in the skin, and extraction of the reservoir, Figure 1-2.

1. Modelling Systemic Drug Concentration: After administration, the drug is absorbed into the blood stream and transported around the body. The amount of drug in the body varies according to distribution, metabolism and excretion of the drug. In this section the amount of drug and its metabolite in different areas of the body (blood, tissues) are modelled in order to estimate drug levels at any given time for a user-specified drug regimen. The outputs from this model provide boundary conditions for Model 2.

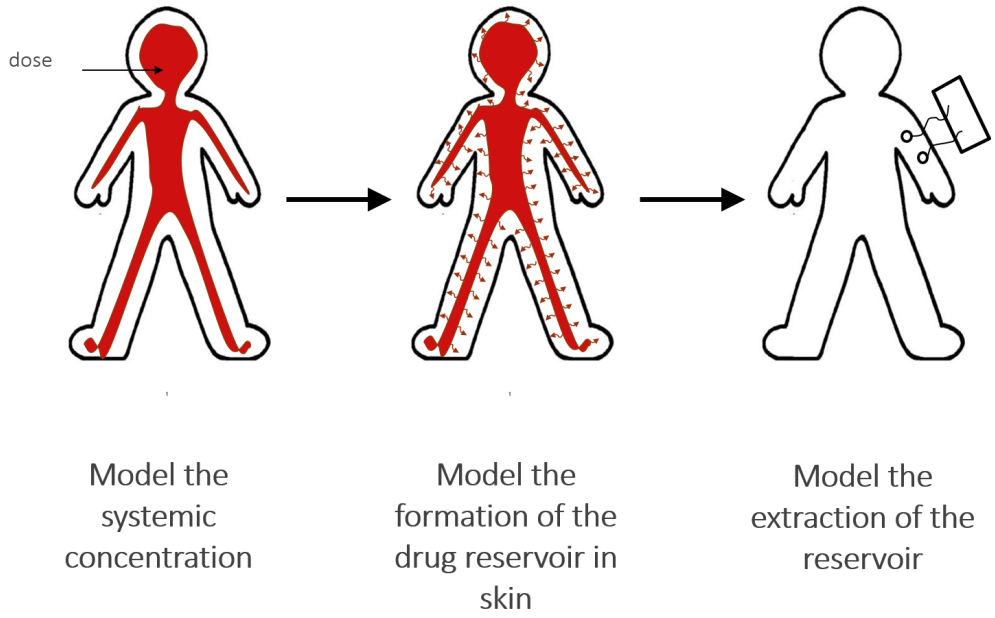

Figure 1-2: The overall aim is to create three composite models which will be linked together to create a model which predicts the expected reverse iontophoresis reading for a given drug administration regimen and therefore interpret reverse iontophoresis readings in the context of historical (order of days/weeks) drug monitoring.

Many of the mechanisms and parameters in this model are motivated by our choice of example drug, buprenorphine. However the model format is highly customisable and could be adapted for a number of different drugs.

2. Formation of a drug reservoir in the skin: Our hypothesis is that drug builds up in the skin over approximately a two week time period (after which time surface skin is shed and drug is lost with it). We create a spatial model of the skin using the output from Model 1 as the boundary conditions at the base of the skin. We use this to relate skin reservoir size to the amount of drug administered. This is a spatial model and the output of this model provides the initial conditions for Model 3.

3. Extraction of the reservoir: We consider two extraction techniques; reverse iontophoresis and tape stripping which are described in detail in Chapters 4 and 6 respectively. Reverse iontophoretic extraction is modelled using spatial and compartmental modelling through use of PDEs and ODEs.

It should be noted that whilst Model 1 feeds into Model 2, the converse is not true. We assume that any drug which enters the skin is not reabsorbed into the blood. Model 2 provides initial conditions for Model 3 which describes the extraction of

this reservoir via reverse iontophoresis and later tape stripping. We assume that active drug is administered and it is the administered drug that we are interested in modelling. A single daily dose is administered in the fully compliant case. The separation of the overall system is reasonable as each stage takes place on a different timescale; moreover, it allows for the potential for each stage to be verified using experimental data.

We conclude with observations about the potential to exploit the SC reservoir as a mechanism for non-invasive drug monitoring and determine important parameters and drug properties that impact on this potential.

As we are combining three distinct models that draw on quite disparate literature, the literature review for each model will appear towards the beginning of the respective chapter to provide foundation and context for the work that follows.

Thesis outline

Chapter 2: Modelling Systemic Drug Concentration This chapter begins by describing current approaches to modelling systemic/plasma concentrations of a drug. A full description of characteristics of the chosen case study drug, buprenorphine, is then provided. A model to describe buprenorphine concentration in the plasma and tissues is developed and compared with data from the literature. The final model in this chapter is referred to as 'Model 1' throughout the thesis.

Chapter 3: Formation of a Drug Reservoir in Skin In this chapter we begin by describing the anatomy of the skin and factors that may affect reservoir formation. We review relevant literature, with a focus on literature on passive drug delivery, as many of the associated processes are similar. We then create a spatial model for the formation of a drug reservoir in the SC. Boundary conditions for this model are set up to accept output from Model 1 from Chapter 2, however, combination of the two models is delayed until Chapter 5. The final model in this chapter is referred to as 'Model 2' throughout the thesis.

Chapter 4: Reverse iontophoresis We begin by describing the process of reverse iontophoresis and the theory and mechanisms involved. We review relevant literature, drawing largely on iontophoretic drug delivery with a focus on model framework and the potential to convert to the case of reverse iontophoresis. We then go on to create a spatial model for reverse iontophoresis extraction of both reservoir and plasma concentrations. The final model in this chapter is referred to as 'Model 3' throughout the thesis.

Chapter 5: Model Combination In this chapter we combine Models 1 - 3 from Chapters 2 - 4 focusing on the impact of chosen parameters and potential for detecting compliance.

Chapter 6: Tape stripping Finally we explore the possibility of verifying/ supporting findings from reverse iontophoresis using the tape stripping technique.

Chapter 7: Conclusions In this chapter we summarise key findings from each chapter and discuss further work.

Chapter 2

Modelling Systemic Drug Concentration

2.1 Introduction

In this chapter we seek to create the first of our three models (Figure 2-1). The purpose of this model is to predict the fluctuating in-body concentrations for a specified administered drug dose in order to provide boundary conditions for Model 2, the formation of the drug reservoir in the skin.

We begin by reviewing the methods and approaches for modelling systemic concentrations used in the literature. We then look at the characteristics of our exemplar drug, buprenorphine, in order to identify key traits that need to be accounted for in the model. We build our model starting with the simplest approach, building in complexities to make the model more realistic.

Note the concluding model in this chapter combined with work in Chapter 3 form the basis of the published paper [26].

In this chapter we focus on compartmental ODE models to describe processes within the human body. Compartmental models are based on the principle of conservation of matter; in our case this is the drug. All drug in the system must be accounted for whether that be by movement from one region (compartment) to another, or by metabolism or excretion of the drug. In mathematics a compartmental model refers broadly to the use of a system of homogeneous well mixed compartments, also known as 'lumped parameter models'. They simplify the behaviours of a spatially distributed physical model into discrete 'compartments' in which entities being modelled are assumed to be uniformly distributed.

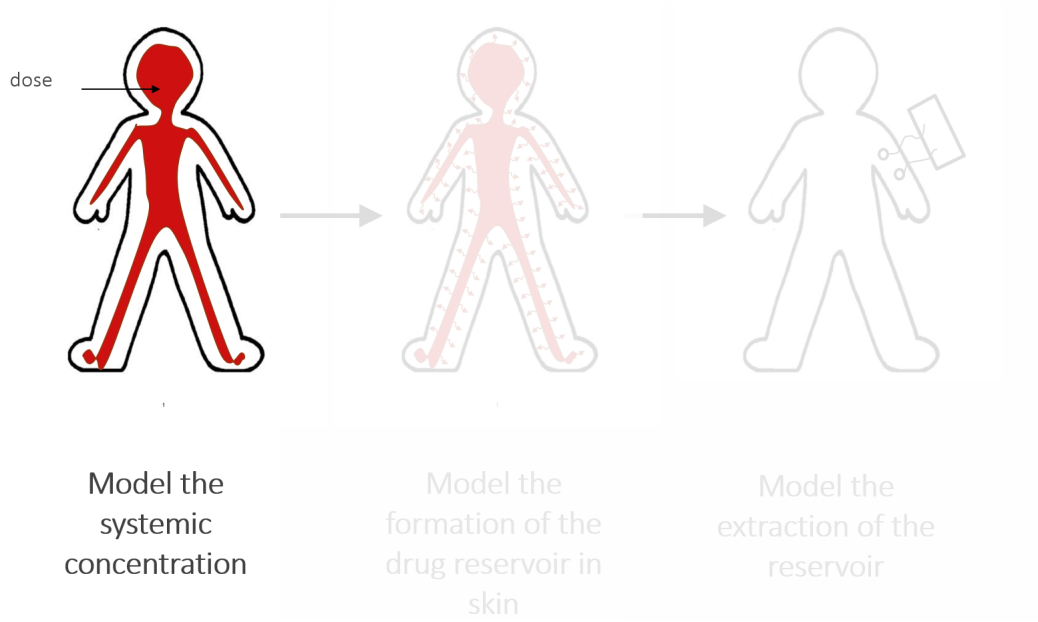

Figure 2-1: The overall aim is to create three composite models which will be linked together to create a model which predicts the expected reverse ionotphoresis reading for a given drug administration regimen and therefore interpret reverse iontophoresis readings in the context of historical (order of days/weeks) drug monitoring. The first model, for the systemic concentration, is the focus of this chapter.

In pharmacology, however, the term compartmental model often refers specifically to conventional pharmacokinetic (PK) models. In PK models, empirically obtained in vivo concentration profile data is 'fitted' to a compartmental model consisting of a 'central' and sometimes one or more 'peripheral' compartments. The central compartment usually refers to the plasma or dosing site; peripheral compartments are added to help the model better fit the data. The site of action and site of elimination for a drug can be located in the central or peripheral compartments depending on properties of the drug. This approach is phenomenological; compartment volumes often take values that would be unrealistic in the human body and don't reflect physiological spaces. PK models are used as a way of describing and comparing drugs to give some idea of how the drug will behave to inform optimal dosing procedures and toxicity risk. As the model is created using a concentration profile, the concentration profile can't be predicted a priori using this type of model. Due to the way the compartments are defined the model cannot necessarily provide predictions such as concentration in a given tissue either.

More recently there has been a move towards more complicated physiologically based pharmacokinetic models (PBPK) which take a mechanistic approach, modelling each component of the body relevant to the passage of a given drug [27]. These are still compartmental models in the mathematical sense but should not

be confused with the conventional PK models. In 1937 Teorell devised a model for which he has now been referred to as 'the father of pharmacokinetics' [27, 28]. In this model, the human body was simplified into compartments, each representing a different organ or functional region of the body, Figure 2-2. Processes acting within and between these compartments were described by a set of differential equations allowing the prediction of the time course for a drug in the body. This model was a precursor to today's PBPK models which incorporate species and chemical specific information to simulate the absorption, distribution, metabolism and excretion of compounds in the body. An increase in computing power and an emphasis on numerical rather than analytical methods has allowed the inclusion of many complexities, causing a rise in the application of PBPK modelling to drug development. This, combined with in vitro-in vivo extrapolation (IVIVE) and statistical techniques to account for population variability, has resulted in the creation of software such as Simcyp and GastroPlus, in which virtual drug trials can be simulated. Software and models such as these are being utilised at all stages of drug development from study design and justification [29] to regulatory procedure [30].

The benefits of PBPK modelling are that, as any relevant information on a drug can be incorporated, models can be used to predict the effects of multiple factors which have not been combined experimentally: PBPK models are also intuitive and therefore can be interpreted and understood by non-clinicians. Tools such as this, however, require a great many experimentally determined parameters which are not trivially obtained. A study by Zhao *et al.* [30] concluded that several in vivo and in vitro studies appear to be indispensable to determine vital system parameters and these require expertise, time and expense.

Our objective is to create a model that describes the movement of a drug within the body which could be used to reasonably convert a given dosing regimen to an in-body concentration profile that can be used in the wider model system (Figure 1-2). We follow the principle of Occam's razor to create a model that is as simple as possible whilst still providing the information that we require. To do this we will begin our modelling by looking at the simplest case scenario, building on the work of Paulley *et al* [24].

In the paper by Paulley *et al.* [24] the change in in-body concentration of lithium is described by a single compartment representing the serum concentration with exponential decay. This is suitable for lithium as it doesn't bind to proteins in the body and displays one-compartment pharmacokinetics. When dealing with more complex drug compounds we need to extend this approach to obtain a realistic plasma profile.

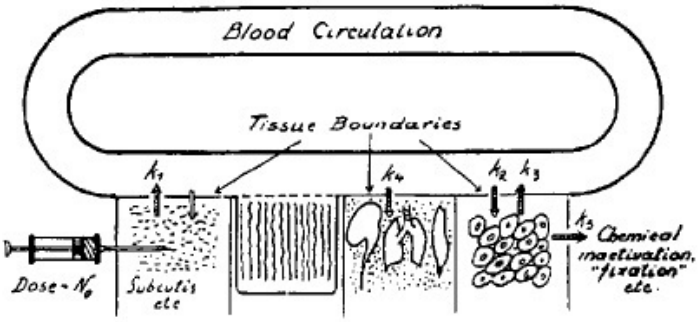

Local	Drug depot	Blood + equivalent Blood vol	Kidney etc elimination	Tissues	Tissue inactivation
Symbol	D	B	K	T	I
Amount	x	y	u	z	w
Volume	V_1	V_2	—	V_3	—
Concentration	x/V_1	y/V_2	—	z/V_3	—
Perm. coeff	k_1'	—	k_4'	k_2'	—
Velocity constant out	$k_1 = k_1'/V_1$	—	$k_4 = k_4'/V_2$	$k_3 = k_2'/V_2$	k_5
Velocity constant in	neglected	—	not existing	$k_2 = k_2'/V_2$	—
Name of process	Resorption	—	Elimination	Tissue take up -n- output	Inactivation

FIG. 1

Scheme of the Concept of Drug Distribution used in this paper.
Instead the *injection* pictured in the figure, the administration of the drug depot can be made *per os*, *per rectum*, *by inhalation*, etc.

Figure 2-2: The original scheme used by Teorell via [27] .

We use buprenorphine as an exemplar drug to motivate our modelling choices and hence we describe the pharmacokinetic processes in terms of buprenorphine. These concepts are applicable to many different drugs.

2.2 Buprenorphine ADME

ADME stands for absorption, distribution, metabolism and excretion. These four aspects describe the disposition of a drug within the body and determine the exposure to the tissues.

2.2.1 Administration

Buprenorphine is administered via a number of routes: sub-lingual (a tablet or liquid beneath the tongue), intramuscular (injected directly into muscle) and subcutaneous (injected just beneath the skin). As the eventual focus of this project will be on movement of drugs such as buprenorphine and its metabolites into the skin, the subcutaneous administration route will not be considered due to the complication of potential diffusion into the epidermis on administration.

It is common for buprenorphine to be administered sub-lingually as this does not require a trained professional (unlike intramuscular or subcutaneous administration). As a result there is more data available for buprenorphine administered via the sub-lingual route and so the preliminary model will be created with this administration route in mind.

2.2.2 Absorption

Bioavailability is defined to be the fraction of an administered dose that reaches the systemic circulation. Bioavailability of buprenorphine following intramuscular, subcutaneous and sub-lingual administration is similar (dependent on dose, individual and length of time retained in mouth for sub-lingual).

Sub-lingual dosing of buprenorphine has an estimated bioavailability of 50% i.e. 50% of that dose enters systemic circulation intact and is carried around the body in the plasma. The mean time to maximum plasma concentration following sub-lingual administration is variable, ranging from 40 minutes to 3.5 hours [31].

2.2.3 Distribution

The rate and extent of distribution of any drug in the body varies depending on the binding of drug to plasma proteins, blood perfusion of a given tissue, and the binding of the drug within the tissue, which is largely dependent on drug lipophilicity, pH and local membrane permeability.

The volume of distribution of a drug is the theoretical volume that would need to be occupied at blood plasma concentration to account for the total amount of drug in the body. Buprenorphine has a high volume of distribution which implies it does not mainly reside in the blood. Volume of distribution however, does not give information about a specific drug distribution; whether the drug is stored in fat, highly bound to specific tissues or remains in the extracellular fluid. Buprenorphine is a lipophilic drug and is therefore more likely to be found in fatty tissues [32].

2.2.4 Metabolism

In the liver, buprenorphine is metabolised via N-dealkylation by CYP3A4 enzymes into norbuprenorphine. This metabolism process can be described by Michaelis-Menten kinetics.

Buprenorphine and norbuprenorphine also undergo 'glucuronidation' in the liver resulting in two further metabolites: conjugated buprenorphine and conjugated norbuprenorphine respectively. Conjugates of buprenorphine and norbuprenorphine are not tested for routinely, consequently there is limited data for these compounds. For this reason emphasis is put on the amount of unconjugated buprenorphine and norbuprenorphine in the body.

2.2.5 Michaelis-Menten Kinetics

Metabolism Reaction N-dealkylation of buprenorphine in humans occurs in the liver via the CYP3A4 isozyme of the P450 enzyme system. The responsible enzyme acts as a catalyst, meaning it enables, but is not consumed by, the reaction. The enzyme attaches to the substrate (in this case buprenorphine) to form a complex; this part of the reaction is reversible. The complex then either breaks down or goes on to produce the product (norbuprenorphine), the original enzyme and some by-product. This can be written

$$\underset{\text{Substrate}}{B} + \underset{\text{Enzyme}}{E} \underset{k_{-1}}{\overset{k_1}{\rightleftharpoons}} \underset{\text{Complex}}{C} \xrightarrow[k_2]{} \underset{\text{Product}}{N} + \underset{\text{Enzyme}}{E} \tag{2.1}$$

which can be converted to the system of non-linear ordinary differential equations

$$\frac{dB}{dt} = -k_1BE + k_{-1}C, \tag{2.2a}$$
$$\frac{dC}{dt} = k_1BE - k_{-1}C - k_2C, \tag{2.2b}$$
$$\frac{dN}{dt} = k_2C, \tag{2.2c}$$

where B, E, C and N denote the concentration (amount/volume) of buprenorphine, enzyme (P450 3A4), complex and norbuprenorphine respectively, and k_1, k_{-1} and k_2 denote the rates of reactions as depicted in equation (2.1).

As this reaction is being considered in a fixed volume, we have

$$E + C = E_0, \tag{2.3a}$$
$$B + C + N = B_0, \tag{2.3b}$$

where E_0 and B_0 are constants.

Quasi steady-state approximation The quasi steady-state approximation is based on the assumption that concentration of the intermediate complex does not change in the time scale of product formation, which gives $\frac{dC}{dt} \approx 0$. Using this and substituting (2.3a) into (2.2b) we have

$$k_1B(E_0 - C) = (k_{-1} + k_2)C, \tag{2.4}$$
$$\implies C = \frac{k_1BE_0}{k_1B + k_{-1} + k_2} = \frac{BE_0}{k_m + B}, \tag{2.5}$$

where

$$k_m = \frac{k_{-1} + k_2}{k_1}.$$

The parameter k_m is known as the *Michaelis constant* which is the concentration of substrate when the reaction rate is at half of its maximum value.

Substituting the above expression for C into (2.2a) and rearranging gives

$$\begin{aligned} \implies \frac{dB}{dt} &= -k_2 C \\ &= -\frac{V_{max} B}{k_m + B}, \end{aligned}$$

where $V_{max} = k_2 E_0$ is the *maximum velocity* or maximum reaction rate at saturating substrate concentrations.

2.2.6 Excretion

Buprenorphine and its metabolites are mainly excreted via the faeces with 10-30% of a dose excreted in the urine. Dose excreted via the urine is primarily composed of conjugated metabolites [33, 34] whereas in the faeces almost all buprenorphine and norbuprenorphine appear in their free forms [31]. The assay techniques employed, however, mean most studies describe the total buprenorphine or norbuprenorphine concentrations "as they include pretreatment of urine with a beta glucuronidase to remove glucurinide conjugates from metabolites' [33]. A comprehensive review compiled by Elkader and Sproule in 2005 [31] reports studies where the mean half-life of buprenorphine ranges between 3 and 44 hours; discrepancies in half-life estimates are assumed to be due to sensitivity of assay techniques when lower doses are administered.

2.3 One Compartment Single Dose Model

Following the model structure from Paulley *et al.* [24] as the simplest scenario, we consider systemic concentrations to be described using a single homogeneous, well mixed compartment. Then, using the principle of conservation of matter, we obtain the following word equations for buprenorphine (bup) and norbuprenorphine (norbup) in the body:

Bup in whole body at time $t + \delta t$ = bup in body at time $t-$ bup metabolised into norbup in$[t, t + \delta t]-$ bup excreted in $[t, t + \delta t]$,

Norbup in whole body at time $t + \delta t$ = norbup in body at time t + bup metabolised into norbup in$[t, t + \delta t]-$norbup excreted in $[t, t + \delta t]$.

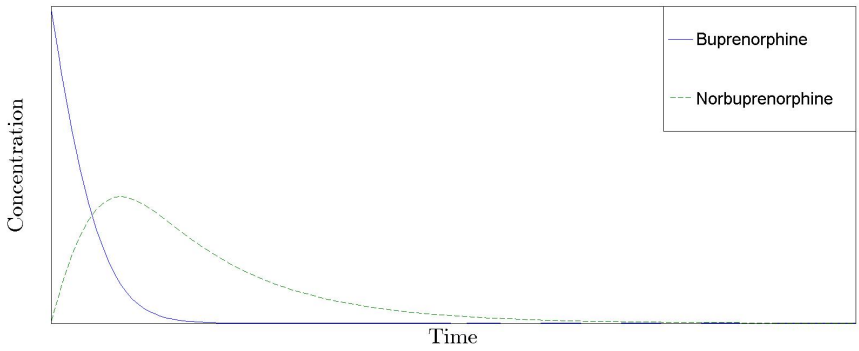

Figure 2-3: Demonstration of model (2.6): concentration of buprenorphine and norbuprenorphine in the body against time with Michaelis-Menten metabolism kinetics and a linear excretion rate. Using ODE45 in MATLAB with $e_B = 0.5$, $e_N = 0.5$, $V_{max} = 1$ and $k_m = 0.5$

Metabolism of buprenorphine to norbuprenorphine is described by Michaelis-Menten kinetics equation (2.4) whilst excretion is first order.

In this first simple model for a single dose, that dose provides the initial condition for the model equation scaled by its bioavailability.

Combining these elements we obtain the model system

$$\frac{dB}{dt} = \frac{-V_{max}B}{k_m + B} - e_B B, \tag{2.6a}$$

$$\frac{dN}{dt} = \frac{V_{max}B}{k_m + B} - e_N N, \tag{2.6b}$$

where $B(t)$ and $N(t)$ are the concentrations of buprenorphine and norbuprenorphine in systemic circulation at time t respectively. The parameters e_B and e_N are the constant excretion rates for buprenorphine and norbuprenorphine respectively and V_{max}, k_m are defined as in Section 2.2.5. Initial conditions are given by

$$B(0) = \alpha D,$$

$$N(0) = 0,$$

where α is the bioavailability and D is the dose.

The predicted profile for the one compartment model of buprenorphine and norbuprenorphine, equation (2.6), is given in Figure 2-3.

2.4 Multi-compartmental Multi-Dose Model

In the model described in Section 2.3 the body was treated as a single homogeneous compartment. As already mentioned in Subsection 2.2.3, buprenorphine does not mainly reside in the plasma and so we separate the body into two compartments: plasma and tissue. The tissue compartment represents the non-blood compartment of the body i.e. all the soft tissues, muscles, and organs. We use 'plasma' instead of whole blood as values for drug concentrations available in the literature are typically given in terms of plasma.

2.4.1 The Model

It is important to note that only 'free' or unbound drug is able to diffuse through membranes from plasma to tissues. Buprenorphine is a highly bound drug [31]; at equilibrium only 4% of the drug in plasma remains unbound to plasma proteins [35]. Buprenorphine binds mainly to α-globulin and β-globulin fractions. Since other drugs bind to albumin there is little risk of competition for binding sites [36, 37] which means we do not need to consider interaction between buprenorphine and other drug molecules.

Taking binding into account, the compartmental model contains 8 state variables. These consist of buprenorphine and norbuprenorphine in a bound and unbound state, both in the plasma and in the tissues.

Figure 2-4 shows a schematic of this new model iteration. In the following sections the terms describing the processes in this schematic are derived.

2.4.1.1 Amount vs. concentration

From this point onwards we will be dealing with concentrations (amount per volume) of buprenorphine and norbuprenorphine. This is because a number of parameters and mechanisms defined in the literature are dependent on concentration differences (movement into the tissue for example). It is important to make this distinction here as we are now dealing with separate compartments with different volumes. The molar mass of a substance is the mass (in grams) of one mole (avagadro's number of particles) of a substance. The amount (number of moles) of a substance can therefore be determined from the mass by dividing through by molar mass.

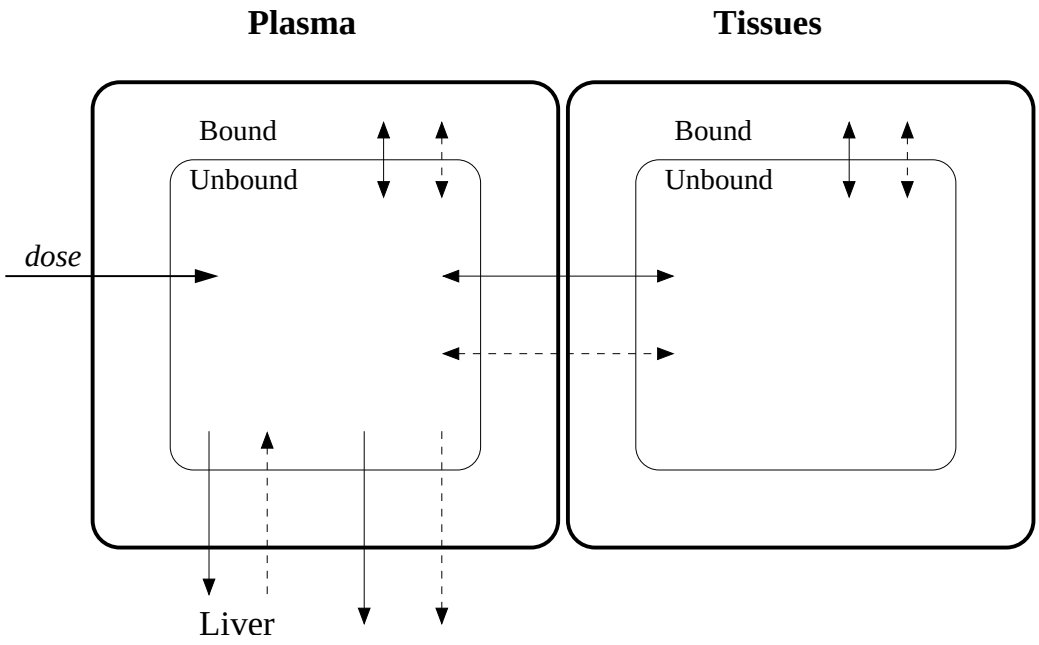

Figure 2-4: Schematic demonstrating the movement of buprenorphine (arrows) and norbuprenorphine (dashed arrows) in the body.

Buprenorphine enters the body in the plasma and is initially unbound.

Nomenclature
Labelling of drug in different regions of the body obeys the following format from this point onwards

$P(t)$ concentration (amount/volume) of a drug in the **Plasma** at time t,
$T(t)$ concentration (amount/volume) of a drug in the **Tissue** at time t,

Subscripts B, N, u, b denote the drug species **Buprenorphine** or **Norbuprenorphine** and whether the drug is **unbound** or **bound** respectively,

T_{Bu} therefore stands for the concentration of buprenorphine that is unbound in the tissue.

First consider the unbound buprenorphine (bup) in plasma. Movement into and out of this region is tracked as follows:

Change in unbound bup in plasma (over time)	=− net binding of bup to plasma proteins	− net movement of bup into tissues	−amount metabolised into norbup
	− bup excreted	+ administered bup.	

Using this equation structure we write the full system of model equations. The mechanisms for each term are described in the following subsections.

2.4.1.2 (Net) Binding

Binding in the plasma is a reversible process where, at equilibrium, unbound drug will be a fraction, f_{up}, of the total drug in the plasma, $(P_{Bu} + P_{Bb})$. We assume that the rate at which this equilibrium is approached is directly proportional to the difference between the amount of unbound drug at time t, $P_{Bu}(t)$, and the amount that will be unbound at equilibrium, $f_{up}(P_{Bu} + P_{Bb})$. This gives rise to a binding rate

$$r_B(P_{Bu} - f_{up}(P_{Bu} + P_{Bb})),$$

where r_B is a positive rate constant. The effect of this term on the amount of unbound drug will be positive if P_{Bu} is below its equilibrium level and negative if above.

2.4.1.3 (Net) Movement into tissue

Again, this process is reversible. As an approximation, the distribution of a drug between tissues and plasma can be estimated using the $\log_{10} P$ (log partition coefficient) or $\log_{10} D$ (log distribution coefficient) which are the logs of the ratio of concentrations of a compound in a mixture of two immiscible phases, usually octanol and water, at equilibrium. The partition coefficient usually refers to the ratio of un-ionised species whereas the distribution coefficient refers to all species (ionised plus un-ionised). This is often taken as an approximation of the ratio of concentrations between fat and plasma. Only unbound drug moves between plasma and tissue. Hence we obtain the rate of movement into tissue as

$$-s_B(P_{Bu} - \frac{1}{k_p} T_{Bu}),$$

where $k_p = 10^{log_{10}D}$ i.e. k_p represents the ratio between concentration of buprenorphine in tissue and plasma at equilibrium.

The parameter s_B is the rate at which this equilibrium is reached and is dependent on a number of factors such as blood flow to tissues and partitioning coefficients.

2.4.1.4 Metabolism

Metabolism of buprenorphine to norbuprenorphine is governed by Michaelis-Menten kinetics and the same term is used as in the initial model; derived in Subsection 2.2.5. Only unbound drug in the plasma is metabolised, hence we obtain the rate of metabolism:

$$\frac{V_{max}P_{Bu}}{k_m + P_{Bu}},$$

where V_{max} and k_m are the maximal velocity and Michaelis constant, respectively.

2.4.1.5 Excretion

Excretion is described by the first order removal rate

$$e_B P_{Bu},$$

where e_B is the excretion rate.

2.4.1.6 Multiple dose

The term describing administration of drug is of the form

$$\sum_{i=0}^{N} \delta k \exp(-k(t-i))$$

as used in the model by Paulley *et al.* [24] for a repeat lithium dose. For simplicity, on administration, the dose is assumed to be distributed homogeneously in the plasma. The parameter δ is the 'size' of the dose that arrives in the body, calculated as the product of the mass of the dose and the bioavailability, and converted to molar concentration by dividing through by molar mass and plasma volume. The dissolution/absorption rate constant for the given route of administration is given by k. This reflects that drug not given intravenously will not all arrive in the body

immediately. Doses are administered at the times T_i where N is the number of doses administered [24, 38]. Note that

$$\int_{T_i}^{\infty} \delta k \exp(-k(t-i))dt = \delta$$

which means that the full dose does eventually reach the plasma.

2.4.1.7 Volume adjustment between compartments

We assume bound and unbound drug occupy the same volume within compartments. We cannot, however, assume that volume between compartments is the same. We introduce the dimensionless variable

$$v_{T/P} = \frac{\text{Vol of tissues}}{\text{Vol of plasma}}.$$

This ensures that the conservation of mass is maintained as drug moves between compartments.

2.4.1.8 Model equations

Combining these processes gives an equation to describe the change in unbound buprenorphine in the plasma over time,

$$\begin{aligned}\frac{dP_{Bu}}{dt} =& - r_B(P_{Bu} - f_{up}(P_{Bb} + P_{Bu})) - s_B(P_{Bu} - \frac{1}{k_p}T_{Bu}) \\ & - \frac{V_{max}P_{Bu}}{k_m + P_{Bu}} - e_B P_{Bu} + \sum_{i=0}^{N} \delta k \exp(-k(t-i)).\end{aligned}$$

Using this same technique we can write equations to describe the change in concentration of burpenorphine and norbuprenorphine in all four regions of Figure 2.4.

$$\frac{dP_{Bu}}{dt} = - r_B(P_{Bu} - f_{up}(P_{Bb} + P_{Bu})) - s_B\left(P_{Bu} - \frac{1}{k_p}T_{Bu}\right) - \frac{V_{max}P_{Bu}}{k_m + P_{Bu}} - e_B P_{Bu} + \sum_{i=0}^{N} \delta k \exp(-k(t-i)), \tag{2.8a}$$

$$\frac{dP_{Bb}}{dt} = r_B(P_{Bu} - f_{up}(P_{Bb} + P_{Bu})), \tag{2.8b}$$

$$\frac{dT_{Bu}}{dt} = s_B\frac{V_p}{V_t}(P_{Bu} - \frac{1}{k_p}T_{Bu}) - t_B(T_{Bu} - f_{ut}(T_{Bb} + T_{Bu})), \tag{2.8c}$$

$$\frac{dT_{Bb}}{dt} = t_B(T_{Bu} - f_{ut}(T_{Bb} + T_{Bu})), \tag{2.8d}$$

$$\frac{dP_{Nu}}{dt} = \frac{V_{max}P_{Bu}}{k_m + P_{Bu}} - e_N P_{Nu} - r_N(P_{Nu} - f_{Nup}(P_{Nb} + P_{Nu})) - s_N\left(P_{Nu} - \frac{1}{k_{Np}}T_{Nu}\right), \tag{2.8e}$$

$$\frac{dP_{Nb}}{dt} = r_N(P_{Nu} - f_{Nup}(P_{Nb} + P_{Nu})), \tag{2.8f}$$

$$\frac{dT_{Nu}}{dt} = s_N\frac{V_p}{V_t}\left(P_{Nu} - \frac{1}{k_{Np}}T_{Nu}\right) - t_N(T_{Nu} - f_{Nut}(T_{Nb} + T_{Nu})), \tag{2.8g}$$

$$\frac{dT_{Nb}}{dt} = t_N(T_{Nu} - f_{Nut}(T_{Nb} + T_{Nu})). \tag{2.8h}$$

Parameter definitions for two compartment model

r_B the rate at which bup binds to protein in the plasma

s_B the rate at which bup perfuses into the tissues from plasma

t_B the rate at which bup binds to protein in the tissue

V_p total volume of the plasma

V_t total volume of tissue

e_B the rate at which bup is excreted from the body

r_N the rate at which norbup binds to protein in the plasma

s_N the rate at which norbup perfusses into the tissues from plasma

t_N the rate at which norbup binds to protein in the tissue

e_N the rate at which norbup is excreted from the body

f_{up} the fraction of bup in plasma which is unbound

k_p a measure of relative binding between plasma and tissue for bup (ratio of concentrations at equilibrium)

V_{max} the 'maximum velocity', as defined in Section 2.2.5

k_m the Michaelis rate constant

f_{ut} the fraction of bup in tissue which is unbound

f_{Nup} the fraction of norbup in plasma which is unbound

k_{Np} the relative binding between plasma and tissue for norbup

f_{Nut} the fraction of norbup in tissue which is unbound

*Note: presence of B or N in the subscript of a term denotes the term relating specifically to **buprenorphine** or **norbuprenorphine** respectively.*

2.4.2 Reducing the number of equations

As the binding of buprenorphine in the plasma happens on a shorter timescale when compared with other processes in the system, such as metabolism and excretion, it is reasonable to assume that at any given time the concentration of bound bup in the plasma can be found directly from the total bup in the plasma as follows:

$$P_{Bb} = (1 - f_{up})(P_{Bu} + P_{Bb}),$$

$$P_{Bu} = f_{up}(P_{Bu} + P_{Bb}).$$

Using these expressions, (2.8a) and (2.8b) can be combined to give an equation for the change in total drug in the plasma over time,

$$\frac{dP_B}{dt} = -s_B(f_{up}P_B - \frac{1}{k_p}T_{Bu}) - \frac{V_{max}f_{up}P_B}{k_m + f_{up}P_B} - e_B f_{up}P_B + \sum_{i=0}^{N} \delta k \exp(-k(t-i))$$

where

$$P_B = P_{Bu} + P_{Bb} = \text{total buprenorphine in plasma.}$$

We extend this approach using

$$f_{ut}T_B = T_{Bu},$$

$$f_{Nup}P_N = P_{Nu}$$

and

$$f_{Nut}T_N = T_{Nu}$$

where T_{Bu} is the unbound buprenorphine in the tissue and P_{Nu} and T_{Nu} are the unbound norbuprenorphine in the plasma and tissue respectively. We then obtain the reduced model system.

$$\frac{dP_B}{dt} = -s_B\left(f_{up}P_B - \frac{1}{k_p}f_{ut}T_B\right) - \frac{V_{max}f_{up}P_B}{k_m + f_{up}P_B} - e_B f_{up}P_B + \sum_{i=0}^{N}\delta k \exp(-k(t-i)) \tag{2.9a}$$

$$\frac{dT_B}{dt} = s_B\frac{V_p}{V_t}\left(f_{up}P_B - \frac{1}{k_p}f_{ut}T_B\right) \tag{2.9b}$$

$$\frac{dP_N}{dt} = \frac{V_{max}f_{up}P_B}{k_m + f_{up}P_B} - e_N f_{Nup}P_N - s_N\left(f_{Nup}P_N - \frac{1}{k_{Np}}f_{Nut}T_N\right) \tag{2.9c}$$

$$\frac{dT_N}{dt} = s_N\frac{V_p}{V_t}\left(f_{Nup}P_N - \frac{1}{k_{Np}}f_{Nut}T_N\right). \tag{2.9d}$$

2.4.3 Parameter estimates from the literature

Parameters such as V_{max} and k_m are related to Michaelis-Menten metabolism by enzymes in the liver. They are measured directly from liver samples in vitro and can be upscaled/converted for whole body use.

Many of the other parameters have not or cannot be directly observed experimentally such as k_p, 'the ratio of concentrations of buprenorphine between tissue and plasma at equilibrium'. Tissue is a term used here to refer to the entire group of tissues in the body in which bup distributes. Therefore this would need to be taken as a weighted average across all tissues, data which is not available for any tissues. Values for this term therefore must be inferred from other information we know about the drug such as the log$P$ value which is the ratio between the concentrations of a substance in octanol and water at equilibrium.

Table 2.1 lists parameters and their estimates along with calculations and appropriate data sources.

From Table 2.1, we see that bup is much more likely to reside in tissue than norbup is (as determined by the value of $\log P$ for each). This, combined with the lack of data available for norbup in the literature, leads us to restrict our model to consider the dynamics of bup only. Moreover norbup is at much lower levels than bup in the body and so we do not expect to detect more norbup in the skin. Metabolism of buprenorphine to norbuprenorphine is irreversible and so removal of the norbuprenorphine model does not impact on our predictions for buprenorphine.

Many of the parameters we have are uncertain. In some cases parameters have been upscaled from in vitro studies (V_{max}, k_m), some have been inferred from characteristics of buprenorphine (k_p inferred from bup lipophilicity) and others have been taken from predictions or estimations from in vivo data in various studies

Parameter	Description	Value	Calculation	Relevant data w/ references
f_{up}	Fraction of bup in plasma unbound	0.04	-	[35]
k_p	Measure of relative binding between plasma and tissue for bup	8511	$= \frac{[conc.intissue]}{[conc.inplasma]}$ $= 10^{3.93}$	logD=3.93[32], [39] [40]
V_{max}	Max velocity (Michaelis-Menten kinetics for bup metabolism) $(\mu moll^{-1}h^{-1})$	829 $(3.62 - 4.04 \times 10^{-3})$	0.712(Vmax) $\times$ 32 $\times$1820(liver weight) $\times$ 60(min$-$ >hr) $\times 10^{-9}$(nmol) /3L(plasma vol)	0.712nmol min^{-1}mg of protein^{-1}[41] $32mg/g$ [42] liver weight= 2.6% of BW [43] 70kg human $(3.14 \pm 0.033$nm min^{-1}mgprotein^{-1}[44])
k_m	Michaelis rate constant for bup $(\mu moll^{-1})$	39.3 $\pm$9.2 $(85 \pm 16 \times 10^{-6})$		$39.3 \pm 9.2 \mu Molar$[41] ($85 \pm 16 \mu Molar$[44])
e_B (k_4)	Rate at which bup is excreted in pure form (h^{-1})	0.30		Mean Value of elimination rate constant estimated for 1.2mg IV [45]
V_p	Volume of the plasma (L)	3.15		Average volume for 70kg human [40]
V_t	Volume of tissues (L)	57.39		All tissues excluding 'negligibly perfused tissues' as determined by [46] Volumes from [40]
k_{Np}	Measure of partitioning between plasma and tissue for norbup	13.8 - 16.6	$k_{Np} = 10^{logD}$ $= \frac{[conc.intissue]}{[conc.inplasma]}$ $10^{1.14} - 10^{1.22}$	logD=1.18+-0.04[39]
δ	Sub-lingual dose of bup $(\mu moll^{-1})$ Intravenous dose of bup $(\mu moll^{-1})$	dose in mg $\times$ 0.3394 dose in mg $\times$ 0.6789	$\frac{\text{dose} \times \text{bioavailability}}{\text{molar mass} \times \text{plasma vol}}$	sub-lingual bioavaliability= 50% [47] molar mass= 467.64 plasma vol= 3.15L

Table 2.1: parameters and their estimates along with calculations and appropriate data sources.

(e_b, bioavailability). Next we take into account variability in parameter estimates and set sensible ranges for the uncertain parameters.

2.4.4 Parameter fitting

Even though we have removed the need to estimate the parameters pertaining to norbuprenorphine alone, there are still a number of unknown parameters in our system; $k_p, s_B, f_{ut}, (V_p, V_t)$. Though these parameters have a physiological interpretation they are not measured directly in experiments and so their values must be inferred from other measurements or other parameters that have been estimated.

V_t and V_p are listed as unknown parameters here as the division of the body into plasma and tissues alone is crude. Typical volumes for each tissue exist in the literature, but the pharmacological compartmentalisation of the body is often divided into 'first' (plasma) and 'second' (tissue) compartments without specifying that this first compartment must be the plasma alone.

In this section we first discuss feasible parameter ranges and then go on to describe the fitting process that we employed to obtain parameter estimates.

2.4.4.1 The unknown parameters

The parameter k_p can be estimated using the $\log P$ or $\log D$ approach described earlier. Buprenorphine is a lipophilic drug, we therefore use

$$k_p = 10^{logD} = 10^{3.93} = 8511$$

as an upper limit for our plasma tissue partition coefficient [32] with the assumption that the plasma is approximated by water, and the 'tissues' are approximated by octanol. Alternatively the fraction of drug outside the plasma at steady state can be calculated using 'volume of distribution at steady state,' V_{ss}, by $\frac{V_{ss}-V_p}{V_{ss}}$ and so $k_p \approx \frac{V_{ss}-V_p}{V_p} = 110.6$ using $V_{ss} = 334.9$ [45].

The parameter s_B determines the rate at which an equilibrium between plasma and tissue concentrations is reached. There are many factors that could affect this value including blood flow and drug affinity for lipids. However as this is not directly measured experimentally there is as yet no simple way to quantify it.

The fraction of buprenorphine in the tissue which is unbound is denoted f_{ut}. This parameter is difficult to estimate as the term 'tissue' here is vague; a value for tissue binding for buprenorphine has not been determined and it is likely that this

value would vary depending on the tissue in question. The only certainty with this value is that it lies between 0 and 1.

As k_p and f_{ut} always appear in combination we define

$$\sigma := \frac{f_{ut}}{k_p}$$

to reduce the number of parameters to fit. We also acknowledge that without further distinguishing information we cannot conclude anything about k_p or f_{ut} independently from the other.

2.4.4.2 Data choice

The multiple dose model (2.9) describes bup concentration in tissues and plasma for a repeated sub-lingual dose. We choose to use data for a single dose to estimate the unknown parameters as a repeat dose would give a non-homogeneous ODE resulting in a much more complicated solution. Additionally the data available in the literature is more detailed for a single dose.

Initially, we fit the model to intravenous dose data so that errors in estimation of parameters, such as bioavailability and absorption rate, do not influence the estimation of other physiological parameters.

The data set chosen is from a study by Kuhlman *et al.* [45] in which 6 healthy men were administered buprenorphine intravenously (1.2 mg) and blood plasma samples were taken for up to 96 hours.

2.4.4.3 Initial conditions

Intravenous administration involves injecting the whole dose directly into the blood stream. This gives a bioavailability of 100%. Therefore, assuming the dose is distributed instantaneously and evenly in the plasma we can calculate the initial plasma concentration from the dose as follows:

$$P_B(0) = \frac{\text{dose in mg} \times 10^3}{\text{molar mass} \times V_p} = \frac{1.2mg \times 10^3}{467.64 \times 3.15} = 0.814\mu\text{mol/L}. \tag{2.10}$$

2.4.4.4 Linearising

The only non-linear term in equation (2.9) is the metabolism. For a dose of 1.2mg it is clear that even at the maximum (initial) plasma concentration we find that

$k_m \gg f_{up}P_B$, therefore we have

$$\frac{V_{max}f_{up}P_B}{k_m + f_{up}P_B} \quad \approxeq \quad \frac{V_{max}f_{up}P_B}{k_m}.$$

As we are not actually fitting metabolism parameters (V_{max} and k_m are already known) the values obtained for s_B and σ, relating to linear processes, should be applicable for higher doses.

Our linearised model for a single IV dose is then

$$\frac{dP_B}{dt} = -s_B(f_{up}P_B - \sigma T_B) - \frac{V_{max}f_{up}P_B}{k_m} - e_B f_{up}P_B \tag{2.11}$$

$$\frac{dT_B}{dt} = s_B\frac{V_t}{V_p}(f_{up}P_B - \sigma T_B). \tag{2.12}$$

This can be written in the form

$$\underline{\dot{B}} = A\underline{B}$$

where

$$\underline{B}(t) = \begin{bmatrix} P_B(t) \\ T_B(t) \end{bmatrix} \tag{2.13}$$

and

$$A = \begin{bmatrix} -s_B f_{up} - \dfrac{V_{max}\, f_{up}}{k_m} - e_B\, f_{up} & s_B\sigma \\ s_B\, f_{up}\dfrac{V_t}{V_p} & -s_B\sigma\dfrac{V_t}{V_p} \end{bmatrix}, \tag{2.14}$$

and $\underline{\dot{B}}$ denotes the time derivative of $\underline{B}$. The analytic solution of the linear model is then of the form

$$\underline{B} = a\underline{v}_1 e^{\lambda_1 t} + b\underline{v}_2 e^{\lambda_2 t} \tag{2.15}$$

where $\underline{v}_i$ are the eigenvectors and λ_i are the eigenvalues of A for i=1,2, dependent on model parameters.

2.4.4.5 Fitting the model to data

The data points used are from a paper by Kuhlman *et al.* [45] in which six healthy males were administered buprenorphine via the intraveneous (IV), sub-lingual and buccal routes. As we know the form of the solution for an IV dose, equation (2.15), we use the IV dosage data from this study. We begin by fitting a biexponential ($X_2(t)$) to the Kuhlman data set [45] using the inbuilt function in MATLAB to get

$$X_2(t) = 0.1034e^{-12.85t} + 0.01166e^{-0.4587t} \tag{2.16}$$

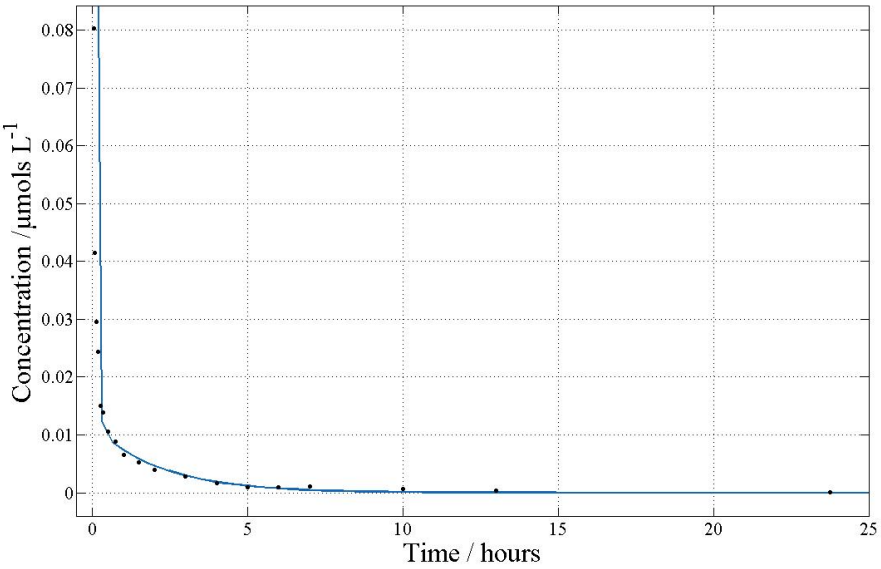

Figure 2-5: Biexponential fit to data for plasma concentration against time for a 1.2mg IV dose of buprenorphine [45] to remove data 'noise'. $K_2(t) = 0.1034e^{-12.85t} + 0.01166e^{-0.4587t}$

(see Figure 2-5).

We then use the numerical values from (2.16) to find parameter values that appear as components of v_i and λ_i (2.15). We do this by performing a parameter sweep across each of the ranges identified for the unknown parameters. For each set of parameters in this sweep we calculate the root mean square of the relative error in plasma prediction given by

$$E_{rms}(\sigma, s_B) = \sqrt{\frac{\sum_i^N \left(\frac{B_p(t_i;\sigma,s_B)-X(t_i)}{X(t_i)}\right)^2}{N}} \tag{2.17}$$

for the sampling points i=1,...,N where $B_p(t_i)$ is the buprenorphine plasma concentration predicted by our model for time points t_i. We then select the parameter set relating to the smallest calculated value of (2.17).

For a dose corresponding to an initial plasma concentration of 0.814 $\mu molL^{-1}$, equation (2.10), using data from Table 2.1 the minimal value of (2.17) was given for

$$\sigma = 0.00694$$

and

$$s_B = 102\text{h}^{-1}$$

resulting in an error estimate between the model and 'smooth' data ($X_2(t)$, equation (2.16)) of E_{rms}=0.3538 and with the unsmoothed data of E_{rms}=0.366.

The main problem with the data fit appears to come from disparity between the predicted and experimental initial plasma concentration (see Figure 2-6).

We test this theory by inputting initial condition of 0.081 $\mu molL^{-1}$ (ten times smaller than the theoretical value of $X_2(0)$) and again seeking the minimal value of the function (2.17). The resulting error for the smoothed data ($X_2(t)$) is then 0.0186 and for unsmoothed data is 0.0236 with σ=0.00694, s_B=102h^{-1}. This is a significant improvement (see Figure 2-7).

If regions of tissue are perfused at notably different rates we may expect a very steep initial decay in plasma concentration as drug diffuses into the rapidly perfused tissues, which would be consistent with the first data points without having to change the initial concentration. Naturally with any substance, movement into tissue will vary between tissues; depending on blood flow, fat content and other physiological factors and properties of the substance.

It appears to be the case here that if tissue compartments were divided further into 'rapidly perfused' and 'slowly perfused' ones, we may expect a very steep inital decay in plasma concentration as drug diffuses into 'rapidly perfused' tissues. This would be consistent with the first data points and the high, predicted initial concentration. We would then expect a triexponential curve solution and a better fit to the data should be obtained. This distribution mechanism is supported by data for buprenorphine in vivo in [48, 49, 50, 51], all of which report a good fit for a triexponential curve.

2.5 Three Compartment Model

We now introduce a third compartment to our model by dividing 'tissues' into 'rapidly perfused tissues' and 'slowly perfused tissues'. The schematic for the new model is given in Figure 2-8. The new model, given only for buprenorphine, without loss of generality, comprises of six time-dependent state variables: unbound drug concentration in plasma, $P_u(t)$; bound drug concentration in plasma, $P_b(t)$; unbound drug concentration in rapidly perfused tissues, $Q_u(t)$; bound drug concentration in rapidly perfused tissues, $Q_b(t)$; unbound drug concentration in slowly perfused tissues, $R_u(t)$ and bound drug concentration in slowly perfused tissues, $R_b(t)$ at time t. The model equations are built from conservation principles as described for the two compartment model and are modified as detailed below.

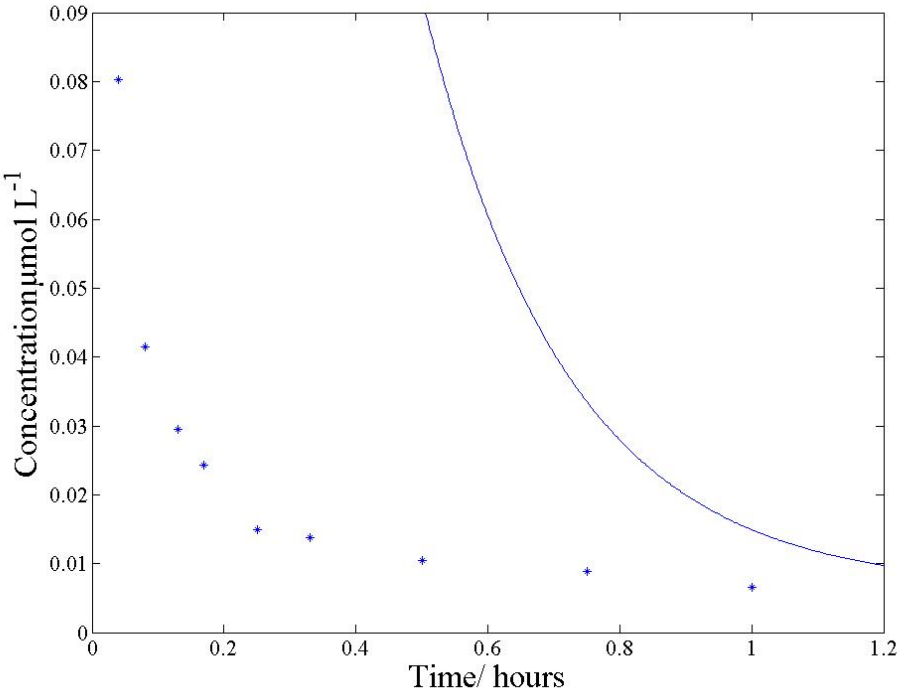

(a)

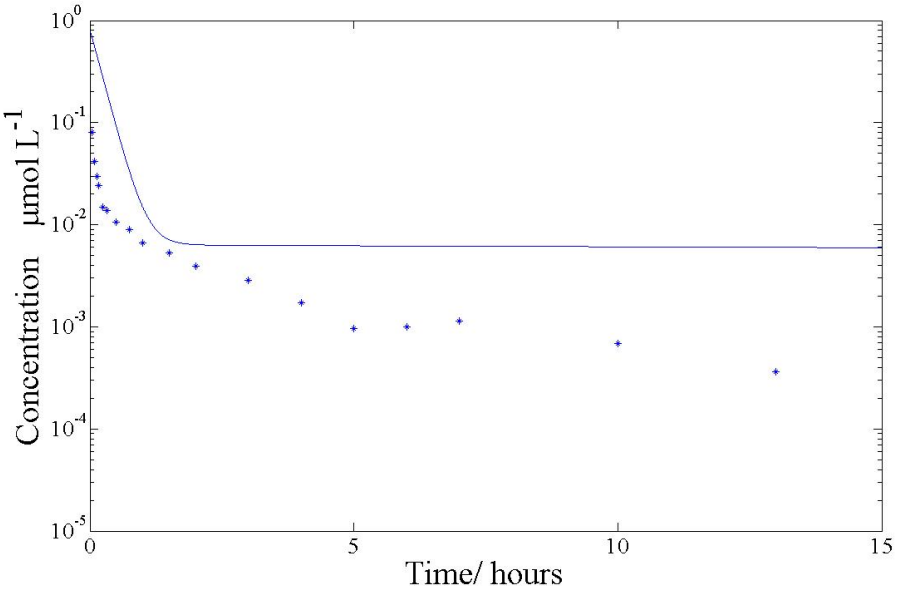

(b)

Figure 2-6: a) Two compartment model solution of plasma concentration after a 1.2mg IV dose compared to in vivo data from [45]. Using data from Table 2.1 with σ=0.00694 and s_B=102 (from equation (2.17)) , with initial conditions $P(0) = 0.814$ (from 2.16). b) The same graph plotted on a log scale.

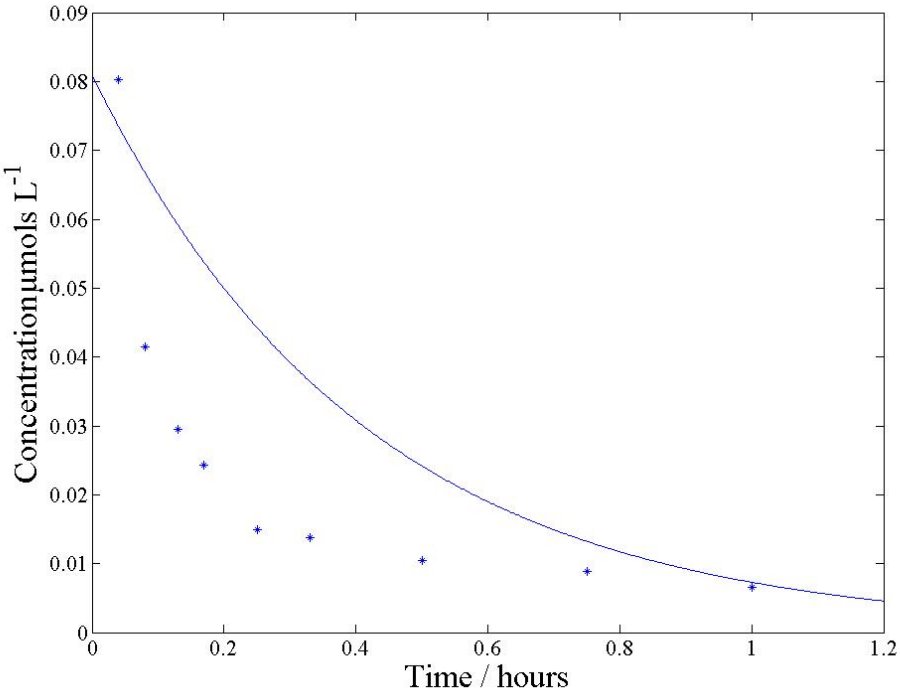

(a)

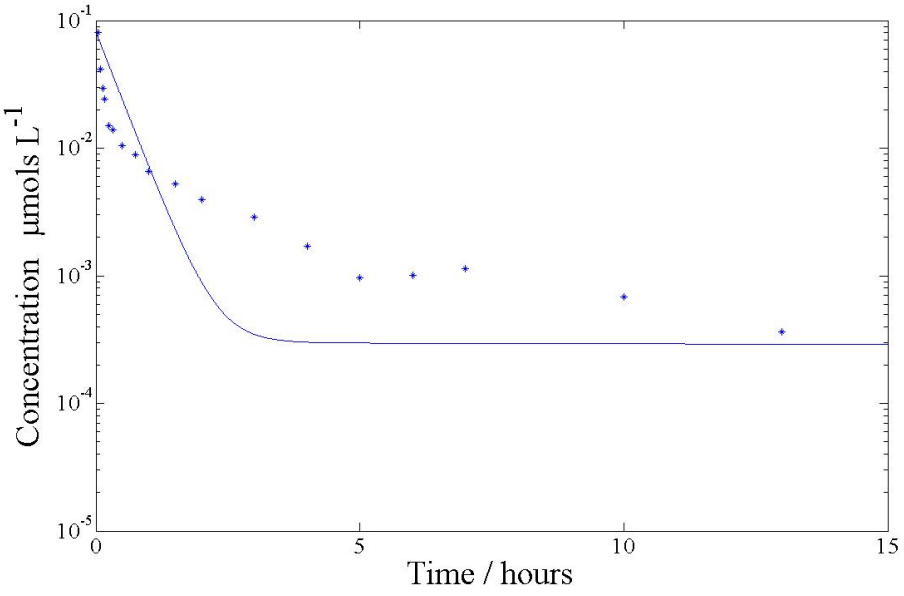

(b)

Figure 2-7: a) Two compartment model solution of plasma concentration after a 1.2mg IV dose (line) compared to in vivo data from [45](stars). Using data from Table 2.1 with σ=0.00426 and s_B=48.54 h^{-1} (from 2.17) , I.C. $P(0) = 0.081\mu moll^{-1}$ (from equation (2.10)). b) The same graph plotted on a log scale.

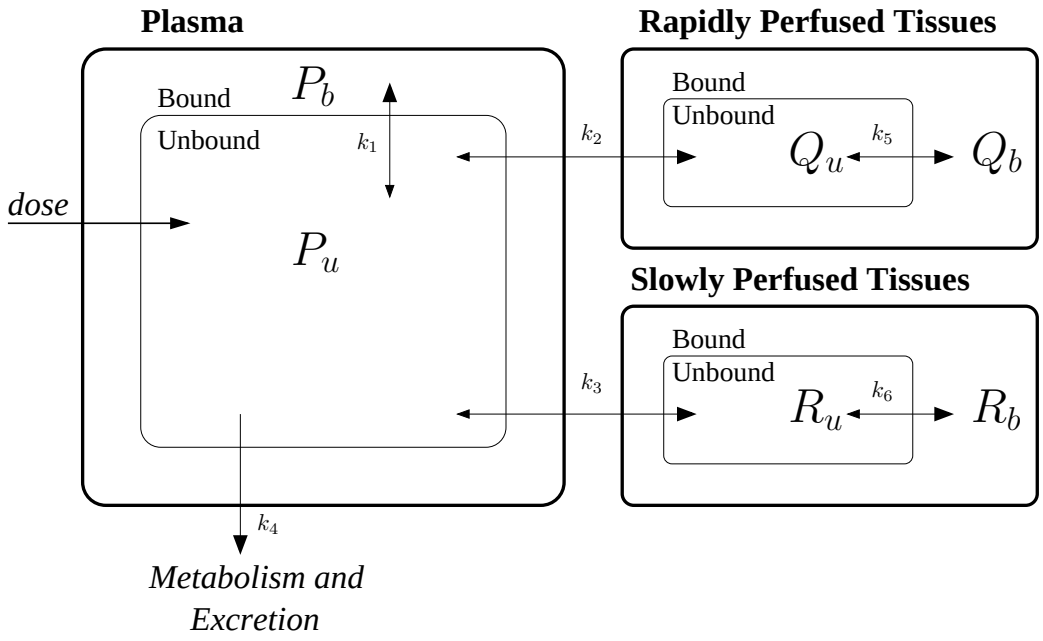

Figure 2-8: Schematic demonstrating the flow of drug within a simplified three compartment body structure. Parameters k_i $(i = 1...6)$ are described in the text.

2.5.1 (Net) Movement into tissue

The term describing movement from plasma into tissues is adjusted to reflect the division of the tissues into rapidly and slowly perfused tissue compartments. This process is reversible. Only unbound drug moves between plasma and tissue which we exploit to give the rate of movement into rapidly and slowly perfused tissue from the plasma as

$$-k_2(P_u - f_2 Q_u) - k_3(P_u - f_3 R_u).$$

The parameters k_2, k_3 are the rates at which movement occurs and are dependent on a number of factors, such as blood flow to tissues and partitioning coefficients.

Tissues are assigned to rapidly perfused or slowly perfused tissue compartments according to blood perfusion values given in [46]. It therefore follows that $k_2 > k_3$. The remaining two parameters, f_2 and f_3 represent the ratio between concentration of drug in plasma and rapidly perfused tissue; and plasma and slowly perfused tissue, at equilibrium respectively. According to the allocation of tissues to each compartment, slowly perfused tissues have a much higher fat percentage than rapidly perfused tissues [46]. As we are considering a lipophilic drug we can also expect $f_2 > f_3$ (higher affinity for fatty tissue).

The terms for binding, metabolism, excretion and repeated dosage are unchanged other than some relabeling. Therefore, the change in concentration of unbound

buprenorphine in plasma for our three compartment model is given by

$$\begin{aligned}\frac{dP_u}{dt} =& -k_1(P_u - f_{up}(P_u + P_b)) - k_2(P_u - f_2 Q_u) - k_3(P_u - f_3 R_u) \\ & - \frac{V_{max} P_u}{k_m + P_u} - k_4 P_u + \sum_{i=1}^{N} \delta k \exp(-k(t - T_i)).\end{aligned} \tag{2.18}$$

Parameter definitions for three compartment model

k_1 the rate at which bup binds to protein in the plasma

k_2 the rate at which bup perfuses into the rapidly perfused tissues from plasma

k_3 the rate at which bup perfuses into the slowly perfused tissues from plasma

k_4 the rate at which bup is excreted from the body

k_5 the rate at which bup binds to protein in the rapidly perfused tissue

k_6 the rate at which bup binds to protein in the slowly perfused tissue

$V_{Q/P}$ ratio of volume of rapidly perfused tissue to volume of plasma

$V_{R/P}$ ratio of volume of slowly perfused tissue to volume of plasma

f_{up} the fraction of bup in plasma which is unbound

f_2 ratio of concentrations of unbound drug in plasma and rapidly perfused tissue at equilibrium

f_3 ratio of concentrations of unbound drug in plasma and slowly perfused tissue at equilibrium

V_{max} the 'maximum velocity', as defined in Section 2.2.5

k_m the Michaelis rate constant

f_{uQ} the fraction of bup in rapidly perfused tissue which is unbound

f_{uR} the fraction of bup in slowly perfused tissue which is unbound

Analogously, we can write equations to describe the change in concentration of drug in all six regions and hence we obtain the full model system:

$$\begin{aligned}\frac{dP_u}{dt} =& - k_1(P_u - f_{up}(P_u + P_b)) - k_2(P_u - f_2 Q_u) - k_3(P_u - f_3 R_u),\\ & - \frac{V_{max} P_u}{k_m + P_u} - k_4 P_u + \sum_{i=1}^{N} \delta k \exp(-k(t - T_i)),\end{aligned} \tag{2.19a}$$

$$\frac{dP_b}{dt} = k_1(P_u - f_{up}(P_u + P_b)), \tag{2.19b}$$

$$\frac{dQ_u}{dt} = k_2 v_{Q/P}(P_u - f_2 Q_u) - k_5(Q_u - f_{uQ}(Q_u + Q_b)), \tag{2.19c}$$

$$\frac{dQ_b}{dt} = k_5(Q_u - f_{uQ}(Q_u + Q_b)), \tag{2.19d}$$

$$\frac{dR_u}{dt} = k_3 v_{R/P}(P_u - f_3 R_u) - k_6(R_u - f_{uR}(R_u + R_b)), \tag{2.19e}$$

$$\frac{dR_b}{dt} = k_6(R_u - f_{uR}(R_u + R_b)). \tag{2.19f}$$

The volumes of each compartment were calculated using tissue volume data from [40] for a 70kg human. As we are still considering a 1.2mg dose, we again linearise the metabolism term. Taking the same approach as in Subsection 2.4.2, we assume that the binding in the plasma and both tissue compartments happens on a much faster timescale than other processes and that in each compartment unbound drug can be determined from total drug in that compartment as follows

$$P_u = f_{up}(P_u + P_b),$$

$$Q_u = f_{up}(Q_u + Q_b),$$

$$R_u = f_{up}(R_u + R_b).$$

Considering a single IV dose which is accounted for by the initial conditions, we can therefore condense the system into three linear equations:

$$\begin{aligned}\frac{dP}{dt} =& - k_2(f_{up}P - f_2 f_{uQ} Q) - k_3(f_{up}P - f_3 f_{uR} R),\\ & - \frac{V_{max} f_{up} P}{k_m} - k_4 f_{up} P,\end{aligned} \tag{2.20a}$$

$$\frac{dQ}{dt} = k_2 v_{Q/P}(f_{up}P - f_2 f_{uQ} Q), \tag{2.20b}$$

$$\frac{dR}{dt} = k_3 v_{R/P}(f_{up}P - f_3 f_{uR} R). \tag{2.20c}$$

These equations can then be written in the form

$$\dot{\underline{B}}(t) = A\underline{B}(t), \qquad \text{where} \qquad \underline{B}(t) = \begin{bmatrix} P(t) \\ Q(t) \\ R(t) \end{bmatrix} \tag{2.21}$$

and

$$A = \begin{bmatrix} -k_2\, f_{up} - k_3\, f_{up} - \dfrac{V_{max}\, f_{up}}{k_m} - k_4\, f_{up} & k_2 f_2 f_{uQ} & k_3 f_3 f_{uR} \\ k_2\, f_{up}\, v_{Q/P} & -k_2\, f_2 f_{uQ}\, v_{Q/P} & 0 \\ k_3\, f_{up}\, v_{R/P} & 0 & -k_3\, f_3 f_{uR}\, v_{R/P} \end{bmatrix}. \tag{2.22}$$

The solution is then of the form

$$\underline{P} = c_1 e^{\lambda_1 t} + c_2 e^{\lambda_2 t} + c_3 e^{\lambda_3 t}. \tag{2.23}$$

Accordingly, we fit a triexponential to the data [45] to find a smooth data set, shown in Figure 2-9

$$X_3(t) = 0.0646e^{-11.241t} + 0.0186e^{-1.299t} + 0.00456e^{-0.200t}. \tag{2.24}$$

We fit our 3 compartment model (2.19) to the smoothed data (2.24) by calculating the error estimate, (2.17), for a range of parameter sets while seeking the minimum value for the error.

The 3 compartment model fit with $P(0) = 0.814\mu\text{moll}^{-1}$ as calculated in (2.10) to the Kuhlman data can be seen in Figure (2-10). The error for the 3 compartment model against smoothed data ($X_3(t)$) was 0.1292 and against unsmoothed data was 0.1416. The fit is also visually much improved from the two compartment model and the additional compartment allows for the high initial plasma concentration.

A triexponential curve does fit the data well, as shown in Figure 2-9, but the fit for the solution to our 3 compartment model (also a triexponential curve) is not as good. This indicates that either some of the parameters that we fixed, Table 2.1, do not exactly match the physiological traits for the individuals in the study by Kuhlman *et al.* [45], that the division into rapidly and slowly perfused tissues could be incorrect, or that the forced initial condition (2.10) is too high, perhaps due to the time taken to inject the dose or an instant distribution into the extravascular space or tissues that isn't accounted for by the 3 compartment simplification of the body.

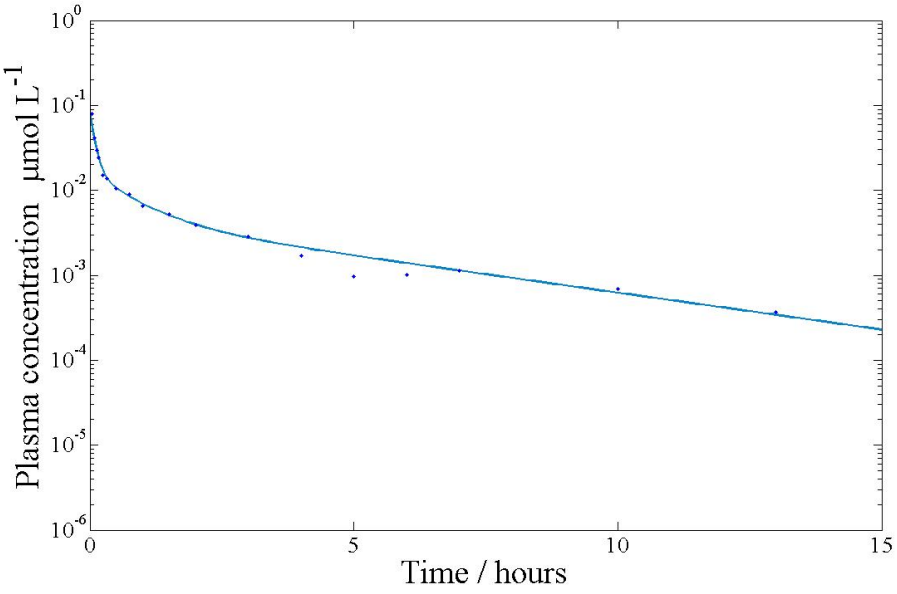

(a)

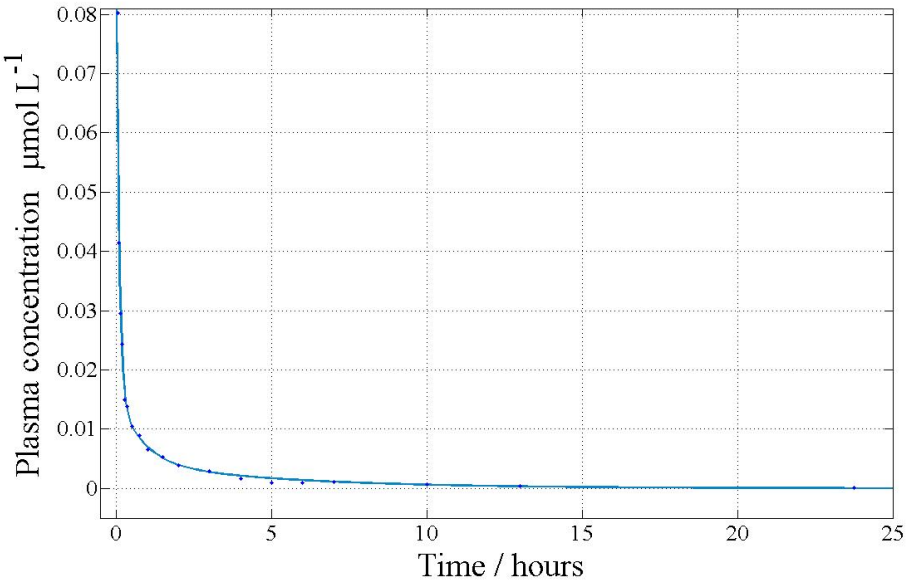

(b)

Figure 2-9: Triexponential fit to data for plasma concentration against time for a 1.2mg IV dose of buprenorphine [45] to remove data 'noise'. Triexponential curve given by $X_3(t) = 0.0646e^{-11.241t} + 0.0186e^{-1.299t} + 0.00456e^{-0.200t}$.

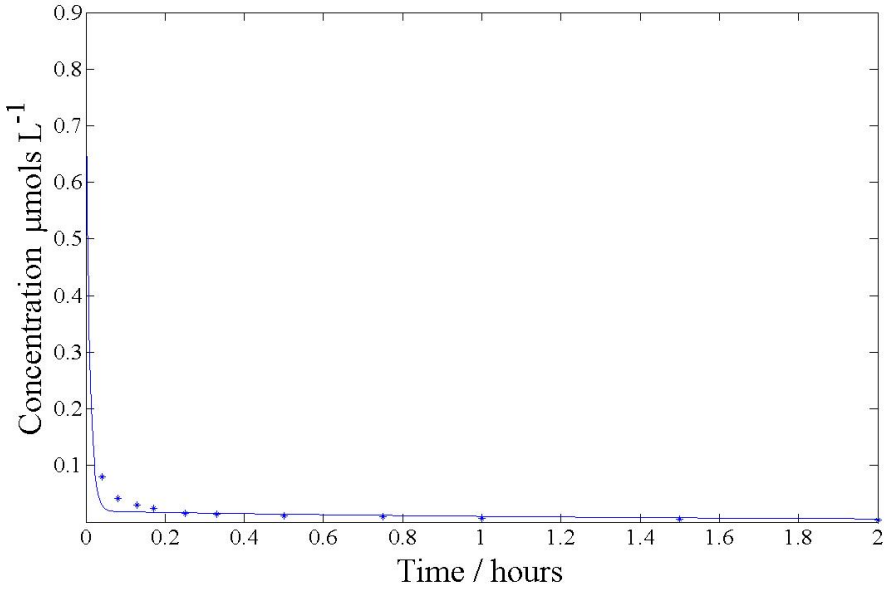

(a)

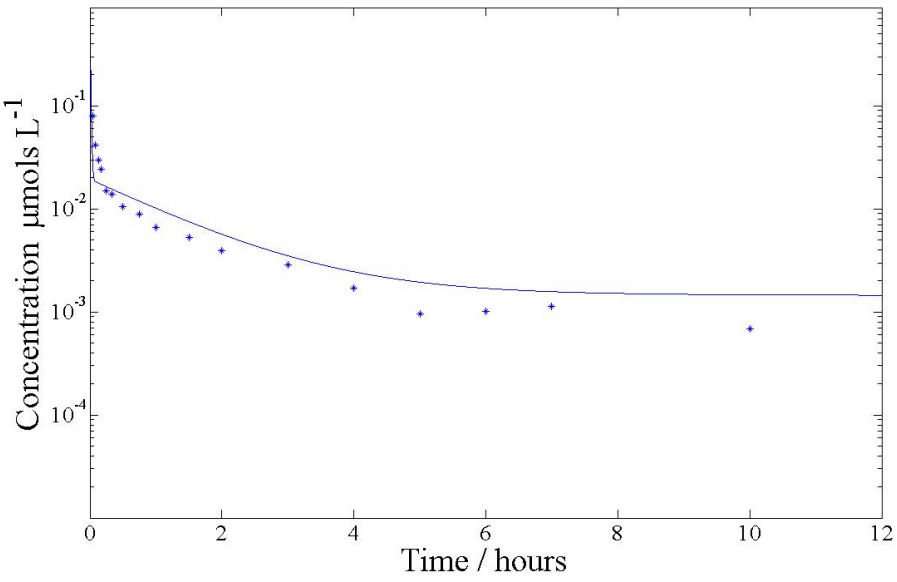

(b)

Figure 2-10: a) Three compartment model (2.19). Solution of plasma concentration after a 1.2mg IV dose (line) compared to in vivo data (stars) from [45](stars). Using data from Table 2.1 with $f_2 f_{uQ} = 5 \times 10^{-4}$, $f_3 f_{uR} = 0.465 \times 10^{-6}$, k_2=2000 and k_3=550 (from (2.17)) , I.C. $P(0) = 0.814 \mu \text{mol} l^{-1}$ (from (2.10)). b) The same graph plotted on a log scale showing first 12 hours after dose.

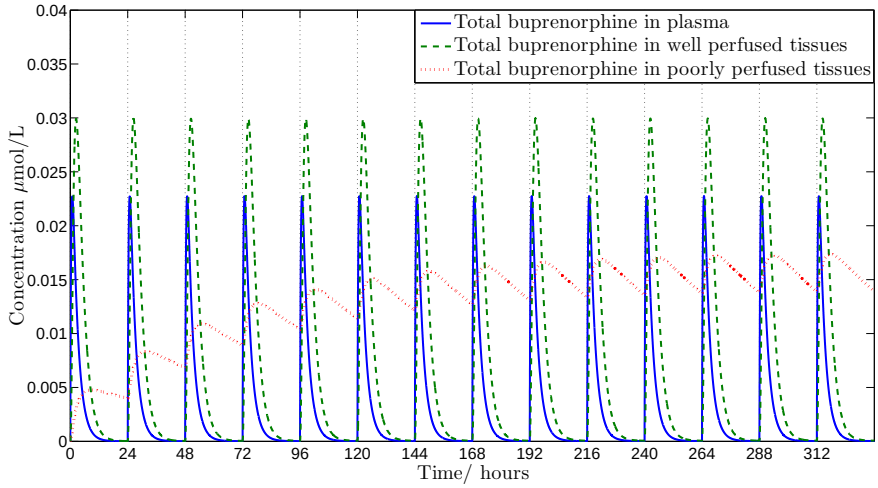

Figure 2-11: Simulation of plasma and tissue concentration profiles for a daily drug administration, using model (2.19) with parameter values as determined in section 2.5 and as given in Table 2.1.

Note If we change the initial plasma concentration to 0.087 ($X_3(0)$) and fit for k_2, k_3, $f_2 f_{uQ}$, $f_3 f_{uR}$ using our parameter sweep method, k_2 and k_3 are both given as 50h^{-1} and $f_2 f_{uQ}, f_3 f_{uR}$ are both given as 0.009, i.e. a two compartment model with similar parameters as predicted by our analytic two compartment fit. This supports the need for a third compartment specifically to account for the initial rapid drop in plasma concentration.

This fitting process has provided us with an estimate of k_2, k_3 and the products $f_2 f_{uQ}$,$f_3 f_{uR}$ to be used with the full non-linear system. Using these combined with parameters described in Table 2.1 (which are estimates for buprenorphine taken from the literature) we obtain concentration profiles for a repeated daily dose as shown in Figure 2-11. We use the profile for poorly perfused tissues as input to Model 2 where drug accumulates in the stratum corneum.

2.6 Conclusion

A model to describe systemic buprenorphine concentration following a repeated daily dose has been developed. The model presented here extends the simple case of a one compartment in-body model for lithium to the case of buprenorphine, where the drug metabolism, binding and unbinding, and distribution into the tissues, are considered. Buprenorphine is used as an exemplar drug to guide modelling decisions and populate the model parameter values used in numerical simulations.

For buprenorphine, a significant improvement in fit to data between a two and a three compartment model is observed. The fit to data could be further improved

by adding additional compartments to reflect the different tissue groups in the body more accurately. Should the appropriate data and mechanistic knowledge for buprenorphine and specific tissues become available, then an increase in the number of compartments to improve model- data fit may become beneficial.

We have created a highly customisable structure which provides an estimate for drug levels in plasma and tissues for a given dosing regimen. The modelling highlights the need for experimental work to obtain parameter estimates; if these can be obtained the model could be usefully extended to reflect different tissue regions. Of course, the model has limitations. It provides a very simplified structure for drug distribution in the body with tissue predictions unable to be verified due to lack of data. The model described gives predictions for a 'typical' 70kg human. These predictions may be affected by inter-patient variability such as age and ethnicity which could be incorporated by careful modification of 'average' model parameter estimates once such data sources are available.

We believe that our model approach is preferable to a classic PK model as it attempts to predict real tissue concentration values directly using realistic compartment volumes. Ideally a full PBPK model describing each functional region of the body would be used, however, this requires a large number of parameter values for which we have no data. We believe that the tissue predictions provided by our model are sufficient to warrant the formulation of a three compartment model. If more data were to become available this would be accommodated by the model structure.

Chapter 3

Formation of a Drug Reservoir in Skin

3.1 Introduction

In this chapter we focus on the second of our three models, shown in Figure 3-1. The purpose of this chapter is to identify key mechanisms and characteristics of skin, and transport across it, to create a description of the formation of a drug reservoir in the skin stemming from a systemic presence of that drug.

There is very little research available in the literature focused on the formation of a drug reservoir in the skin from systemic concentrations. We therefore draw on research and theories from drug delivery models and experiments to inform our own model.

The reservoir function of the skin is a recognised phenomena in the field of percutaneous absorption [8]. A reservoir in the skin was first identified for the case of corticosteroids after a prolonged therapeutic effect was observed [9, 10]. Presence of a reservoir in the skin has since been demonstrated for many other drugs [8]. Moreover it has been shown, via tape stripping, that the main site of this skin reservoir is the stratum corneum (SC), the layer of dead cells at the skin surface [8, 9, 11].

Research on the presence of a reservoir in the SC is generally focussed on formation from an external source, specifically topically applied drugs and chemical exposure [8]; drug that comes into contact with the skin surface enters the body via passive diffusion. As only unbound drug diffuses, the cause of a reservoir forming in the SC is thought to be high keratin binding and slow desorption kinetics [12]. Binding within the skin is most typical for lipophilic drugs with high molecular weight

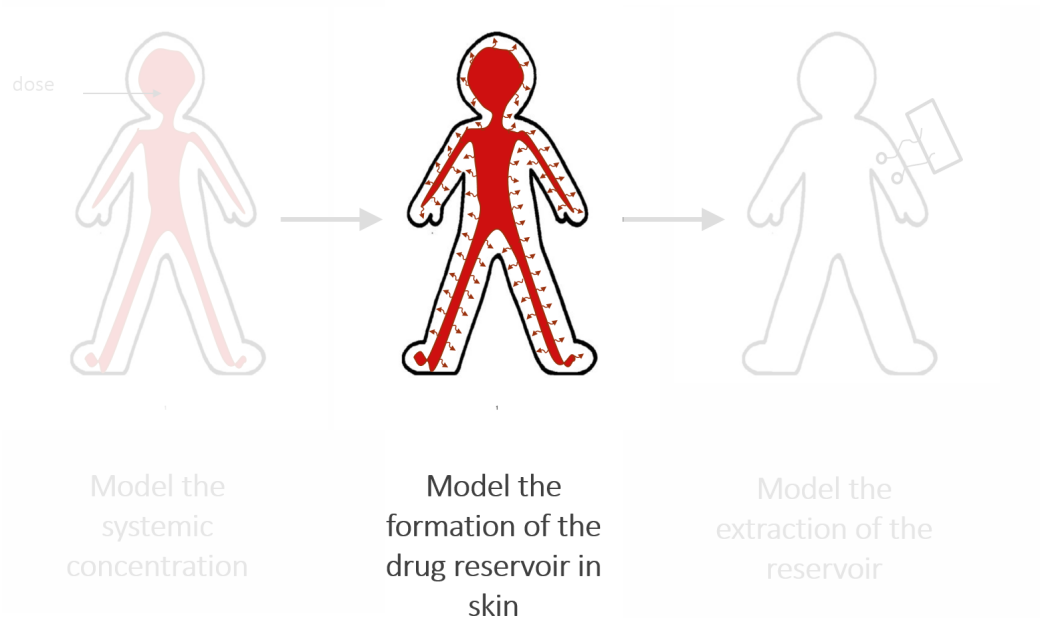

Figure 3-1: The overall aim is to create three composite models which will be linked together to create a model which predicts the expected reverse iontophoresis reading for a given drug administration regimen and therefore interpret reverse iontophoresis readings in the context of historical (order of days/weeks) drug monitoring. The second model, for the formation of the drug reservoir in the skin, is the focus of this chapter.

[13, 14]. We therefore intend to continue to focus on lipophilic drugs to guide our modelling decisions.

In this chapter we first provide a description of the structure of human skin, before going on to review models of reservoir formation and passive drug delivery in the literature to explore the ways in which various complexities have been incorporated. We also identify mechanisms which are considered important to include and consider how these might be altered to suit a non-delivery model. We then create a model for the formation of a reservoir in the SC. The inclusion of various model features are then analysed and the effect of different boundary conditions are considered. In Chapter 5 we combine the model for reservoir formation with models for in-body concentration (Chapter 2) and extraction (Chapter 6).

3.2 Anatomical Structure of Human Skin

3.2.1 Introduction

Skin is the largest organ in the human body, making up approximately 10 - 20% of an individual's total mass [52, 53]. The purpose of the skin is manifold; it is a vital barrier against infection, UV radiation and physical damage and it plays a key role

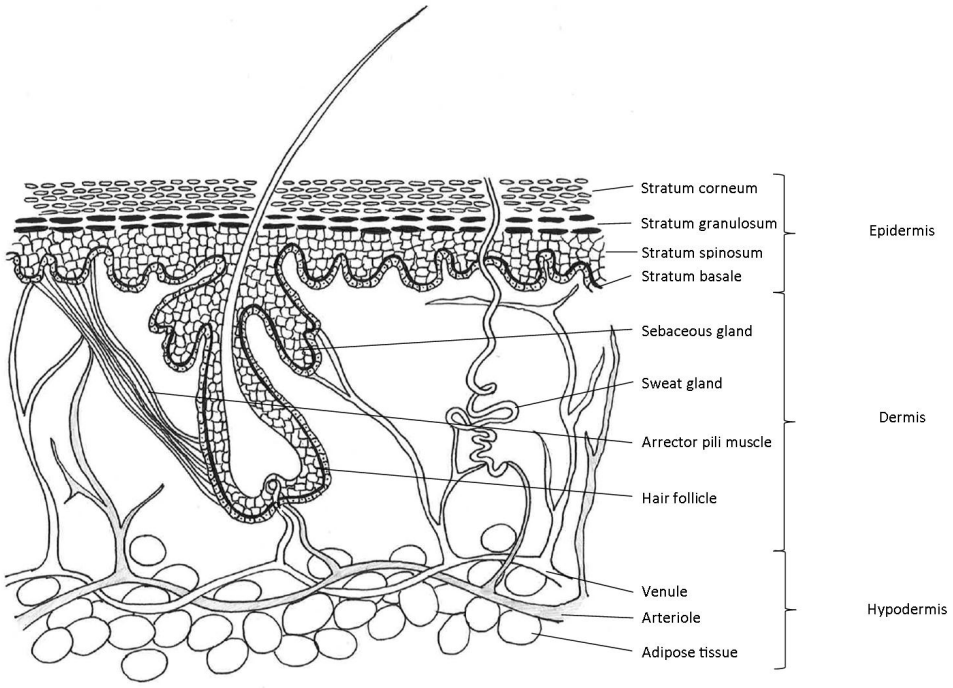

Figure 3-2: Cross sectional diagram of human skin (adapted and redrawn from [52])

in the regulation of temperature, electrolyte and fluid balance in the body; it is also important for its sensory ability and vitamin D production. A cross sectional diagram of human skin is given in Figure 3-2. There are two distinct layers of the skin; the outermost epidermis and beneath that, the dermis. The interface joining the dermis and epidermis is irregular; protrusions of the dermis, called papillae, interlock with epidermal ridges of the stratum basal. Beneath the dermis lies the hypodermis or subcutaneous tissue though this is not generally considered part of the skin.

3.2.2 Dermis

The deepest layer of the skin is the dermis, usually 3-5mm thick [52, 53], containing capillaries, nerves, sweat and sebaceous glands, hair follicles, and small arrector pili (hair supporting) muscles embedded in a mucopolysaccharide gel. In terms of transdermal movement, appendages such as hair follicles and sweat ducts may have a key role to play as they provide an alternative route for some molecules crossing the skin, the so called 'shunt route'.

3.2.2.1 Appendages

Hairs are found all over the body except the load bearing soles and palms and the lips. On average there are 60 hairs/cm^2 on any given area other than the head which has substantially more at 600 hairs/cm^2 [53]. These hairs, however, only occupy a total body area fraction of 10^{-3} [54, 55]. Sweat glands occupy an area fraction of 10^{-4}, appearing as frequently as 100-200 per cm^2 [54]. Despite the small area that the appendages proportionally occupy, many hydrophilic solutes can potentially permeate via the appendages at a much faster rate [56, 57] especially when considering electrically assisted movement, for example iontophoresis [52, 58].

3.2.3 Epidermis

The epidermis is a multi-layered membrane covering the whole body, varying in thickness between 0.06mm and 0.8mm. Keratinocytes make up 95% of the epidermis, the remaining 5% are melanocytes, Langerhans and Merkel cells [59]. The surface layer of the epidermis is the stratum corneum, a layer of dead, keratinised cells providing the primary barrier to percutaneous penetration. Beneath the stratum corneum is the viable epidermis which is itself a multi-layered membrane, each layer representing different stages of cell differentiation. The layers of the viable epidermis, starting from the deepest, are the stratum basale, stratum spinosum and stratum granulosum. The process of cell differentiation from the metabolically active cells of the stratum basale through to the stratum corneum typically takes 14 days with cells remaining in the stratum corneum for a further 14 days before shedding [52, 53]. There are no blood vessels supplying the epidermis. Nutrients are delivered to the living cells of the epidermis via diffusion from underlying dermal capillaries through the stratum basale and metabolic products of the active cells enter the circulatory system by diffusing in the opposite direction [60].

3.2.3.1 Stratum Basale

Cells in the stratum basale or basal layer are metabolically active and are therefore similar to those of other tissues in the body. Keratinocytes within the stratum basale are the only cells in the epidermis undergoing cell division, making the basal layer the primary source of cell renewal in the epidermis [60]. Cell division in the stratum basale occurs via mitosis; a parent basal cell divides creating two new cells, one cell remains attached to the basal layer whilst the other differentiates towards the surface. The cells in the stratum basale are columnar and rest on the

basal laminar at the dermal- epidermal interface. They contain protein laments (tonofilaments) about 10nm in diameter.

3.2.3.2 Stratum Spinosum

As cells progress towards the surface layer of the skin, the number of tonofilaments increase and group, forming tonofibrils [60]. In the stratum spinosum the cells begin to change shape from cuboidal to pentagonal.

3.2.3.3 Stratum Granulosum

Above the stratum spinosum is the stratum granulosum, approximately 2-5 cell layers thick [52, 53]. In this layer the keratinocytes begin to flatten and produce keratin. Enzymes are contained in the stratum granulosum which break down the viable cell nuclei and organelles. Lipid bilayers of the stratum granulosum form rod-like structures known as lamellar granules or keratinosomes, characteristic of this layer. These are membrane coating granules which, when fused with a cell membrane, deposit lipid containing sheets into the intercellular space of the stratum granulosum. These lipid sheets will later become the intercellular lipid lamellae seen in the stratum corneum.

3.2.3.4 Stratum Corneum

Sometimes the stratum lucidum is described as a separate layer; a translucent layer, observed most clearly in thicker portions of the skin, such as that on the soles of the feet. Here the cell nucleus disintegrates, cells become flatter and further keratinised. The stratum lucidum is, however, generally considered as the lower layer of the stratum corneum. Although the stratum corneum is only 10-20 cell layers thick [52, 53, 59] it is key in the regulation of movement through the epidermis, imposing the rate limiting step in the majority of transdermal processes. The stratum corneum is composed of dead, flat, keratinised cells embedded in a non-polar lipid matrix arranged as lamellar lipid layers. The structure of the transverse cross section of the SC is usually referred to as 'bricks and mortar' where the corneocytes are represented by the bricks and the lipid by the mortar [59, 61, 62, 63, 64]. Figure 3-3 shows this configuration. The exact displacement between 'bricks' within cell layers is not known but many models that incorporate this structure allow for different arrangements. The corneocytes are thought to be approximately hexagonal in shape and the bricks and mortar arrangement can be recreated by assuming corneocytes are arranged as regular hexagons when viewed from the transverse direction [65].

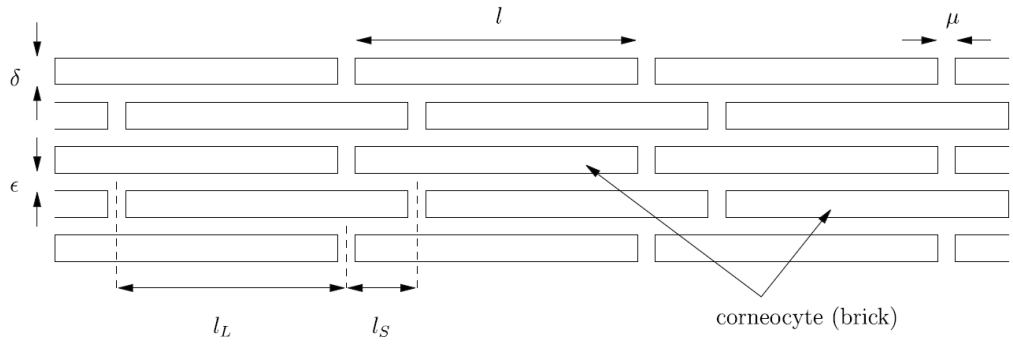

Figure 3-3: "Schematic transverse cross-section of corneocytes in the SC, commonly referred to as a bricks and mortar arrangement. The bricks represent corneocytes and the mortar the intercellular lipid. Bricks have mean length l and mean width δ. The mean horizontal distance between adjacent corneocytes is μ and the mean vertical separation distance is ϵ. The distance l_L is the mean largest horizontal distance from the centre of a lipid channel above a corneocyte to the centre of one of the adjacent lipid channels. Finally, $l_S = l + \mu - l_L$." Taken from [64].

3.2.4 Homoeostasis in the skin

Stem cells located in the stratum basale, or 'mitotic layer', are responsible for epidermal homoeostasis. Normal cell replication occurs at a rate which balances desquamation (skin shedding) at the surface of the stratum corneum and so a relatively constant thickness of epidermis is maintained. Differentiation occurs as a reaction to external chemical cues [66, 67] causing cells to undergo mitosis; a parent cell divides into two daughter cells. In adult humans, one cell stays in the basal layer and the second moves into the cell layer above. In embryos and infants, however, the skin is not yet in homoeostasis and cells move sideways to account for growth [66, 68].

The structure of the epidermis is generally thought to be divided into columns or 'epidermal proliferating units' (EPUs) [68, 69, 70, 71]. Here 1 stem cell in 10 in the basal layer is responsible for cell renewal within that column [72]. This structure is, however, largely based on research in mouse epidermis. The EPU model has more recently been disputed by Doupe and Jones [73] who propose an alternative structure termed the 'committed progenitor' (CP) model; which is a probabilistic model where "the outcome of progenitor cell division is random, with a chance of generating either two progenitor cells, two differentiating cells or one cell of each type" [73]. The CP model does not rely on a predetermined fate of cells as described for an EPU model. A comparison between the two theories presented by Doupe and Jones [73], finds that the CP model is consistent with historical and recent data for human skin but conclude that more evidence and improved assay techniques are needed to resolve this. Considering either of these models on the

membrane scale, we see the characteristic behaviours of cell turnover observed in vivo with the whole SC renewing after about 14 days.

3.2.5 Models of skin homoeostasis in the literature

Models of transdermal drug delivery and percutaneous absorption don't always include cell turnover in the SC, as often the time scale under consideration is too short. We expect SC turnover to play a significant role in the formation of the reservoir and therefore review some models of skin renewal described in the literature. These models are usually focussed on growth and repair, and consider the skin on a cellular level. Therefore stochastic models have been used to describe the skin renewal process from cell division to cell migration [74, 75, 76, 77].

The model presented by Loeffler *et al.*[75] is typical of the type of stochastic model used to describe epidermal homoeostasis and focuses on cell proliferation in the basal layer. A two dimensional 32×32 matrix of hexagonal cells is set up representing a top down view of the basal layer. The possibility of EPUs is discussed and accounted for by dividing the matrix into subunits of 10 cells with at least one stem cell positioned in each. Stem cells are assumed to be anchored but lateral displacement by daughter cells is allowed, as well as upward migration. Five stages of cell development exist in this model: stem cell, three progressive transit cells and a post mitotic cell. The algorithm starts with the whole cell layer being scanned for mitotic cells. A selected mitotic cell then divides according to the value of its 'cell cycle index' (assigned to each cell at creation as 'time until division' and adjusted at each time step). Cell displacement is executed according to the age of neighbouring cells. A dividing cell selects the oldest of the six immediate neighbouring cells which is then displaced (removed from the layer). If the selected cell is the oldest cell this cell migrates out of the layer. When the model is established, a cell labelling scenario is applied in which allocation of labelling 'grains' to daughter cells upon cell division were varied to determine the most realistic scenario. This kind of cell labelling could be adapted to describe the presence of a drug in order to apply the model to a scenario of reservoir formation to consider the movement of a drug within the skin. The disadvantage of this model type, for our purpose, is that once a cell leaves the layer it can no longer be detected and is lost from the analysis. It also only considers cell movement and not the lipid bilayer between cells. Though exact pathways through the SC and binding mechanisms aren't known, it is suspected that lipophilic drugs move through the lipid bilayers around the cells. This cell movement model may therefore be more appropriate for a scenario where drug binds to, or partitions into, aqueous cells.

Nakaoka *et al.* describe a model for division and differentiation of stem cells as a response to chemical cues [76]. A system of delay differential equations is

established in which cells respond to a 'growth factor' (also modelled by differential equation). The model formulation potentially has more scope to be utilised in a drug reservoir formation scenario as diffusion through cells is already an established mechanism, and more skin cell layers are modelled. Again, however, only cells are considered and there is no immediate way of including movement via lipid bilayers.

Although these models may be of use in the future for drug reservoir formation in the skin, we believe that their approach is too detailed for our current needs.

3.3 Pathways

In the case of passive transdermal delivery and chemical exposure, the SC has been identified as the rate limiting barrier. As such, considerable effort has gone into determining the route of particles traversing this membrane. Three possible routes have been identified; transcellular (through corneocytes and lipid); intercellular (through lipid domains only); or via appendages (shunt routes) [52].

The transcellular route refers to the direct route through the SC, partitioning in and out of cells. It is thought, however, that the cells of the SC may be impermeable especially for large, lipophilic molecules [78].

The intercellular route refers to diffusion in the intercellular space between the cells, i.e. through the lipid matrix. This is thought to be the dominant route through the SC especially for lipophilic drugs [62, 79, 80, 81].

The shunt route could be thought of as the most direct route, bypassing the SC entirely. These aqueous pathways are thought to be a potential route for hydrophilic drugs but as appendages only occupy a small area fraction, this route is generally dismissed in the case of passive delivery [79].

3.4 Review of reservoir formation and passive transdermal delivery models

The only current instance of a mathematical model describing the formation of a reservoir in the SC caused by the systemic presence of a drug is that of Paulley *et al.* [24]. This model for the formation of a lithium reservoir using a non-spatial compartmental transfer model. The SC compartment is joined to a serum compartment, and drug enters and leaves the SC compartment via a constant rate term, representing the turnover of cells. Diffusion of lithium in the SC is not considered. The model, which comprises a pair of coupled ODEs, is in good

agreement with available data for both serum levels and extracted fluxes by reverse iontophoresis (relating to reservoir size calculations). However, as explained earlier, this is in many ways the simplest case scenario.

In percutaneous absorption models and experiments, we are considering a scenario where a substance placed on the skin surface enters the body through the skin via passive diffusion only. In practice this is usually a cream or patch of known concentration applied to a fixed area of skin in vivo or patch of excised skin in vitro.

The simplest approach to SC penetration is to assume an idealised, homogeneous SC [82]. The change in concentration of a drug at a depth x in the SC is then described by Fick's second law of diffusion,

$$\frac{\partial C(x,t)}{\partial t} = D_{sc}\frac{\partial^2 C(x,t)}{\partial x^2},$$

with the diffusion coefficient in the SC, D_{sc}, a constant. The steady state flux, J_{ss}, through the SC is given by the amount of solute, Q_{ss}, passing across a surface area, A, of the skin over a time period T, which is proportional to the concentration gradient across the SC, ΔC_{sc}, and the diffusion coefficient, D_{sc}, and inversely proportional to the diffusion path length. For a SC of thickness h_{sc}, this gives

$$J_{ss} = \frac{Q_{ss}}{AT} = \frac{D_{sc}\Delta C_{sc}}{h_{sc}},$$

which represents Fick's first law of diffusion. If we make the further assumption that the concentration on each boundary is fixed, with sink conditions on one side of the SC, the equation simplifies further to

$$J_{ss} = \frac{D_{sc}C_{sc}}{h_{sc}}.$$

These equations are used as a starting point for many models [83, 84, 85, 54, 86, 87, 88]. Complexities such as heterogeneous skin structure, dynamics in vehicle, binding, more skin layer compartments and other features are subsequently added.

3.4.1 Models of passive transdermal delivery through heterogeneous SC

As described in Subsection 3.2.3.4, the SC isn't a homogeneous membrane, and actually has a bricks and mortar like structure. Many authors have devised techniques to incorporate the structure of the SC into their passive delivery models.

One way to incorporate the heterogeneous nature of the SC is to introduce an 'effective diffusion coefficient' or increased path length to reflect the tortuous route through the SC.

Heisig *et al.* [89] and Frasche and Barbero [90] use a 2D bricks and mortar structure of the SC, taking a fixed value for concentration at the skin surface, and sink conditions at the base of the SC, and using PDEs to describe diffusion through the SC. Heisig *et al.* consider a drug that is able to diffuse through both lipids and corneocytes with a reduced diffusion coefficient through corneocytes, whereas Frasch and Barbero restrict the movement to lipids only. Heisig *et al.* demonstrate the dependence of results on inclusion of permeable corneocytes and the diffusion coefficients in them. Both models allow for different displacement ratios of the 'bricks' between layers and analysis highlights the importance of SC geometry for predicted time to cross the SC.

Mollee and Bracken [64] consider an alternative method to model passive diffusion of a lipophilic drug through the lipid bilayers of a bricks and mortar structure. The pathway of particles is modelled by a one-dimensional PDE using a 'trapping and release' methodology. The x-direction is taken to be transverse to the surface of the skin. Drug travels between cells from the surface of the skin until it reaches an obstructing cell, where it remains trapped for the duration of lateral movement and then continues in the x-direction until arriving at the next cell (corneocyte). Parameters in their model allow for different alignment of bricks and mortar and both square and hexagonal cell profiles are considered. Their work supports previous research demonstrating the impact of considering SC structure on parameter estimation [61, 63, 89, 90].

3.4.2 Models of passive transdermal delivery that include cell turnover in the SC

In transdermal delivery, epidermal turnover opposes the absorption of drugs through the SC.

Cell turnover in the SC was included in the model by Reddy *et al.* [13], who also included the turnover of the viable epidermis (VE) and therefore partitioning between the SC and VE, as determined by chemical properties of the drug. The focus of this paper was to link the turnover of SC to loss of chemical from the surface layer. They concluded that epidermal turnover may significantly reduce systemic absorption for highly lipophilic or high molecular weight (MW) chemicals, but is not expected to have a huge impact on most other chemicals.

Motivated by the reservoir effect of the SC for corticosteroids, Roberts *et al.* investigated the impact of desquamation on this reservoir [8]. The paper uses a well

mixed compartment to represent the SC connected to a VE compartment, which is in turn linked with a systemic circulation compartment. Diffusion wasn't directly considered, but was accounted for by a first order rate term for movement of drug from the SC compartment to the VE compartment. Desquamation was accounted for by a constant removal rate from the SC compartment. The authors conclude that desquamation will only affect the reservoir formation when the penetration rate of the solute is comparatively slow. The effect of desquamation is therefore also more pronounced for diseased skin, where turnover is increased.

In 2011, Simon *et al.* included the effects of epidermal turnover in their mathematical drug delivery model to explore the influence of turnover on the time taken to reach steady state delivery [85]. A single species of drug in the SC and viable epidermis is considered, using a pair of coupled one-dimensional PDEs, diffusion and desquamation are modelled in both skin layers using diffusion-advection equations. The model is solved using Laplace transforms and the residue theorem to provide an analytical solution. They conclude that lipophilicity and high MW hamper transport due to a low diffusion coefficient, supporting the findings of Reddy *et al.* [13] and Roberts *et al.* [8].

3.4.3 Models of passive transdermal delivery that include binding

Binding of drug in the SC has been considered in a number of cases [12, 91, 92, 93]. As only unbound drug is free to diffuse, binding of a drug in the SC may impact the rate at which a drug crosses the SC.

Nitsche and Frasch explore the consequences of linear reversible binding on dermal absorption [12]. A coupled system of equations is used representing bound and unbound drug in the skin with linear transfer between the two and only unbound drug free to diffuse. In this paper they consider the SC on a cellular level with a bricks and mortar like structure. The goal is to approximate the behaviour observed here on a membrane scale, and to estimate effective coefficients for this analogous membrane scale model. They find that, when considering transcellular transport, forward and reverse binding rate constants for each microscopic phase (lipid and corneocyte) must be included. However they acknowledge that data for these parameters is generally unavailable and call for further experimental work to determine a relation between these values and properties of a chemical such as lipophilicity (K_{oct}) and MW. They also conclude that a significant fraction of transdermal delivery does not occur at steady state but instead at the 'transient regime'.

Pontrelli and de Monte also addressed binding dynamics in passive transdermal delivery [92]. In this model they consider bound and unbound drug in homogeneous

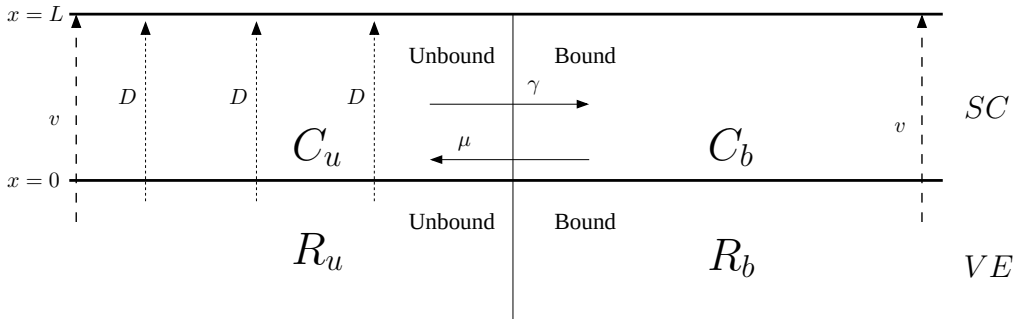

Figure 3-4: Schematic for Model 2 where SC ($x = [0, L]$) is the stratum corneum and VE is the viable epidermis represented by 'poorly perfused tissues' from Model 1, C_u, C_b are the unbound and bound drug in the SC and R_u, R_b are the unbound and bound drug in poorly perfused tissues (from model 1). Dotted arrows denote diffusion of unbound drug (diffusion coefficient D) and dashed arrows denote convective movement of bound and unbound drug due to the renewal of the stratum corneum at rate v.

skin and the delivery vehicle, with reversible binding in both. This is modelled in one spatial dimension, normal to the skin surface. Initially all drug is bound in the vehicle, drug unbinds (and binds) at a constant rate, and unbound drug partitions into skin where it can reversibly bind. At the base of the skin drug is cleared by a capillary system following first order kinetics. Only unbound drug is free to diffuse and partition from vehicle into skin. Analysis highlights the importance of the ratio of binding to unbinding parameter values in both the vehicle and skin, as these affect the whole drug transfer process. The authors suggest that the analytic results provide important information for drug selection and experimental design for optimal drug transport.

3.5 Modelling

In this section we create a mathematical model to describe the formation of a drug reservoir in the stratum corneum. Our hypothesis is that the systemic presence of a drug causes a build up in the SC to create a reservoir, where inflow from poorly perfused tissues is balanced by a loss from the skin surface.

Drug binding in skin In Model 1 (equation 2.19) in Chapter 2, we considered bound and unbound drug in the plasma and tissues. Drug binds to keratin in the skin [14] and the dynamics of binding in the skin have been shown to be linear [91]. As only unbound drug is free to diffuse [12], binding may be an important factor in the formation of a SC reservoir. We therefore consider both bound and unbound drug in the SC and allow for the possibility of binding and unbinding.

Passive diffusion through the skin Movement of unbound drug into the skin occurs via passive diffusion down a concentration gradient and is described by Fick's law of diffusion assuming a constant diffusion coefficient, $D > 0$.

Movement with the differentiating cells Cells and intercellular material in the skin move from the viable epidermis to the skin surface where they are shed [52, 94]. We are considering the movement of drug from the base of the SC to the skin surface i.e. with the direction of movement of renewing cells. Epidermal turnover and desquamation is affected by many variables including hydration, time of day and skin condition. Here we focus on the underlying mechanism and assume that the skin moves towards the body surface at constant velocity, $v > 0$.

We consider a one-dimensional spatial domain for the SC since we assume that the drug is distributed homogeneously across the viable epidermis (VE), the layer below the SC, and approximate the SC as laterally homogeneous. We take $x = 0$ to correspond to the boundary between the SC and VE, and $x = L$ to the surface of the skin.

We let $C_u(x,t)$ and $C_b(x,t)$ denote the concentration of unbound and bound drug at x, at time t, respectively and develop a diffusion-convection model based on the schematic shown in Figure 3-4, assuming that

1. unbound drug diffuses across the SC with diffusion coefficient $D > 0$.
2. bound and unbound drug move towards the surface of the skin at constant velocity, $v > 0$, corresponding to the cell renewal in the SC.
3. bound drug becomes unbound at the rate $\mu > 0$, and unbound drug becomes bound at rate $\gamma > 0$.
4. at $x = 0$, concentrations of bound and unbound drug correspond to those values obtained from the poorly perfused tissue in the compartmental model, $R_b(t), R_u(t)$ respectively.
5. at $x = L$, we assume no diffusion across the surface of the skin of the unbound drug i.e. at $x = L$ flux is vC_u.

Combining these elements we obtain the model system:

$$\frac{\partial C_u}{\partial t} = D\frac{\partial^2 C_u}{\partial x^2} - v\frac{\partial C_u}{\partial x} + \mu C_b - \gamma C_u, \tag{3.1a}$$

$$\frac{\partial C_b}{\partial t} = -v\frac{\partial C_b}{\partial x} - \mu C_b + \gamma C_u. \tag{3.1b}$$

At $x = 0$, the interface between the stratum corneum and viable epidermis, the boundary conditions are

$$C_u(0,t) = \alpha R_u(t), \tag{3.2a}$$

$$C_b(0,t) = \alpha R_b(t), \tag{3.2b}$$

where α represents partitioning between poorly perfused tissues and the SC and where $R_u(t)$ and $R_b(t)$ are outputs from Model 1. Boundary conditions at the surface are given by

$$D\frac{\partial C_u}{\partial x}\bigg|_{x=L} = 0 \qquad \text{(no diffusion across skin surface).} \tag{3.3}$$

3.5.1 Calculation of Steady State Drug Distribution in the SC

Assuming a constant dosing regime, we approximate plasma and tissue concentrations by their average values and assume constant boundary conditions

$$C_u(0,t) = \alpha R_u(t) = \alpha \bar{R}_u,\ \alpha R_b(t) = \alpha R_b = \bar{C}_b(o,t),$$

At steady state we set the left-hand side (LHS) of equation (3.1) equal to zero.

We define

$$\underline{C} = \begin{bmatrix} C_u \\ C_b \\ \omega \end{bmatrix}, \tag{3.4}$$

with $\omega = \dfrac{dC_u}{dx}$ and use this to rewrite equation (3.1) at steady state as

$$\begin{bmatrix} \dot{C}_u \\ \dot{C}_b \\ \dot{\omega} \end{bmatrix} = \begin{bmatrix} 0 & 0 & 1 \\ \dfrac{\gamma}{v} & -\dfrac{\mu}{v} & 0 \\ \dfrac{\gamma}{D} & -\dfrac{\mu}{D} & \dfrac{v}{D} \end{bmatrix} \begin{bmatrix} C_u \\ C_b \\ \omega \end{bmatrix}, \tag{3.5}$$

where $\dot{C}_u = \dfrac{dC_u}{dx}$ and $\dot{C}_b = \dfrac{dC_b}{dx}$.

The eigenvalues of the system are

$$\lambda_0 = 0, \tag{3.6}$$

$$\lambda_+ = \frac{\frac{v}{D} - \frac{\mu}{v} + \sqrt{\left(-\frac{v}{D} + \frac{\mu}{v}\right)^2 + 4\left(\frac{\mu}{D} + \frac{\gamma}{D}\right)}}{2}, \tag{3.7}$$

$$\lambda_- = \frac{\frac{v}{D} - \frac{\mu}{v} - \sqrt{\left(-\frac{v}{D} + \frac{\mu}{v}\right)^2 + 4\left(\frac{\mu}{D} + \frac{\gamma}{D}\right)}}{2}, \tag{3.8}$$

with corresponding eigenvectors

$$\underline{\mathrm{v}}_0 = \begin{bmatrix} \frac{\mu}{\gamma} \\ 1 \\ 0 \end{bmatrix}, \underline{\mathrm{v}}_+ = \begin{bmatrix} \frac{\mu + \lambda_+ v}{\gamma} \\ 1 \\ \frac{\lambda_+ \mu + {\lambda_+}^2 v}{\gamma} \end{bmatrix}, \underline{\mathrm{v}}_- = \begin{bmatrix} \frac{\mu + \lambda_- v}{\gamma} \\ 1 \\ \frac{\lambda_- \mu + {\lambda_-}^2 v}{\gamma} \end{bmatrix} \tag{3.9}$$

Hence the steady state distribution in the SC is given by.

$$\underline{C} = a\underline{\mathrm{v}}_0 + b\underline{\mathrm{v}}_+ \exp(\lambda_+ x) + c\underline{\mathrm{v}}_- \exp(\lambda_- x), \tag{3.10}$$

where a, b and c are constants, found using boundary conditions (3.2) to be

$$a = \alpha\bar{R}_b - b - c, \tag{3.11}$$

$$b = \left(\alpha\bar{R}_u - \frac{\alpha\mu\bar{R}_b}{\gamma} - \frac{cv\lambda_-}{\gamma}\right)\frac{\gamma}{\lambda_+ v}, \tag{3.12}$$

$$c = \frac{\alpha\left(\gamma\bar{R}_u - \mu\bar{R}_b\right)\left(\frac{\mu}{v} + \lambda_+\right)\exp(\lambda_+ L)}{\lambda_-[(\exp(\lambda_+ L)(\mu + \lambda_+ v) - \exp(\lambda_- L)(\mu + \lambda_- v)]}. \tag{3.13}$$

We use these distributions to explore the form and size of a drug reservoir in the skin.

Note that if we consider binding and unbinding occurring at an equal rate ($\mu = \gamma$) and constant boundary conditions with equal concentrations of bound and unbound drug ($\alpha R_u = \alpha R_b$) then from equations (3.11-3.13) c=0 and so b=0 giving a=αR_b. Using this in equation (3.10) the steady state solution of drug in the SC for equal binding and unbinding rates and equal bound and unbound drug on the boundary is

$$\underline{C} = \alpha R_u \begin{bmatrix} 1 \\ 1 \\ 0 \end{bmatrix} \tag{3.14}$$

i.e. we expect no spatial dependence in the steady state reservoir concentration. The reservoir size per unit surface area of the skin is then given as

$$S_u = \alpha R_u L = S_b. \tag{3.15}$$

3.5.2 Reservoir Size

We define the size of the reservoir to be the amount of drug across the entire thickness of the stratum corneum at steady state for a given unit of cross sectional area of skin. The size of the unbound and bound reservoir (S_u, S_b) at steady state are given by

$$\begin{aligned} S_u = \int_0^L C_u(x)\mathrm{d}x &= \frac{a\mu L}{\gamma} + b\left(\frac{\mu+\lambda_+ v}{\gamma\lambda_+}\right)(\exp(\lambda_+ L)-1) \\ &+ \int_0^L c\left(\frac{\mu+\lambda_- v}{\gamma\lambda_-}\right)(\exp(\lambda_- L)-1)\,, \end{aligned} \tag{3.16}$$

$$S_b = \int_0^L C_b(x)\mathrm{d}x = aL + \frac{b}{\lambda_+}(\exp(\lambda_+ L)-1) - \frac{c}{\lambda_-}(\exp(\lambda_- L)-1)\,, \tag{3.17}$$

where a, b, and c are constants as defined by equations 3.11-3.13 and $\lambda_+$and λ_- are given by equations (3.7) and (3.8).

We use these expressions to explore how changes in model parameters affect reservoir size.

3.5.3 Bricks and mortar structure

To cover the thickness of the SC (a distance, L) solely by diffusion would take average time $\tau_D = L^2/D$ and by convection would take average time $\tau_C = L/v$ which means that when $D = Lv$, the time taken to transit the SC is the same for both movement mechanisms. The stratum corneum is known to have a bricks and mortar like structure [54, 61]. For lipophilic drugs we expect the primary route of diffusion will be via the lipid matrix i.e. intercellularly [62]. To follow this route, the drug molecules must move around the flat keratinised cells that are embedded in the matrix [52], which means that their path length through the SC L_D will typically be longer than the domain size L. To account for this in our one-dimensional model, the model diffusion coefficient D is modified from the actual coefficient D_{L_D} by equating the time to travel along both paths. This gives

$$\tau_D = \frac{L^2}{D} = \frac{L_D^2}{D_{L_D}},$$

and hence

$$D = \frac{L^2}{L_D^2} D_{L_D} < D_{L_D}.$$

Based on this argument we represent a longer, more tortuous route through the SC with a lower diffusional coefficient in our one-dimension spatial model.

3.6 Results

In this section we explore the dependence of the reservoir size and time to steady state on key parameters including binding and unbinding parameters, diffusion coefficient and drug distribution at the lower SC boundary.

3.6.1 Parameter Values used in Numerics

The thickness of the SC (L) is dependent on many variables including region of the body, age, gender and health. In a study by Sandby-Moller *et al.*. [95] the average thickness of the SC for the forearm, where skin sampling is usually taken, is given as 18.3μm and it is this value chosen for L in numerical simulations.

The time taken to renew the SC is typically taken to be 14 days for a healthy adult [96, 97, 94] and we therefore take v to be $0.054\mu\text{m}h^{-1}$.

Values of D, μ and γ are drug dependent and are often uncertain or unknown. Boundary values αR_u and αR_b come from the first model and are consequently variable and depend on drug and drug intake. We therefore explore the dependence of our reservoir size on these unknown parameters.

3.6.2 Dependence of reservoir size on binding

The importance of binding parameters in transdermal drug delivery has been highlighted recently in a paper by Pontrelli and de Monte [92]. A comparison between reservoir size and diffusion coefficient, D, for different binding rates with different bound/unbound ratios at the boundary is given in Figures 3-5 and 3-6. From this we can see that for sufficiently large D, reservoir size approaches a constant value dependent on the boundary conditions and binding rates. The relative proportion of bound to unbound drug in the reservoir at steady state appears to be controlled by the binding rates, γ and μ, whereas the scale of the reservoir is affected by a combination of the ratio of bound/unbound drug at the boundary and the rates of binding, γ, and unbinding, μ, in the SC.

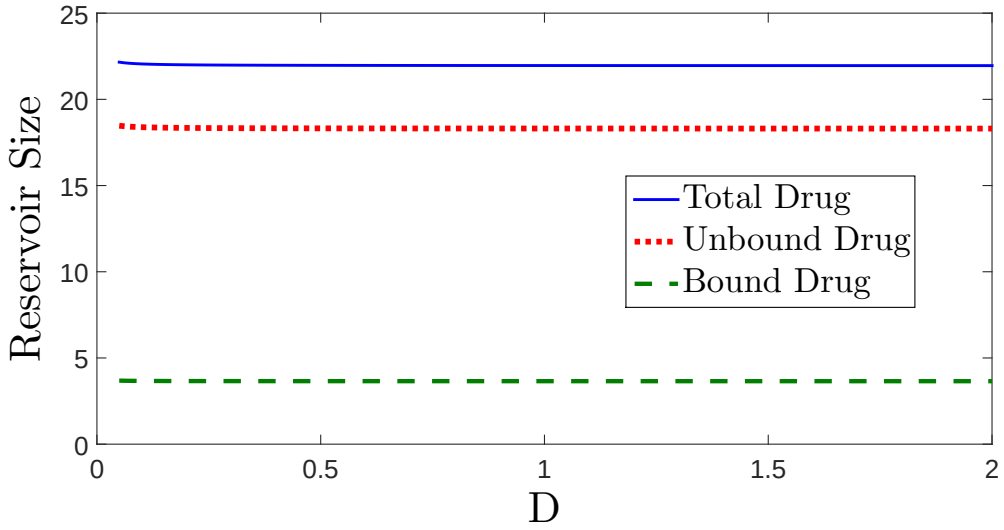

(a) μ=5, γ=1, $\alpha R_u = \alpha R_b$=1

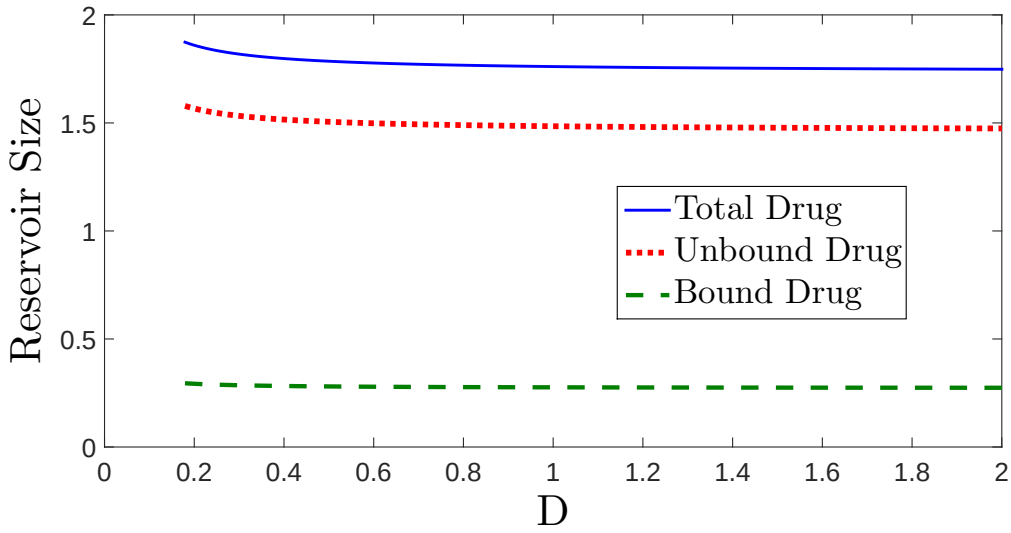

(b) μ=5, γ=1, αR_u=0.08 αR_b=1.92

Figure 3-5: Steady state reservoir size plotted against D for the cases $\mu > \gamma$ with (a) even ($\alpha R_u = \alpha R_b = 1$) and (b) uneven ($\alpha R_u = 0.08, \alpha R_b = 1.92$) binding on the constant boundary at $x = 0$. As parameter values chosen here are for qualitative exploration, units of reservoir size have been omitted.

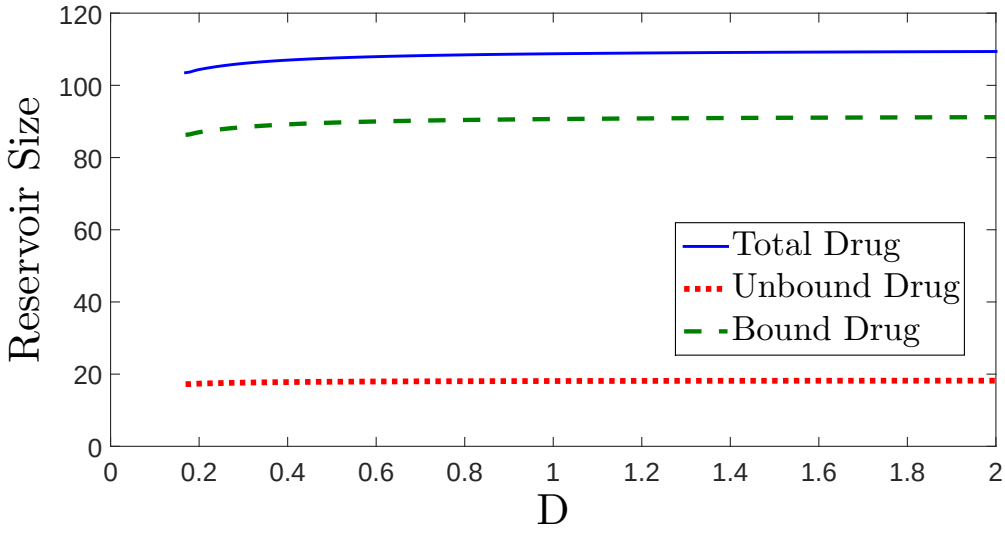

(a) μ=1, γ=5, $\alpha R_u = \alpha R_b$=1

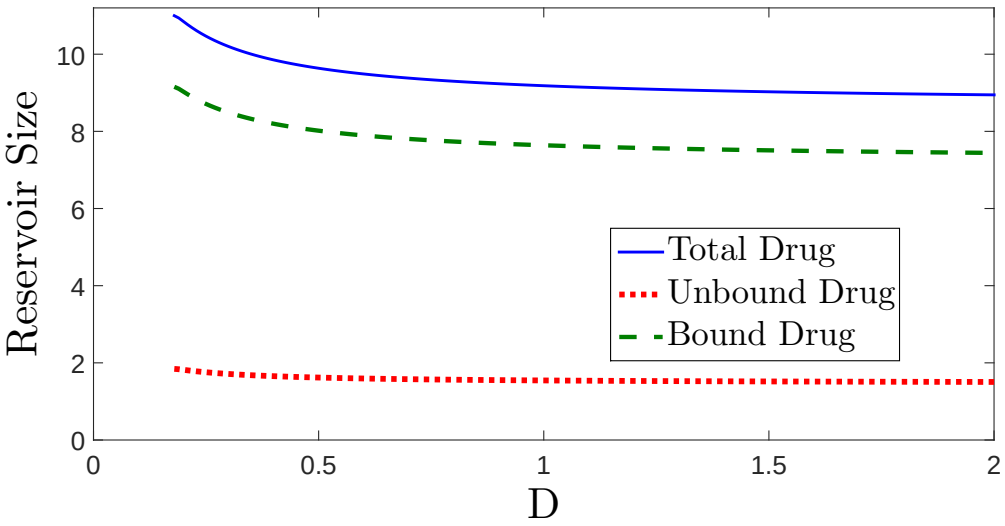

(b) μ=1, γ=5, αR_u=0.08 αR_b=1.92

Figure 3-6: Steady state reservoir size plotted against D for the cases $\mu < \gamma$ with (a) even ($\alpha R_u = \alpha R_b = 1$) and (b) uneven ($\alpha R_u = 0.08, \alpha R_b = 1.92$) binding on the constant boundary at $x = 0$. As parameter values chosen here are for qualitative exploration, units of reservoir size have been omitted.

Next we explore how the reservoir size depends on the binding and unbinding rates whilst keeping D fixed, and boundary conditions constant. In Figure 3-7(a) we vary γ and observe that the total reservoir size increases essentially linearly with γ, driven by an increase in the amount of bound drug. Variation in γ has no effect on the amount of unbound drug in the reservoir at steady state (due to the non-zero value of D).

In Figure 3-7(b), we vary μ (unbinding) and in this case observe that the total reservoir size is inversely proportional to μ, again driven by a similar relation between bound drug and μ. From both graphs we see that binding mechanisms of drug within the SC may prove a crucial factor in expected reservoir size. Moreover the comparative levels of bound and unbound drug may be significant when considering extraction of the reservoir. If, for example, only unbound drug is retrieved with a given extraction method, high binding and low unbinding may decrease rather than increase observed reservoir size.

3.6.3 Dependence of reservoir size on boundary drug distribution

In Figure 3-8 we show how the binding ratio for drug in the poorly perfused tissue (Figure 2-11) impacts on reservoir size. From this figure we note that; in all cases, as the percentage of drug that is unbound increases in the body, the reservoir size increases, and when the rate of binding exceeds the rate of unbinding in the SC, the reservoir size is significantly larger than when this relation is reversed. Again this has relevance for the extraction process as detailed above in Subsection 3.6.2.

3.6.4 Time to form reservoir

Whilst steady state reservoir size provides valuable information about the scale of the drug storage in the skin, it does not provide any information on how long it takes for the reservoir to form. This is an important measure as it indicates how sensitive the reservoir size is to a change in the boundary condition and therefore how quickly it will reflect a change in dose.

In the case where the rate of unbinding is greater than the rate of binding ($\mu > \gamma$), illustrated by Figures 3-9(a) and 3-9(b), the time taken to reach steady state decreases with an increase in D, i.e. the faster the diffusion of unbound drug, the quicker the reservoir is able to settle to its steady state level. For small D the accumulation of the reservoir is initially slower than for large D but over time this reverses. This is because initially, greater diffusion allows unbound drug to access the whole region before becoming bound and so the reservoir builds rapidly but

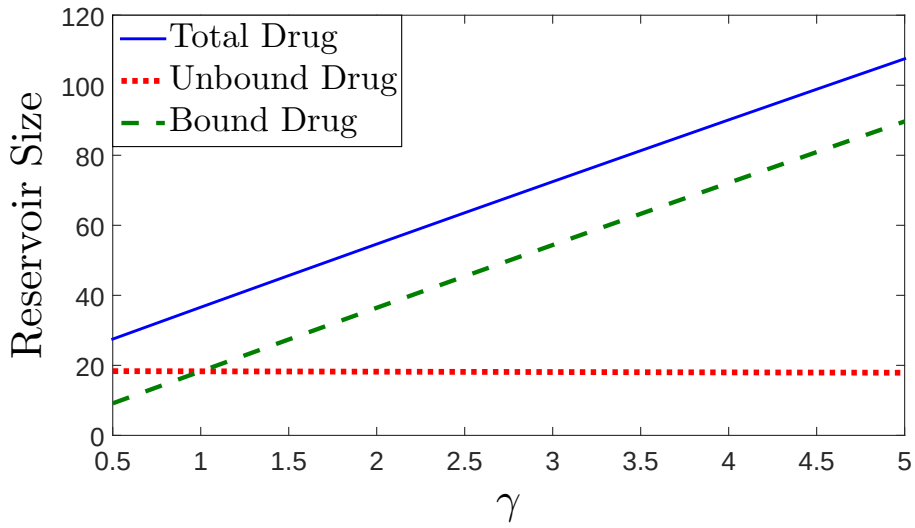

(a) $D = 0.5$, μ=1, $\alpha R_u = \alpha R_b$=1

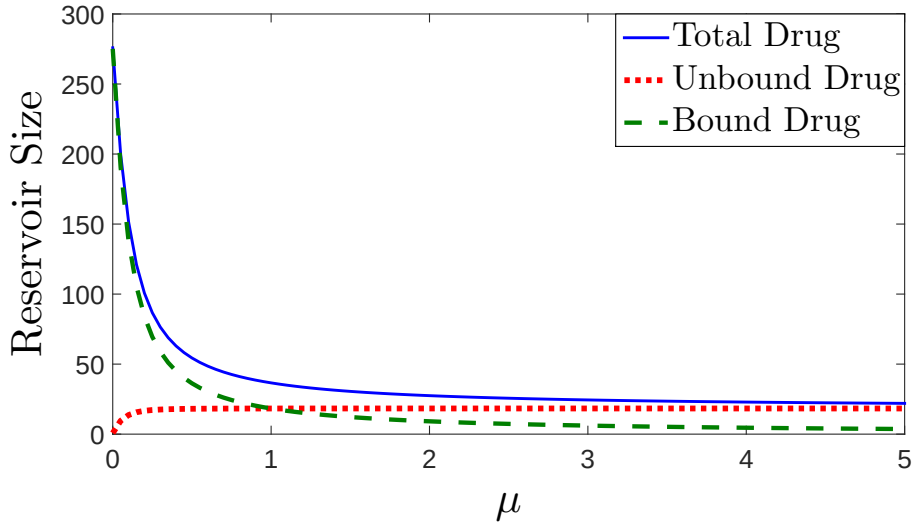

(b) $D = 0.5$, γ=1, $\alpha R_u = \alpha R_b$=1

Figure 3-7: Steady state reservoir size plotted against (a) binding rate, γ with constant $\mu = 1$ and (b) unbinding rate μ, with constant $\gamma = 1$ both graphs plotted using constant diffusion, $D = 0.5$ and constant boundary conditions at $x = 0$, $\alpha R_u = \alpha R_b = 1$. As parameter values chosen are for qualitative exploration, units of reservoir size have been omitted.

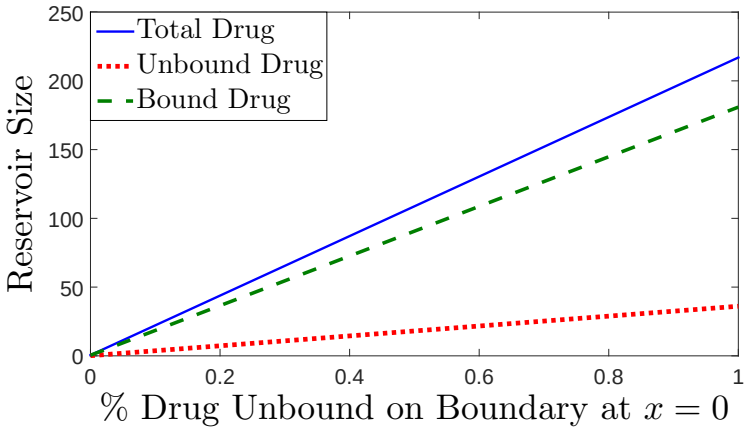

(a) $\mu = 1$, $\gamma = 5$, $D = 1$

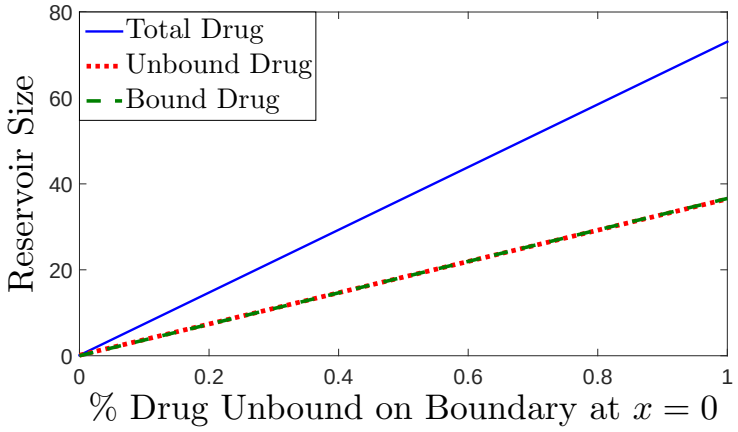

(b) $\mu = 1$, $\gamma = 1$, $D = 1$

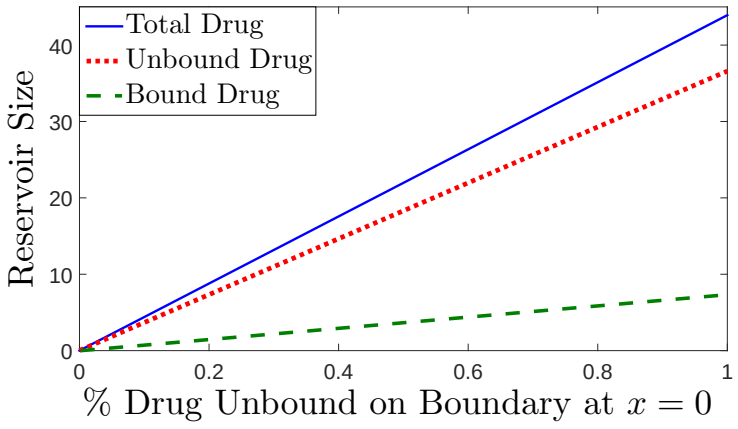

(c) $\mu = 5$, $\gamma = 1$, $D = 1$

Figure 3-8: Steady state reservoir size plotted against percentage of drug unbound on boundary $x = 0$ for constant total boundary condition $\alpha R_u + \alpha R_b$=2 for (a) $\mu > \gamma$ (b) $\mu = \gamma$ (c) $\mu < \gamma$. As parameter values chosen are for qualitative exploration, units of reservoir size have been omitted.

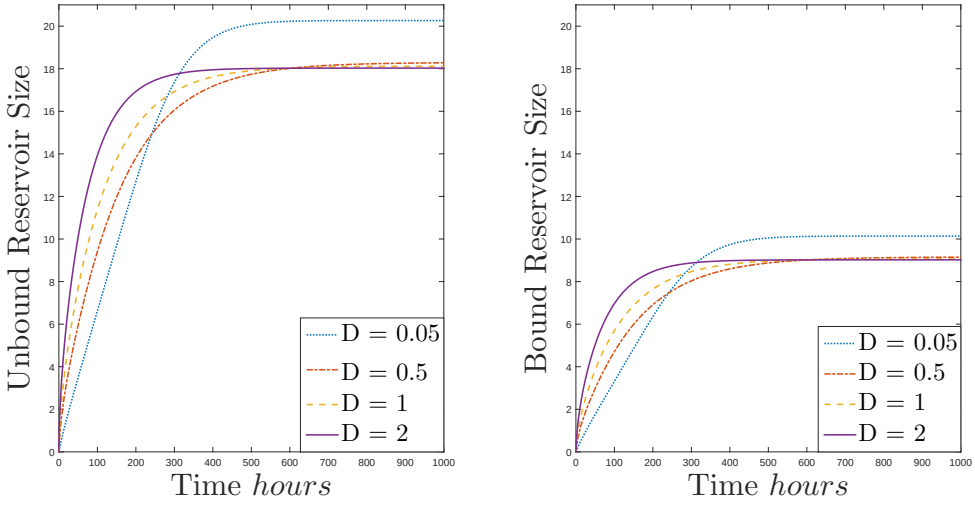

(a) $\mu = 2$, $\gamma = 1$

(b) $\mu = 2$, $\gamma = 1$

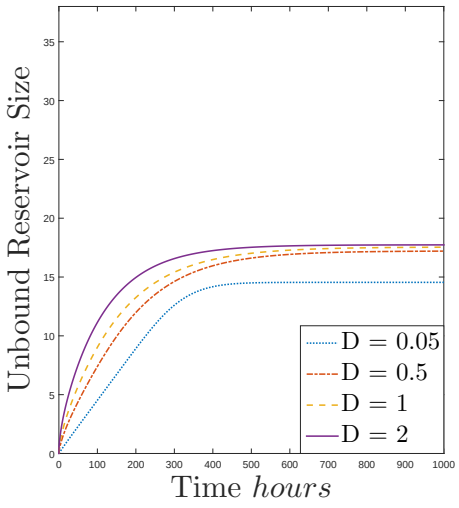

(c) $\mu = 1$, $\gamma = 2$

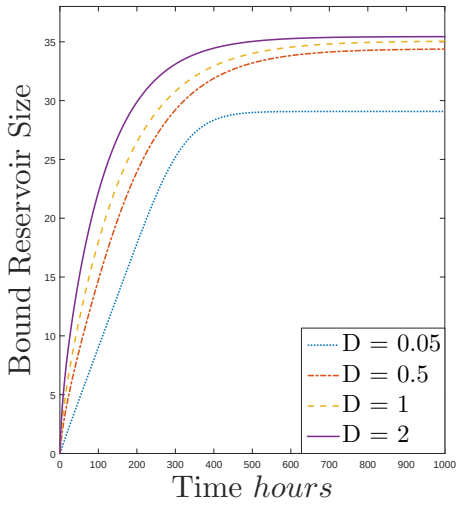

(d) $\mu = 1$, $\gamma = 2$

Figure 3-9: Reservoir size plotted against time for diffusion coefficient $D = 0.05$, 0.5, 1 and 2 with constant boundary conditions, $\alpha\bar{R}_u = \alpha\bar{R}_b = 1$ for unbinding rate μ and binding rate γ a) unbound drug with $\mu > \gamma$, b) bound drug with $\mu > \gamma$, c)unbound drug with $\mu < \gamma$, d) bound drug with $\mu < \gamma$. As parameter values chosen are for qualitative exploration, units of reservoir size have been omitted.

as the unbound drug spreads through the region, having smaller diffusion allows more drug to become bound and hence the reservoir size increases.

In the case where the rate of binding is greater than the rate of unbinding ($\gamma > \mu$), Figures 3-9(c), 3-9(d), the time taken to reach steady state increases with an increase in D. This is because in this case at steady state we expect more bound than unbound drug in the reservoir. The dominant equation in this case is therefore equation (3.1b). When D is sufficiently small, the governing equation for unbound drug (equation (3.1a)) is in agreement with the bound equation and both bound and unbound drug move through the domain with the skin (v), allowing for local binding dynamics to settle quickly and therefore reaching steady state quickly. However presence of diffusion in equation (3.1a) disrupts the system, with larger D values causing a greater perturbation and therefore taking longer to reach steady state.

In Figure 3-10(a) we show how quickly a perturbation to the drug concentrations at the boundary affects the reservoir size, depending on the diffusion coefficient. To explore this behaviour μ, γ are set to 1 so that the effect of differing binding rates does not influence our results and similarly we take $\alpha\bar{R}_u = \alpha\bar{R}_b = 1$ so that drug concentrations at the boundary $x = 0$ are equal. In this figure, at $t = 500h$ a perturbation is applied at the boundary for 24 hours, we see that for larger values of D, the effect of the perturbation is more pronounced than for small D values but that the time taken to return to a steady reservoir size is much less for large diffusion coefficients than small diffusion coefficients.

This will be of importance when considering a fluctuating boundary condition as we have in the body. A larger D would result in a shorter time to steady state (i.e. equilibrating with in body concentrations quickly) which means that the reservoir size would reflect changes in body concentration more dramatically; meaning traces of a fluctuation will also be removed more quickly. Whereas a smaller D would result in a reservoir that is less sensitive to in-body concentration fluctuations.

Note that choices of γ and μ in the above figures are arbitrary. Figures shown are representative of the cases where $\mu > \gamma$ and $\gamma > \mu$ and similar profiles were obtained for other choices of these unknown parameters.

3.7 Conclusion

Using information available in the literature, the SC was identified as the most likely location for a reservoir to form in the skin. A model to describe the formation of a reservoir in the SC was then created which includes both bound and unbound drug with linear reversible binding, diffusion of unbound drug, and cell renewal in

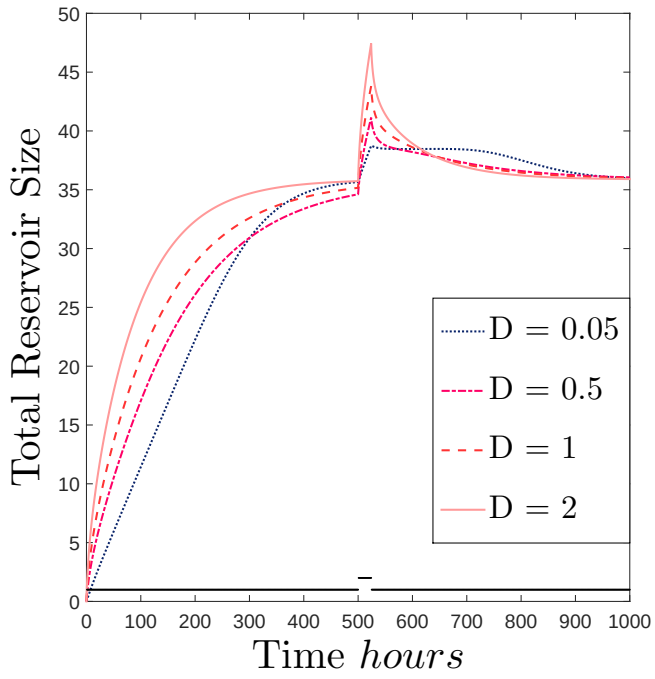

(a)

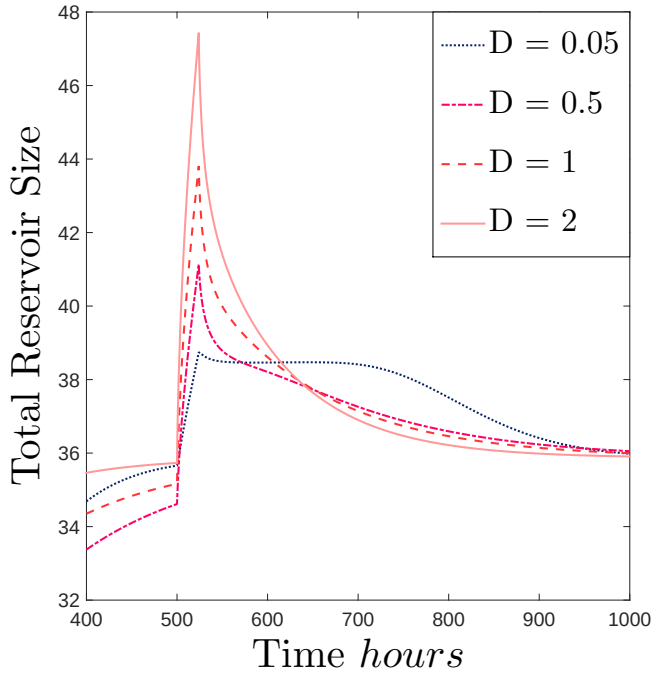

(b)

Figure 3-10: (a) Total reservoir size plotted against time for diffusion coefficient $D = 0.05$, 0.5, 1 and 2 with constant boundary conditions, $\alpha\bar{R}_u = \alpha\bar{R}_b = 1$ and equal binding and unbinding, $\mu = \gamma = 1$. with a perturbation to the boundary conditions at $t = 500h$ for 24 hours of $\alpha\bar{R}_u = \alpha\bar{R}_b = 2$. (b) Enlarged view of Figure 3-10(a). As parameter values chosen are for qualitative exploration, units of reservoir size have been omitted.

the form of a linear advection term which moves both bound and unbound drug to the skin surface. The bricks and mortar structure of the SC was also accounted for by use of an effective diffusion coefficient.

The importance of binding in transdermal delivery has been shown previously [12, 92]. Our model demonstrates that binding may also be an important factor in the formation of a reservoir from systemic presence affecting both reservoir scale and time to reach steady state.

One of the key movement mechanisms included in our model is SC turnover and desquamation. Though SC turnover isn't always considered in drug delivery models it is the only mechanism of drug movement through the SC included in the model by Paulley *et al.* [24], and as the main method of removal of drug from the SC it provides the rate limiting factor for storing of drug information in skin.

Analysis has also provided insight into the time scales associated with reservoir formation and response to in-body changes in drug concentration. Moreover, the system lends itself well to the exploration of non-invasive extraction and drug monitoring techniques across the skin as it describes both total amount in the SC and also spatial distribution of drug in the SC. The first measure is relevant to extraction techniques such as reverse iontophoresis whilst the second lends itself to the process of tape stripping. This model was created to take values from Model 1 in Chapter 2 and provide a description for resulting reservoir size. This model will be used to give IC for the extraction model developed in Chapter 4. In Chapter 5 the combination of these three models will be explored.

This work was conducted with a lipophilic drug in mind and so only the intercellular pathway was considered. In the future this model could be expanded to consider other routes through the SC. The transcellular pathway could be incorporated using a trapping and release method as used by Mollee and Bracken for an intercellular approximation [64]. This method could be adapted with the use of a partitioning term in and out of cells for the transcellular route. In the introduction to this chapter various models of skin homeostasis were discussed. It is not currently fully understood where the drug in the SC resides as techniques involve breaking down the SC structure when sampling. However if this information becomes available in the future, stochastic cell based models may provide useful insight into reservoir formation.

Chapter 4

Reverse Iontophoresis

4.1 Introduction

In this chapter we focus on the third of our three models as shown in Figure 4-1. When a drug reservoir has become established in the SC we want to detect its presence and, if possible, determine something about the magnitude of the reservoir. We consider reverse iontophoresis as a mechanism for extracting drug that has accumulated in the SC.

We begin by describing the process of (reverse) iontophoresis and the necessary mathematical background. We go on to review models of (reverse) iontophoresis in the literature and use ideas here to create a model for reservoir extraction via reverse iontophoresis. We then examine the impact of assumptions made in the modelling process.

4.2 Reverse Iontophoresis

Iontophoresis is a transdermal drug delivery technique. Two cells are placed on the skin surface, one attached to an anode, the other to a cathode, as shown in Figure 4-2. The drug for delivery is placed in the 'donor' cell which is determined by the properties of the drug being delivered. A current is passed between the two cells which causes an ion flow; positive ions move towards the cathode and away from the anode and negative ions move in the opposite direction. This encourages movement of the drug from the donor cell into the body.

Reverse iontophoresis is a relatively new technique for non-invasive drug monitoring. It works on the same principles as iontophoresis but initially there is no drug in either cell. Empty cells, or 'collection pads' attached to electrodes are placed

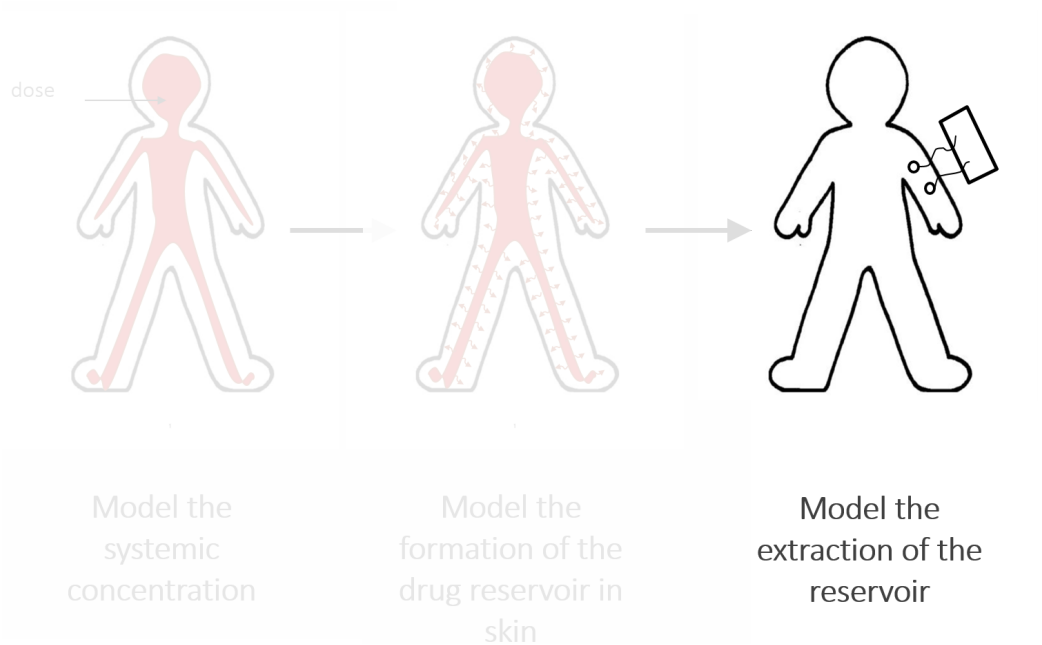

Figure 4-1: The overall aim is to create three composite models which will be linked together to create a model which predicts the expected reverse iontophoresis reading for a given drug administration regimen and therefore interpret reverse iontophoresis readings in the context of historical (order of days/weeks) drug monitoring. The third model, for the extraction of a drug reservoir in the skin, is the focus of this chapter.

on the skin surface and again a current is passed between them causing positive and negative ions to move towards the opposing electrode and accumulate on the collection pads there.

Transdermal iontophoretic drug delivery is a much more widely used and well established technique than reverse iontophoresis and as such there is much more literature on iontophoretic delivery. However, the principles and mechanisms of movement involved are similar, and so much of the literature for iontophoretic delivery is relevant for reverse iontophoretic extraction modelling.

There are some key differences between iontophoresis and reverse iontophoresis that need to be considered when creating the model. In iontophoretic drug delivery, the source of the drug being considered is the donor cell on the skin surface; in reverse iontophoresis the source of the drug comes from within the body. An in-body concentration would usually refer to systemic concentration as determined by blood plasma concentration but in our case we also consider drug initially in the SC, which is in the path between the collection pads and the plasma. In transdermal delivery studies, drug administered is therefore at comparatively large concentrations, whereas during extraction the concentration in the blood will, generally speaking, not be significantly greater than the therapeutic blood

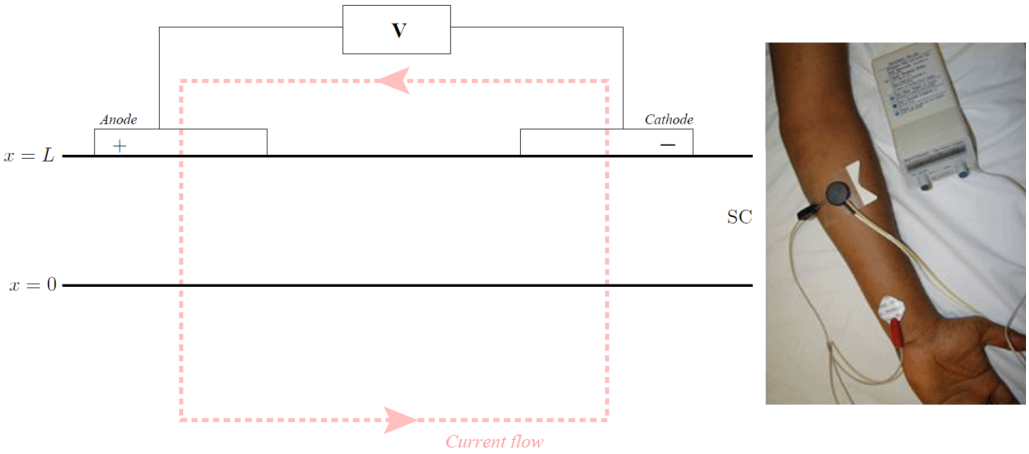

Figure 4-2: Diagram of iontophoretic set up with photo of apparatus taken from Tesselaar and Sjöberg [98].

concentration; moreover, concentrations of drug present in the stratum corneum reservoir are expected to be smaller still.

During delivery it is often assumed that the continual clearance of drug from lower (viable) skin levels by the blood provides constant sink conditions at the boundary. During extraction collection pads are replaced at regular intervals in order to maintain sink conditions at the boundary.

In both cases the movement of particles can be described by three key processes; electromigration, electroosmosis, and increased passive diffusion, as described in the following sections.

4.2.1 In vitro experimental set up

The process of (reverse) iontophoresis is mimicked in vitro by placing a sample of skin (SC or SC+VE) between two cells, one filled with a 'donor' solution and the other with a 'receptor' solution. An anode is placed in one cell and a cathode in the other (determined by the drug being delivered). The donor solution contains the drug for delivery and often also contains a buffer to maintain a constant pH. The receptor solution also contains a buffer, usually to replicate physiological pH. Depending on the experiment the receptor solution may be continually replaced to maintain sink conditions.

Plasma has a lower resistivity than lower layers of the epidermis and so we expect the lateral current flow in Figure 4-2 to be through the plasma (see Figure 4-3). As the comparative resistivity of the SC is so high, no lateral movement of current is expected in this layer. For this reason, as we are usually only interested in movement of drug in one direction, the in vivo set up (electrodes on the same side

of the skin) can be approximated by the in vitro set up (electrodes on opposite sides of the skin).

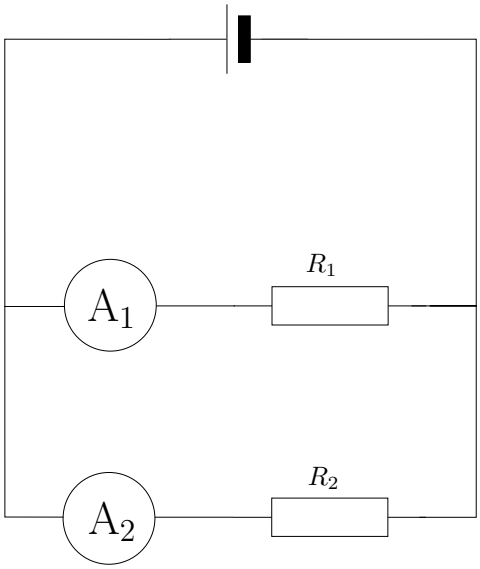

Figure 4-3: Simple circuit diagram of 2 resistors in parallel to explain why we expect no lateral movement through the SC. Provided the separation between the collection pads is sufficiently large, the resistance of the path through the SC (represented by R_1 here) is much greater than the resistance of the path through the plasma (R_2) and we expect the current reading at $A_2 \gg A_1$ i.e the current travels almost completely through the plasma. It is for this reason we don't consider lateral movement through the SC and only consider movement through the plasma (and not lower levels of the epidermis).

4.2.2 Pathways

The exact pathway of permeants through the SC during iontophoresis is not known for sure. It is currently thought that the most likely route through the SC during iontophoresis is via the appendages (shunt route). Appendages in humans include hair follicles, sweat ducts and sebaceous glands. It is thought that during iontophoresis these aqueous routes are dominant as they offer a low resistance pathway [99]. However the appendages listed do not account for the number of pathways observed [100]. A porous skin model has been suggested which includes these appendages with other pores made up of localised skin imperfections where porous pathways 'open up' on the application of an electric field [100]. Evidence presented by Bath *et al.* [101] suggests that bulk flow, as described by electroosmosis, is exclusively through aqueous pores.

The intercellular route is the tortuous route via the lipid domain, suggested as the route of passive diffusion of lipophilic substances. As electrical current takes the path of least resistance, movement due to electrostatic repulsion (electromigration)

and bulk fluid flow (electroosmosis) is unlikely to be through the lipid domain as lipids are poor conductors. It has, however, been hypothesised that due to an increase in temperature caused by the current flow, fluidity of lipid bilayers is increased leading to enhanced passive diffusion in this domain during iontophoresis.

Hydration of the skin can cause pores to swell and close, suggesting hydration of the SC may significantly impact movement via this route. It has been shown that iontophoresis can directly affect the hydration levels, particularly in in vitro experiments where skin samples have been (partially) dehydrated or frozen prior to use.

4.2.3 Electromigration

Electromigration describes the movement due to direct electrostatic repulsion of ions from an electrode of the same charge. This transport is only relevant for ionic (charged) particles and is more prominent for small, mobile (unbound) ions [19]. Electromigration has been identified as the key movement mechanism for charged species [101].

Electrical current is defined as the flow of charged particles through a conducting material. It therefore follows that the flux of any given ion is proportional to the current, as given by

$$\mathbf{J_i} = \frac{-\mathbf{I}t_i}{Fz_i}, \tag{4.1}$$

where F is Faraday's constant, $\mathbf{I}$ is the current, z_i is the valency of ion i, and t_i is the transport number. The transport number of a given ion is the proportion of total charge carried by that ion, $\mathbf{I}_i = t_i\mathbf{I}$ and is given by

$$t_i = \frac{C_i z_i \mu_i}{\sum_j C_j |z_j| \mu_j}, \tag{4.2}$$

with μ_i, the ion mobility and C_i the concentration of the ion. The transport number of an ion is dependent on all ions present.

Faraday's law of electrolysis, equation (4.1), has been used to describe electromigratory flux in transdermal iontophoresis in a number of publications [19, 102, 103]. More commonly, however, electromigratory flux of an ion, i, is described using the Nernst-Planck (N-P) equation

$$\mathbf{J}_i = -D_i \frac{dC_i}{dx} + \frac{D_i z_i e \mathbf{E} C_i}{kT}, \tag{4.3}$$

where D_i is the diffusion coefficient of the ion, z_i is the valency of the ion, C_i is the concentration of ions, kT is the thermal energy of the system, e is the charge of

an electron and **E** is the magnitude of the electric field. The first term in equation (4.3) relates to passive diffusion, and the second term to electromigration.

Equivalence between the electromigratory term in the Nernst-Planck equation (4.3) and Faraday's law (4.1) is shown below.

First we consider an ion, i, in a viscous fluid (the SC) with imposed electric field **E**. The force on the particle due to the field is given by

$$\mathbf{F}_i = z_i e \mathbf{E}, \tag{4.4}$$

where $z_i e$ gives the charge on the particle. This force is balanced by the drag on the particle given by Stokes' law for drag on a small spherical object in a viscous fluid. This can be derived by solving Stokes' flow limit for small Reynolds number in the Navier-Stokes equations, which gives

$$\mathbf{F}_i = 6\pi\eta r_i \mathbf{v}_i \tag{4.5}$$

where η is the viscosity of the SC, r_i is the radius of the particle and $\mathbf{v}_i$ is the flow velocity relative to the object (drift velocity). Equating (4.4) and (4.5) and rearranging, we can find the drift velocity,

$$\mathbf{v}_i = \frac{z_i e \mathbf{E}}{6\pi\eta r_i}. \tag{4.6}$$

Drift velocity for an ion in electric field **E** is also given by Ohm's law as

$$\mathbf{v}_i = \mu_i \mathbf{E}. \tag{4.7}$$

The electrical mobility for a spherical ion in a viscous fluid, μ, is therefore given by

$$\mu_i = \frac{z_i e}{6\pi\eta r_i}. \tag{4.8}$$

Comparing this with the Stokes-Einstein-Sutherland equation,

$$D_i = \frac{kT}{6\pi\eta r_i}, \tag{4.9}$$

which is the diffusion coefficient for a sphere in a low-Reynold's-number viscous fluid, we have

$$\mu_i = \frac{D_i z_i e}{kT}. \tag{4.10}$$

Now, if we consider the electromigratory component of flux as given in the Nernst-Planck equation (4.3) as

$$\mathbf{J_i} = \frac{D_i z_i e \mathbf{E} C_i}{kT}, \tag{4.11}$$

using equation (4.10) we can rewrite equation (4.11) to give

$$\mathbf{J_i} = \mu_i \mathbf{E} C_i. \tag{4.12}$$

Again, using Ohm's law (as reformulated by Kirchhoff),

$$\mathbf{I_i} = \sigma_i \mathbf{E} \tag{4.13}$$

where σ_i, the conductivity, is given by $\sigma_i = |z_i| F C_i \mu_i$, we have

$$\mathbf{J_i} = \frac{\mu_i C_i I_i}{|z_i| F C_i \mu_i}. \tag{4.14}$$

Finally, using the definition of transport number in equation (4.2), equation (4.14) becomes

$$\mathbf{J_i} = \frac{t_i I}{z_i F}, \tag{4.15}$$

as required.

The approach of Nernst Planck usually coincides with a fixed electric field, which means that, as the resistivity of the SC changes during iontophoresis the flux of ions will change too. A fixed current however, corresponds to a fixed flux of ions, with the relative flux of each ion determined by properties of all of the ions present. Moreover, as the (change in) resistance of the SC is subject to significant inter and intra patient variability a fixed current may significantly reduce this variability [102, 104, 105, 106].

It is for this reason that many studies choose a fixed current over a fixed electric field in experimental work.

As stated previously, the concentration of drug considered in transdermal delivery is orders of magnitude greater than the concentrations of drug expected in an extraction scenario. Therefore competition for charge with other ions present is usually ignored in delivery studies. In transdermal extraction more than one ion is present in the SC and we expect that the ion of interest will not be the most abundant; effects of ion competition may therefore become more significant. We therefore choose to maintain a constant current and include ion competition through the use of Faraday's law to model electromigratory flux.

4.2.4 Electroosmosis

Uncharged species have no direct interaction with an applied electric field. However, it has been shown that iontophoresis enhances the delivery of neutral species [105, 106, 107]. The cause of this increased transport is thought to be

electroosmosis [108]. Electroosmosis has been identified as the key movement mechanism for iontophoretic delivery of neutral substances [101] and large cations (>1000 Dalton)[109].

Electroosmotic flow is bulk solvent flow under an electric field. It occurs in membranes with a net charge, and the direction of flow is always in the direction of counter ion flow [110, 111, 112]. Electroosmotic flow can therefore be with or against the current flow. As skin is negatively charged above pH 4, flow is from anode to cathode [108]. Electroosmosis in the skin therefore reinforces movement due to electromigration for cations whilst acting against electromigration of anions.

As mentioned previously, electrical current takes the path of least resistance and so it is generally accepted that electroosmosis will occur solely in the aqueous domain [101, 113, 114]. Assuming a porous skin model, we therefore consider electroosmosis occurring exclusively in pores or channels.

For uncharged particles and particles with Stoke's radius $> 1nm$ this is the dominant flow mechanism. Moreover, both theory and experimental data indicate that electroosmotic flow increases in importance as the size of the ion increases [108]. This is because, although electroosmosis itself is independent of molecular size [113, 110, 115] (provided it doesn't approach the size of the pathway [111, 116]), as size increases, relative contributions of passive and electromigratory flux decrease [109].

When temperature, pressure, and fluid composition on both sides of the membrane are equal, electroosmotic volume flow is directly proportional to the potential gradient [117]. Flux due to electroosmosis can therefore be written

$$J_v = L_{VE}\left(\frac{-d\phi}{dx}\right) \tag{4.16}$$

where J_v is the volume flow, L_{VE} is the electroosmotic flow coefficient, and $\frac{-d\phi}{dx}$ is the potential gradient.

The flux due to electroosmosis, J_v, can be described in terms of the velocity of the flow, v_f, as

$$J_v = v_f A \tag{4.17}$$

where A is the area considered for the flux, and v_f for zero pressure gradient is given by Brett & Brett [118, pp.67] to be

$$v_f = \frac{\epsilon\zeta E}{\eta}, \tag{4.18}$$

where ϵ is the permittivity, η is the absolute viscosity and ζ is the zeta potential. As we have chosen to consider a constant current approach we can rewrite this as

$$v_f = \frac{\epsilon \zeta I \rho}{\eta A}, \tag{4.19}$$

where ρ is the resistivity.

However, as the values for concentration, mobility etc. are for within the SC, estimation is difficult and values are subject to significant inter-patient and intra-patient variability. We therefore follow the lead of many transdermal delivery models [101, 119, 120] and use the simplification

$$J_i = J_v C_i, \tag{4.20}$$

where

$$J_v = v_{eo} I$$

and we take v_{eo} to be a constant value over the area of interest (beneath the collection pad). Experimental work by Pikal and Shah [121] gives

$$v_{eo} = (6 - 19)\mu l h^{-1} m A^{-1}. \tag{4.21}$$

4.2.5 Enhanced Passive Diffusion

It has been shown in many studies that, provided the safe limit of $0.5 m A cm^{-2}$ [122, 123] is not exceeded, there is no long lasting damage to the skin i.e. passive permeability coefficients post-iontophoresis return to their original values [120, 124]. However there is some evidence to suggest that during iontophoresis there is a drop in resistivity of the SC which also causes the passive flow of ions and neutral species to increase during this time [121, 122, 123, 125].

It is thought that the cause of this reduction in resistivity may be the 'opening of porous pathways' [99]. Resistance is given by

$$\rho_i = \frac{1}{\sigma_i} = \frac{1}{|z_i| F C_i \mu_i}. \tag{4.22}$$

A decrease in resistance relates to increased mobility of ions, μ_i. On inspection of the diffusion coefficient, $D_i = \dfrac{kT\mu_i}{z_i e}$, we see that an increase in mobility μ_i, would also increase the diffusion coefficient, therefore increasing the contribution of passive diffusion. However, the impact of an increase in passive diffusion is not expected to be large as the contribution of passive diffusion compared to

electromigration (EM) and electroosmosis (EO) is still small. The effect becomes more noticeable when the reverse iontophoresis is stopped and passive diffusion is still temporarily increased. This concept is explored by Nugroho *et al.* [126, 127], described in detail in the literature review Section 4.3.

4.2.6 Skin pH and Ionisation

The ionisation of a substance depends on the pH of the environment that it is in. The pH of the stratum corneum varies depending on the depth within the SC, with the surface pH estimated to be 4.5 for men (and 5.3 in women) increasing to a pH of 6.8 (6.9) in the stratum granulosum at the base of the SC [128]. pH variation in the SC is dependent on a number of factors such as race [129, 130], age [131, 132], gender [128, 131] and even time of day [133].

As only ionised drug will move via electromigration [19] it is important to have an idea of the proportion of drug that is ionised in the skin. Again we use buprenorphine as the exemplar drug by which we make modelling decisions. The pH at which the substance is exactly half dissociated (ionised) is known as the pKa and for buprenorphine $pKa = 8.31$. Buprenorphine is a base, meaning that we expect buprenorphine ions to have a positive charge; a buprenorphine ion has valency +1. To determine the proportion ionised in the skin we use the Henderson Hasselbalch equation for bases,

$$pH = pKa + \log_{10}\left(\frac{[B]}{[BH^+]}\right), \tag{4.23}$$

where $[B]$ denotes concentration of neutral substance and $[BH^+]$ denotes concentration of (positive) ions. For simplicity we consider skin to have pH within the range pH4-6 [132], using this with the pKa for buprenorphine in (4.23) we expect buprenorphine to be 99.9%-99.5% ionised in the SC. Therefore for the possible range of pH values in the SC, bup is essentially completely ionised. Moreover, considering physiological pH 7.3, we would expect bup to be 91.1% ionised in the plasma and so we expect that change in pH and therefore change in ionisation will not have a significant impact on the predicted or observed transport.

For drugs with a lower pKa, especially drugs with pKa close to skin pH, changing ionisation may be an important factor for extraction.

4.3 Literature Review

There is very little in the literature specific to reverse iontophoresis and even less in the way of mathematical models. In fact the only mathematical model

of reverse iontophoresis known is the 2010 paper by Paulley *et al.* [24]. In this paper the authors consider a chronic administration of lithium where the drug has built up to form a reservoir in the SC over time. It is assumed iontophoretic extraction of lithium, a small positively charged ion, is by electromigration only. It is modelled using a system of ODEs with movement via electromigration based on Faraday's law of electrolysis, using transport numbers as described in Section 4.2.3. A constant current is assumed. Lithium is extracted via reverse iontophoresis from well mixed SC and mixed plasma compartment through independent routes. The results show an initially high extraction which levels off as the reservoir is emptied, with subsequent extraction from plasma only, which is in agreement with available data. However, during reverse iontophoresis for a drug-naive patient, a lag time (lower initial extraction) is expected due to the time taken to cross the skin. In this paper the extraction from plasma is independent of extraction from the SC and is modelled using non-spatial compartments. Therefore the expected lag time is not replicated by this model (not shown in paper). This lag time from plasma would still be present in a chronically dosed patient but the initial low reading is masked by the high reading for the reservoir extraction. This means that, for a given reservoir size, initial readings would be over predicted by this model, potentially causing reservoir sizes to be underestimated. The results in this paper, however, show good qualitative agreement with data for chronically dosed patients and the model provides a starting point for modelling of reservoir extraction via reverse iontophoresis.

The most simple models for iontophoretic delivery describe the in vitro experimental set up with a homogeneous membrane and usually focus on one, two or all three of the transport mechanisms (electromigration, electroosmosis and diffusion) as determined by the drug of interest. Some papers have attempted to make models more realistic by addressing the membrane structure, pathway of the drug or by including more drug specific characteristics.

Keister and Kasting consider iontophoretic delivery under a uniform electric field [125]. They consider movement of an ionised drug across an uncharged homogeneous membrane (i.e. no electroosmosis) with infinite sink conditions on the acceptor side of the membrane. They therefore model the movement through the membrane using the Nernst-Planck equation (electromigration and diffusion) as described in Section 4.2.3. They quantify the effects of iontophoresis by an 'enhancement ratio' i.e. ratio of steady state flux under applied voltage to steady state passive flux, and ratio of iontophoretic lag time to passive lag time. They conclude that the application of an electric field leads to an enhancement in drug delivery proportional to the magnitude of the electric field applied.

Bath *et al.* consider constant current iontophoresis of an anion, cation and neutral molecule through hair follicles in hairless mouse skin, to determine the relative

contribution of electromigration, electroosmosis and diffusion in each case [101]. Their work is mainly empirical. In their model, movement via electromigration is expressed using the Nernst-Planck equation, with electroosmosis described by a simple linear convection term. In this paper they consider the impact of changes in skin pH on the electroosmosis term. To avoid dealing with a change in diffusion due to a change in resistance of the skin, the work considers steady state transport. In order to do this experimentally, a constant current is applied across the skin sample until a steady state skin resistance is reached before taking any measurements. Their findings show electroosmotic flow velocity is independent of the charge of the permeant, which is supported by findings of Guy *et al.* [109]. They also find that electroosmotic flow velocity is directly proportional to the applied current. They conclude that a significant fraction of iontophoretic transport for all permeants occurs through hair follicles.

Roberts *et al.* consider iontophoretic delivery of partially ionised drugs of a range of radii through a porous model of the SC [116]. Movement mechanisms through aqueous pores considered are electromigration, electroosmosis and diffusion. Simultaneous passive diffusion via lipids is also considered with the pathways independent of each other. Pores only occupy a certain area fraction of the SC and it is predicted that solutes with radius approaching the size of pore radius may be more impeded than small molecules. Two separate approaches are considered to model the porous structure of the SC, based on the papers by Yoshida and Roberts [134, 135]; a free volume model in which there is limited space where molecules can enter to transport through pores; and a pore restriction model where there is steric hindrance on entry into the pore and movement within the pore due to friction with the pore wall. Both forms of the model were found to be consistent with experimental data, with the pore-restriction model outperforming the free volume model for prediction of solute size effects on iontophoresis.

Imanidis and Luetolf [120] make the distinction between aqueous and lipid domains in the SC for delivery of a weak electrolyte by iontophoresis under a constant electric field. It is known that as current will take the path of least resistance, it will travel predominantly through the aqueous domain of the SC, meaning drug permeating the lipoidal route will not be directly affected by current. In this paper the authors consider diffusion, electroosmosis and electromigration in the aqueous route and diffusion only through the lipid route. The Nernst-Planck equation is used to describe movement in the aqueous domain with an additional constant flux term included for electroosmosis. Drug is allowed to pass between the lipid and aqueous domains dependent on partition coefficients and pH (which affects ionisation). They found that diffusion via the lipid domain provided a non-negligible contribution to overall delivery and demonstrate consistency with experimental work. The results highlight the importance of pH and ionisation in

partitioning and iontophoretic delivery of weak electrolytes.

Nugroho *et al.* consider an in vitro iontophoretic delivery set up, with skin clamped between two cells [126]. In this paper electromigration and electroosmosis are grouped together and referred to as an iontophoretic driving force (IDF). They claim that although enhanced passive diffusion may not provide significant contribution during iontophoresis, when iontophoresis has been stopped and there is no IDF, enhanced passive diffusion becomes significant. This hypothesis is explored by modelling the in vitro set up using two well mixed homogeneous compartments, one representing the skin the other representing the acceptor solution. The donor solution is not modelled, as it is assumed the concentration here is constant. They consider two separate scenarios. In the first, movement into the skin compartment is described by a zero-order influx rate constant from the donor compartment driven by the IDF. Drug is then removed from the skin, with a first order rate constant to the acceptor compartment described as a 'skin release rate constant'; in the second scenario they consider a similar two compartment set up but alter the removal term from the skin to acceptor compartment, so that it includes IDF (this remains a first order rate constant). The authors go on to consider the post iontophoresis period in both cases. They find that both models could be fitted to data for the iontophoresis and post-iontophoresis period and that incorporation of the IDF in the 'removal from skin' term, in the second model, didn't improve the model fit. The authors claim that this suggests a negligible iontophoretic driving force contribution in the mass transfer from skin to acceptor compartment. However, it could be argued that, as the two models are mathematically equivalent (apart from a step change in the parameter value in question when the machine is turned off) that, although they have found parameters that fit and provide good agreement with data, that clearance from skin to acceptor compartment during iontophoresis may still be dependent on the electromigration and electroosmosis. This could be tested by repeating the experiment at different currents which, if their claim is correct, would see the clearance rate from skin to acceptor compartment unchanged. They conclude that drug delivery post iontophoresis into an acceptor compartment in vitro is well described by a first order clearance term from the skin compartment.

Note that for the purpose of reverse iontophoresis (extraction) that enhanced passive diffusion post iontophoresis will not have an effect as we assume that when iontophoresis has stopped the pad is also removed.

Much of what is known about iontophoresis has been determined from in vitro studies in which a skin (SC) sample is clamped between two cells filled with buffer solution used to replicate the pH of the body and donor solution. In vivo however, electrodes are placed next to each other, not on either side of the membrane. Lai *et al.* explore the in vivo set up using a mathematical model and consider both

vertical and lateral transport [113]. In this paper, skin is modelled as a set of well stirred compartments, where movement out of each compartment is described by a 'clearance' term based on the Nernst-Planck equation. The model considers the set up at "moderate time" i.e. after a pseudo steady state is reached. Their results predict that lateral transport in the SC during iontophoresis is minimal. This is supported by experimental work in the same paper which uses iontophoresis on rats with cells spaced at 2 and 7cm. It is found that the concentration of a given substance decreases exponentially with distance from an electrode.

4.4 Model Formation

We consider two electrodes connected to 'collection pads' on the skin surface, with a fixed current passed between them, and create a model to describe the movement of a positively charged molecule from the SC and plasma towards the cathodal collection pad, see Figure 4-4. We assume that the separation between pads is sufficiently large such that current doesn't directly travel between the two via the SC. We therefore consider movement in the vertical direction only.

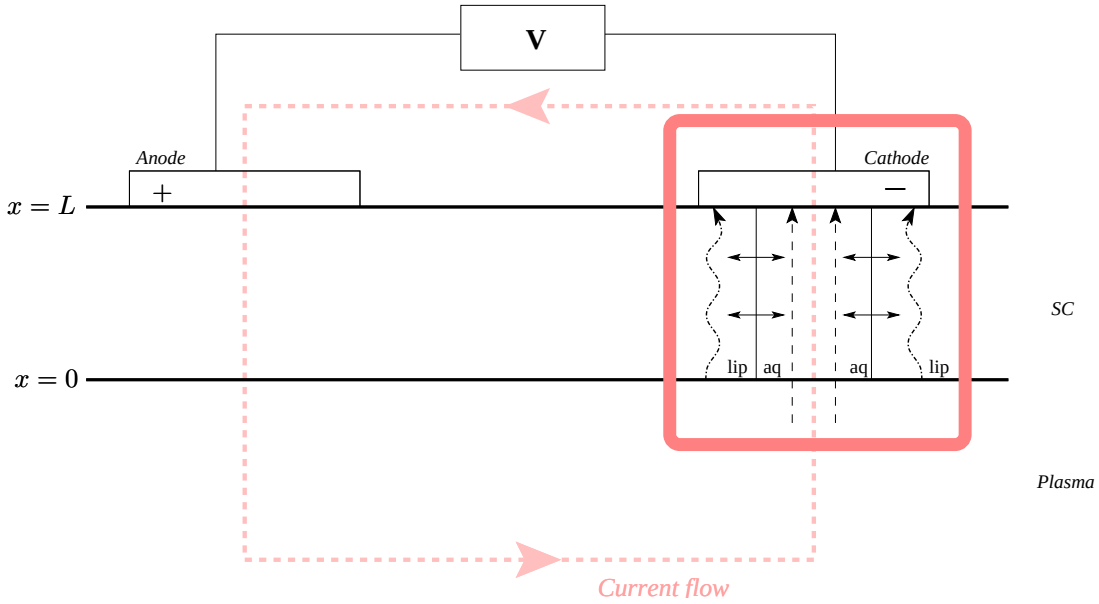

Figure 4-4: Schematic for reverse iontophoresis showing the movement of drug from and through the aqueous domain of the SC (dashed arrows) and from the lipid domain (wavy dotted arrows). The bold box highlights the area of interest which is modelled in Subsection 4.4.

It has been shown that on application of an electric field, aqueous pathways 'open up' in the SC and these are the main route of current through the SC. We therefore consider the SC constituent 'aqueous' and 'lipid' domains. In the aqueous domain we expect ionised drug to move via electromigration, electroosmosis and

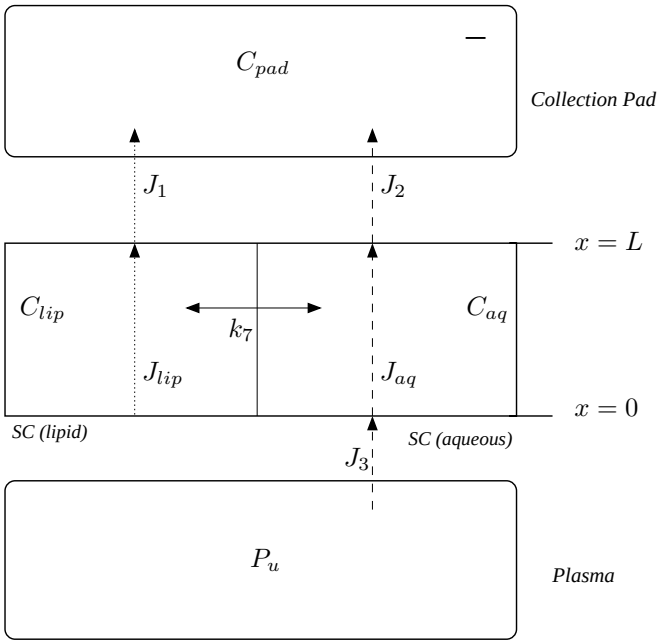

Figure 4-5: Simplified schematic for reverse iontophoresis model set up. The top compartment represents the collection pad, the middle compartment, $x = 0$ to $x = L$, represents the SC which is separated into lipid and aqueous domain with k_7 representing the reversible movement between lipid and aqueous domains, and the bottom compartment represents the plasma from model 1 (Chapter 2). Full details of the model are provided in Section 4.4 - 4.6

diffusion. As current takes the path of least resistance (aqueous domain) we don't expect the movement of solute in the lipid domain to be directly affected by the current. However, as discussed in Section 4.2.5, there may be some increase in passive diffusion during iontophoresis. Therefore, the only movement mechanism in the lipid domain is passive diffusion. Any enhancement in passive diffusion is accounted for by an increase in the diffusion coefficient. Movement between the two domains is accounted for via a partitioning term, represented by horizontal, reversible arrows in Figure 4-4.

The experimental set up in Figure 4-4 is simplified in Figure 4-5 to show the model layout. Here, plasma is taken as a single homogeneous compartment which provides boundary conditions at $x = 0$ for the spatial SC compartment. As only a small amount of drug is extracted during reverse iontophoresis we assume drug in the plasma is not depleted by the process. We also initially assume that the drug concentration of plasma does not change significantly during the time period of reverse iontophoresis. We therefore take the plasma concentration to be constant.

Electromigration is modelled using Faraday's law of electrolysis as detailed in Section 4.2.3. We therefore also consider the movement of sodium, chloride and potassium ions as these are the most abundant in the SC and are likely to be the

main charge carriers [24]. Though other ions are present, these are at a much lower concentration so we consider competition with them to be negligible. We assume that due to their abundance and the comparatively small amount collected by reverse iontophoresis there is no notable depletion of sodium, chloride and potassium ions during the sample period due to reverse iontophoresis.

As electroosmosis is independent of the molecule being transported, it is taken to be a constant experimentally determined flow rate, proportional to the current.

Let $C_{id}(x,t)$ denote the concentration of ion i in domain d at time t, at position x in the SC, where $x = 0$ is the base of the SC and $x = L$ is the SC-collection pad interface.

Flux of drug in the aqueous domain (pores) of the SC is therefore given by the sum of flux due to enhanced passive diffusion, electromigration and electroosmosis,

$$J_{iaq} = -D_{iaq}\frac{\partial C_{iaq}}{\partial x} + \frac{It_i}{Fz_i} + v_{eo}C_{iaq}I, \tag{4.24}$$

where J_{iaq} denotes the flux ($mols^{-1}$) of ion i in the aqueous domain of the SC, D_{iaq} is the diffusion coefficient of ion i in the aqueous domain, I is the current intensity, t_i is the transport number of ion i, F is Faraday's constant, z_i is the valency and v_{eo} is the volume flow due to electroosmosis. By conservation,

$$\frac{\partial C_{iaq}}{\partial t} = -\frac{\partial J_{iaq}}{\partial x}. \tag{4.25}$$

Taking D_{iaq} and v_{eo} constant, we have

$$\frac{\partial C_{iaq}}{\partial t} = D_{iaq}\frac{\partial^2 C_{iaq}}{\partial x^2} - \frac{I}{Fz_i}\frac{\partial}{\partial x}\left(\frac{C_{iaq}z_i\mu_{iaq}}{\sum_j C_{jaq}|z_j|\mu_{jaq}}\right) - v_{eo}I\frac{\partial C_{iaq}}{\partial x}. \tag{4.26}$$

As we assume the change of concentration of Na^+, Cl^-, K^+ over the period of reverse iontophoresis is negligible and that the concentration of the drug of interest is small compared to the concentration of Na^+, Cl^-, K^+, we assume that it's contribution to the sum is small and so we can write,

$$\frac{\partial C_{iaq}}{\partial t} = D_{iaq}\frac{\partial^2 C_{iaq}}{\partial x^2} - \frac{I}{Fz_i}\frac{z_i\mu_{iaq}}{\sum_j C_{jaq}|z_j|\mu_{jaq}}\frac{\partial C_{iaq}}{\partial x} - v_{eo}I\frac{\partial C_{iaq}}{\partial x}. \tag{4.27}$$

The movement in the lipid domain of SC can be written

$$\frac{\partial C_{ilip}}{\partial t} = D_{ilip}\frac{\partial^2 C_{ilip}}{\partial x^2} \tag{4.28}$$

where D_{lip} is the diffusion coefficient in the lipid. As we are considering the concentration of only one drug, we drop the 'i' and write $C_{iaq} = C_{aq}$, $C_{ilip} = C_{lip}$with $z_i = z, \mu_{iaq} = \mu_{aq}, D_{iaq} = D_{aq}, D_{ilip} = D_{lip}$. Incorporating movement between lipid and aqueous domains we have the spatial model system in the SC compartment given as

$$\frac{\partial C_{aq}}{\partial t} = D_{aq}\frac{\partial^2 C_{aq}}{\partial x^2} - \frac{I}{Fz}\frac{z\mu_{aq}}{\sum_j C_{jaq}|z_j|\mu_{jaq}}\frac{\partial C_{aq}}{\partial x} - v_{eo}I\frac{\partial C_{aq}}{\partial x} - f(C_{aq}, C_{lip}), \tag{4.29a}$$

$$\frac{\partial C_{lip}}{\partial t} = D_{lip}\frac{\partial^2 C_{lip}}{\partial x^2} + f(C_{aq}, C_{lip}). \tag{4.29b}$$

where

$$f(C_{aq}, C_{lip}) = k_7(C_{aq} - f_{aq}(C_{lip} + C_{aq}))$$

with f_{aq} the fraction of drug in the aqueous domain at equilibrium and k_7 the rate at which drug moves between the lipid and aqueous domains.

The drug collected on the pad at $x = L$ is then given by

$$\frac{dC_{pad}}{dt} = \int_0^t J_{lip}|_{x=L} + J_{aq}|_{x=L}\, dt$$

where $J_{lip}|_{x=L}$ and $J_{aq}|_{x=L}$ are the flux of ions at $x = L$ in the lipid and aqueous domains respectively.

4.5 Boundary Conditions

At $x = 0$ (base of the SC) the only movement into the SC is the drug being pulled through from the plasma due to iontophoresis (electromigration, electroosmosis and enhanced passive diffusion) and only unbound drug is extracted via reverse iontophoresis. Drug entering the SC due to desquamation (as in Model 2, Chapter 3) happens on a much longer time scale than iontophoresis and contribution from this is therefore negligible. We therefore have the the boundary condition in the aqueous domain at $x = 0$ given by

$$C_{aq}(x = 0, t) = \beta P_u \tag{4.30}$$

where β is the partitioning coefficient and P_u is the concentration of unbound drug in the plasma.

The boundary condition in the lipid domain at $x = 0$ is given by

$$\left.\frac{\partial C_{lip}}{\partial x}\right|_{x=0} = 0. \tag{4.31}$$

At $x = L$, as the collection pad has a comparatively large volume to the SC and we assume it is replaced regularly during the iontophoretic extraction, we impose infinite sink conditions at the boundary $x = L$ for both the lipid and aqueous domains and we therefore have

$$C_{iaq}(x = L^+, t) = 0, \tag{4.32}$$

$$C_{ilip}(x = L^+, t) = 0. \tag{4.33}$$

4.6 Initial Conditions

Only unbound drug is available to be extracted via reverse iontophoresis [25]. Initial conditions consist of a spatial reservoir profile. In the full model system (explored in Chapter 5) initial conditions are given by the unbound reservoir size at the time of extraction (end time of reservoir formation= t_0) distributed between the lipid and aqueous domain as according to the prescribed value of f_{aq}. For the purpose of exploration in this chapter, we consider a uniform distribution of drug in the reservoir prior to extraction given by

$$C(x = [0, L], t = t_0) = C_0,$$

distributed between the lipid and aqueous domains depending on the value of f_{aq} such that

$$C_{iq}(x = [0, L], t = t_0) = f_{aq}C_0, \tag{4.34}$$

$$C_{lip}(x = [0, L], t = t_0) = (1 - f_{aq})C_0. \tag{4.35}$$

4.7 Numerical Scheme for Model 3

We seek to solve the system of equations (4.29) with boundary conditions (4.30)-(4.33) and initial conditions (4.34), (4.35) numerically.

We first consider the simplified system where $f(C_{aq}, C_{lip}) = 0$ so there is no exchange between lipid and aqueous domains during reverse iontophoresis,

$$\frac{\partial C_{aq}}{\partial t} = D_{aq}\frac{\partial^2 C_{aq}}{\partial x^2} - v\frac{\partial C_{aq}}{\partial x}, \tag{4.36a}$$

$$\frac{\partial C_{lip}}{\partial t} = D_{lip}\frac{\partial^2 C_{lip}}{\partial x^2} \tag{4.36b}$$

with v a constant given by

$$v = \left(\frac{1}{Fz}\frac{z\mu_{aq}}{\sum_j C_{jaq}|z_j|\mu_{jaq}} + v_{eo}\right) I.$$

We start by discretising the domain $x \in [0, L]$ using a uniform mesh on N points with mesh width $\Delta x = L/N$.

Define $C := C_{aq}$,$U := C_{lip}$, we can then approximate (4.36a) using

$$(C_i)_t = D_{aq}\delta^2 C_i - v\delta_- C_i,$$

where $(C_i)_t$ denotes the time derivative of C (C_{aq}) at spatial point $x_i := i\Delta x$, δ^2 denotes the standard finite difference approximation for the second derivate given by

$$\delta^2 C_i = \frac{C_{i+1} - 2C_i + C_{i-1}}{\Delta x^2},$$

and δ_- is the estimate for the first spatial derivative under an up-winding scheme given by

$$\delta_- C_i = \frac{C_i - C_{i-1}}{\Delta x}.$$

This is known as backwards difference and is used in this case due to the direction of the advection (from x_0 to x_N).

We write this in matrix form as

$$\delta^2 C_i = \frac{1}{\Delta x^2}\begin{bmatrix} -2 & 1 & 0 & . & . & 0 \\ 1 & -2 & 1 & & & . \\ 0 & 1 & -2 & 1 & & . \\ . & & . & . & . & 0 \\ . & & & . & . & . \\ 0 & . & . & 0 & 1 & -2 \end{bmatrix} C_i + b \tag{4.37}$$

where b is a vector which will be used to incorporate boundary conditions,

$$\delta_- C_i = \frac{1}{\Delta x}\begin{bmatrix} 1 & 0 & . & . & 0 \\ -1 & 1 & & & . \\ 0 & -1 & 1 & & . \\ . & & . & . & 0 \\ 0 & . & 0 & -1 & 1 \end{bmatrix} C_i.$$

Next we need to take account of boundary conditions. At $x = 0$ for the aqueous domain we take $C_0 = \beta P_u$

$$(C_1)_t = D_{aq}\left(\frac{\beta P_u - 2C_1 + C_2}{\Delta x^2}\right) - v\left(\frac{C_1 - \beta P_u}{\Delta x}\right),$$

we therefore need to add $\frac{D_{aq}P_u}{\Delta x^2} + \frac{vP_u}{\Delta x}$ into the first entry of the boundary condition vector, b.

At $x = L$ for the aqueous domain we have infinite sink conditions (for the diffusion)

$$(C_N)_t = D_{aq}\left(\frac{C_{N+1} - 2C_N + C_{N-1}}{\Delta x^2}\right) - v\left(\frac{C_N - C_{N-1}}{\Delta x}\right),$$

as we have an up-winding scheme, advection is already taken care of. We have sink conditions on the right-hand side (RHS) and so set $C_{N+1} = 0$, therefore the RHS boundary conditions are already taken care of by our matrices δ_- and δ^2.

Following the same procedure for the lipid domain we have

$$(U_i)_t = D_{lip}\delta^2 U_i.$$

At $x = 0$ in the lipid domain we have zero diffusion and so we let $C_0 = C_2$. We therefore change the matrix for δ^2 (equation (4.37)) to

$$\delta^{2'}C_i = \frac{1}{\Delta x^2}\begin{bmatrix} -2 & 2 & 0 & . & . & 0 \\ 1 & -2 & 1 & & & . \\ 0 & 1 & -2 & 1 & & . \\ . & & . & . & . & 0 \\ . & & & . & . & . \\ 0 & . & . & 0 & 1 & -2 \end{bmatrix} C_i. \tag{4.38}$$

At $x = L$ in the lipid domain we again have sink conditions. Finally we reintroduce movement between the aqueous and lipid domains.

We first write matrix A, relating to

$$\frac{\partial C}{\partial t} = D_{aq}\frac{\partial^2 C}{\partial x^2} - v\frac{\partial C}{\partial x} - \nu C,$$

Such that

$$C_t = AC + b$$

$$A = D_{aq}\delta^2 - v\delta_- - \nu I$$

where I is the $n \times n$ identity matrix and $\nu = k_7(1 - f_{aq})$

We then write the matrix B, relating to

$$\frac{\partial U}{\partial t} = D_{lip}\frac{\partial^2 U}{\partial x^2} - \mu U,$$

$$B = D_{lip}\delta^{2'} - \mu I$$

where $\mu = k_7 f_{aq}$.

We can then write the whole model system (4.29) as

$$\begin{bmatrix} C_t \\ U_t \end{bmatrix} = \tilde{A}\begin{bmatrix} C \\ U \end{bmatrix} + b$$

where $\tilde{A} = \begin{bmatrix} A & \mu I \\ \nu I & B \end{bmatrix}$ and b, a zero vector of length 2N with

$$b(1) = \frac{D_{aq}\beta P_u}{\Delta x^2} + \frac{v\beta P_u}{\Delta x},$$

the vector of boundary conditions.

4.8 Nondimensionalisation

We wish to explore the dependence of drug collected on the parameters in the system because exact parameter values are not all available in the literature, and those that are are subject to error due to assumptions made in their approximation (the radius of a molecule is required when estimating the diffusion coefficient of the molecule, for example, and this is estimated under the assumption that molecules are spherical which is not often the case). We choose to rescale the system so that parameter values are comparative. Taking

$$v = \left(\frac{1}{Fz} \frac{z\mu_{aq}}{\sum_j C_{jaq}|z_j|\mu_{jaq}} + v_{eo} \right) I$$

we write the system (4.29) as,

$$\frac{\partial C_{iaq}}{\partial t} = D_{iaq}\frac{\partial^2 C_{iaq}}{\partial x^2} - v\frac{\partial C_{iaq}}{\partial x} - f(C_{iaq}, C_{ilip}), \tag{4.39a}$$

$$\frac{\partial C_{ilip}}{\partial t} = D_{ilip}\frac{\partial^2 C_{ilip}}{\partial x^2} + f(C_{iaq}, C_{ilip}). \tag{4.39b}$$

where $f(C_{iaq}, C_{ilip}) = k_7(C_{iaq} - f_{aq}(C_{ilip} + C_{iaq}))$.

We then nondimensionalise the concentration by C_0, the average (lipid + aqueous) initial reservoir concentration over x and the time by L/v; the characteristic time scale for drug to cross the stratum corneum by advection alone. Hence equation (4.39) can be written

$$\frac{\partial \overline{C}_{iaq}}{\partial \bar{t}} = \overline{D}_{iaq}\frac{\partial^2 \overline{C}_{iaq}}{\partial \overline{x}^2} - \frac{\partial \overline{C}_{iaq}}{\partial \overline{x}} - \overline{k}_7(\overline{C}_{iaq} - f_{aq}(\overline{C}_{ilip} + \overline{C}_{iaq})), \tag{4.40a}$$

$$\frac{\partial \overline{C}_{ilip}}{\partial \bar{t}} = \overline{D}_{ilip}\frac{\partial^2 \overline{C}_{ilip}}{\partial \overline{x}^2} + \overline{k}_7(\overline{C}_{iaq} - f_{aq}(\overline{C}_{ilip} + \overline{C}_{iaq}))). \tag{4.40b}$$

$$C_{iaq}(\bar{x} = 1, \bar{t}) = 0, \tag{4.41}$$

$$C_{ilip}(\bar{x} = 1, \bar{t}) = 0. \tag{4.42}$$

with bars denoting nondimensionalised parameters and state variables, as given by

$$\bar{C}_{iaq} = \frac{C_{iaq}}{C_0}, \quad \bar{C}_{ilip} = \frac{C_{ilip}}{C_0}, \quad \bar{D}_{iaq} = \frac{D_{iaq}}{Lv}, \quad \bar{D}_{ilip} = \frac{D_{ilip}}{Lv},$$
$$\bar{k}_7 = \frac{k_7 L}{v}, \quad \bar{x} = \frac{x}{L}, \quad \bar{t} = \frac{tv}{L}.$$

4.9 Results

4.9.1 No diffusion

First we explore the impact of the inclusion of a lipid compartment on the predicted drug extracted. In order to do this we consider the system (4.29) in the case where the diffusion coefficient in the lipid and aqueous domains are zero (diffusion free case). We solve equations numerically for the cases

i) reservoir entirely in aqueous domain (f_{aq}=1)

ii) reservoir distributed between the aqueous and lipid domain (f_{aq}=0.6) with k large (equilibrium between aqueous and lipid reached quickly) and

iii) reservoir distributed between the aqueous and lipid domain (f_{aq}=0.6) with k small (equilibrium between aqueous and lipid reached slowly).

A value of $f_{aq} = 0.6$ is chosen for illustrative purposes in the cases ii) and iii) so that values for the lipid and aqueous domains can be easily distinguished. The results shown here are qualitatively representative of results for $0 < f_{aq} < 1$.

The total reservoir concentration over time in each case is shown in Figures 4-6(a)-4-6(c). The amount collected on the pad over time for each case i)-iii) is presented in Figure 4-7(a) with the case where the reservoir is initially empty (relating to a drug naïve patient) also shown for comparison. The information in Figure 4-7(a) is also given as a histogram of extracted fluxes in half hour intervals in Figure 4-7(b),this mimics the data that would be collected in a reverse iontophoresis experiment, where the collection pad is typically changed every half hour and the total drug on each pad measured.

The model results are as follows

i)If all the drug in the stratum corneum is in the aqueous domain it is readily available for extraction. Therefore the reservoir is completely emptied before

readings begin to reflect plasma concentrations (Figures 4-6(a),4-7(a)) and the reservoir size can be easily distinguished.

ii)If only a portion (60% in this example) of the drug is in the aqueous domain, the reservoir isn't immediately emptied and we see a much smaller initial reading Figure 4-7(b). In this case the reservoir size is more difficult to distinguish as subsequent readings reflect a combination of plasma concentration and the emptying lipid reservoir.

iii)In the case where the drug is distributed between the aqueous and lipid compartments and equilibrium between these compartments is slow (Figure 4-6(c)) we again see a smaller initial reading. Estimation of the total reservoir size is arguably more difficult if f_{aq} is unknown, as it is not clear from subsequent readings whether the reservoir has been emptied (Figure 4-7(b)), this could also lead to over prediction of plasma concentration.

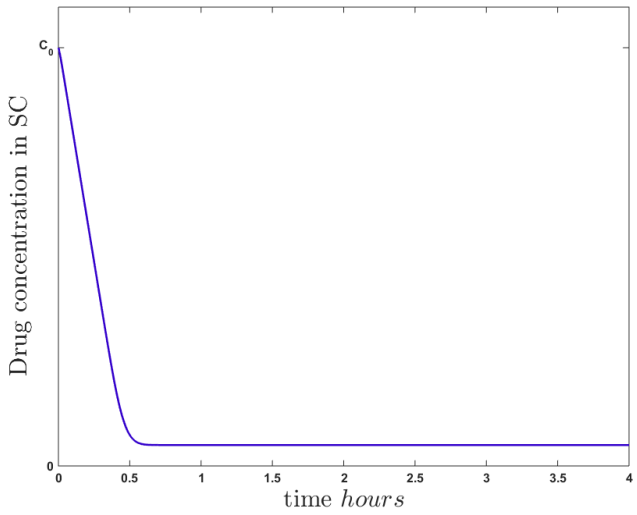

(a) $f_{aq} = 1$

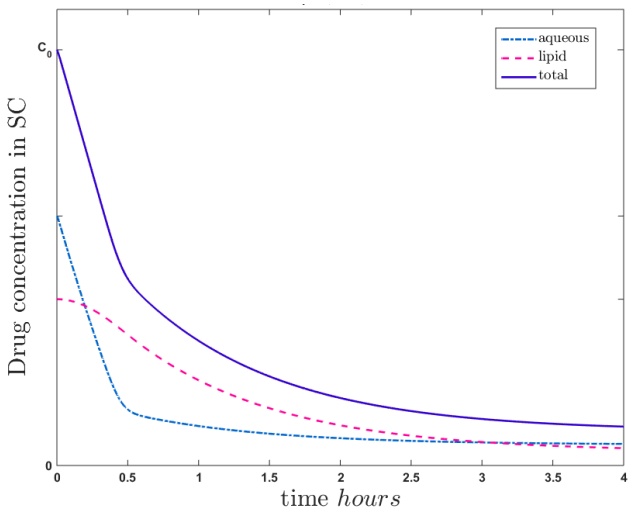

(b) $f_{aq} = 0.6$, fast

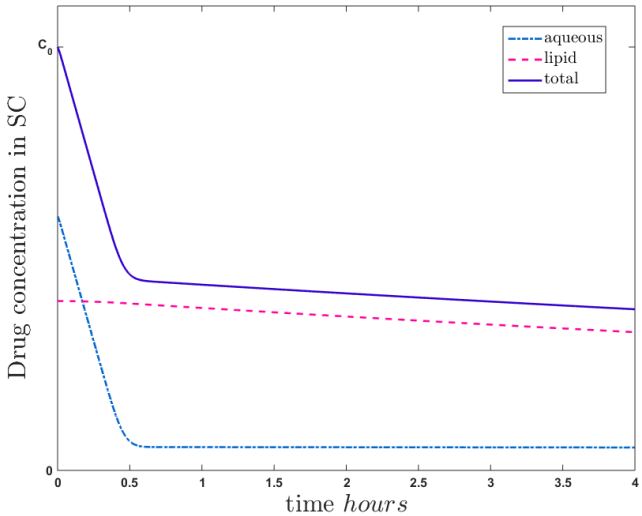

(c) $f_{aq} = 0.6$, slow

Figure 4-6: Unbound drug concentration in the lipid and aqueous domains of the SC during extraction shown for: a) f_{aq}=1, b)f_{aq}=0.6, k_7=2 (large), and c)f_{aq}=0.6, k_7=0.1 (small).

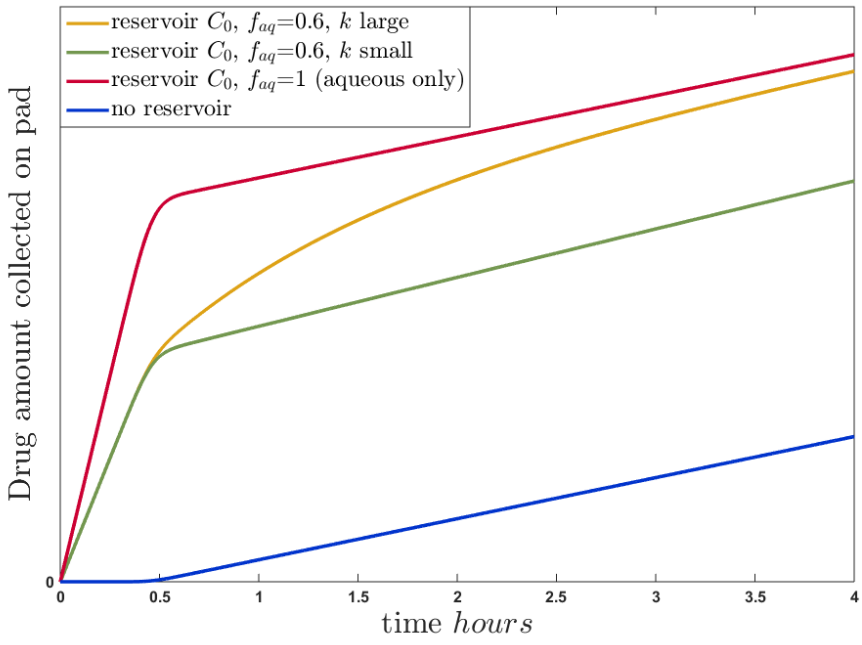

(a)

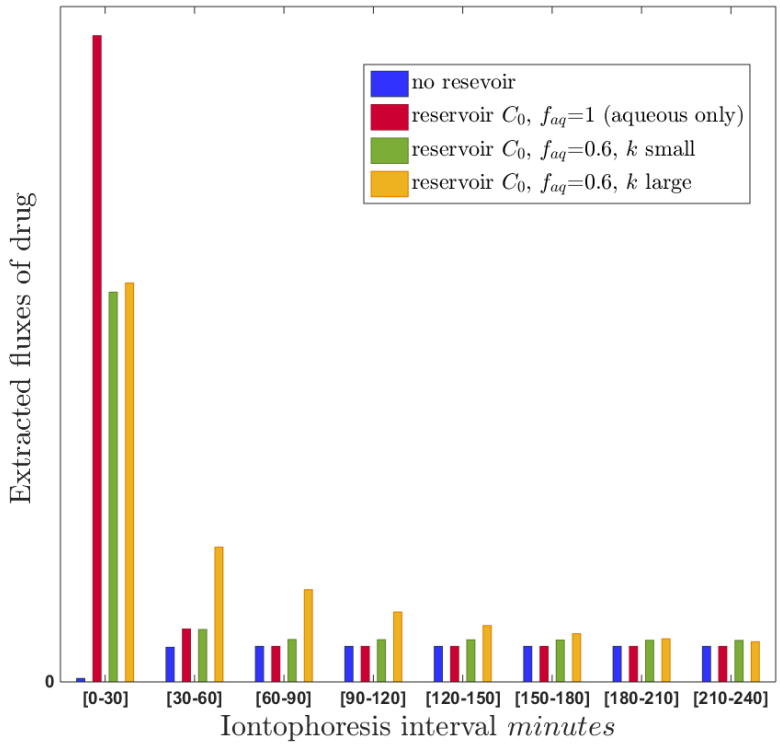

(b)

Figure 4-7: Amount of drug extracted over time for the cases: f_{aq}=0.6, k_7 large, (yellow); f_{aq}=0.6, k_7 small, (green); f_{aq}=1 (red) and the reservoir free case (blue). Shown as the continuous extraction over time (top) and as extracted flux in iontophoresis intervals (bottom).

4.9.2 Diffusive flux included

Initially we consider the aqueous only case. The dependence on diffusion is shown for extraction times $\bar{t} \in [0, 3]$ as the impact of the diffusion coefficient displays time dependence. We show results for values of $\bar{D}_{aq} \in [0, 1.5]$. From Figure 4-8 we can see that at small times, non-zero diffusion < 1 hinders the movement into the collection pad. This means that results observed in iontophoretic extraction for small, non zero diffusion coefficient will have a smaller initial peak than in the diffusion free case. What we observe here is that the introduction of diffusion reduces the clarity in change between extracting reservoir and extracting plasma drug.

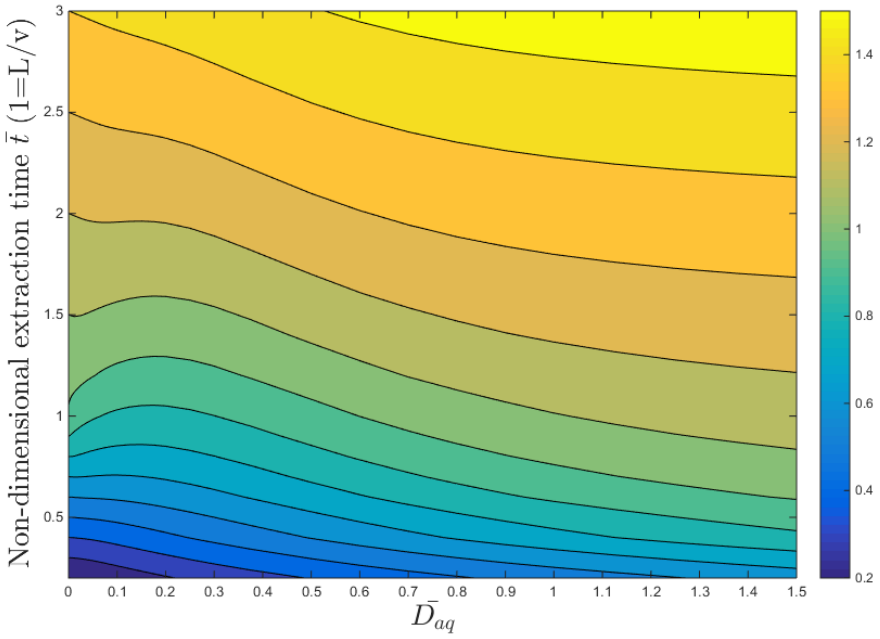

Figure 4-8: Dependence of amount of drug extracted on diffusion for different extraction times using the nondimensional model with $f_{aq} = 1$, $k_7 = 0$, P_u=0.2, $C_u(t = 0)$=1.

Comparing the impact of the diffusion in the lipid and aqueous domains we again consider the nondimensional system (4.40). Drug accumulated on the collection pad in time $\bar{t} = 1$ is given in Figure 4-9 for values of $\bar{D}_{lip}$ and $\bar{D}_{aq}$ ranging from 0 to 0.5. This graph shows that the presence of diffusion in the lipid domain has a greater impact on drug collected than diffusion in the aqueous domain, and that this contribution is consistently positive. Diffusion in the aqueous domain can increase or reduce drug collected for small times depending on the value of $\bar{D}_{aq}$ as seen in Figure 4-8.

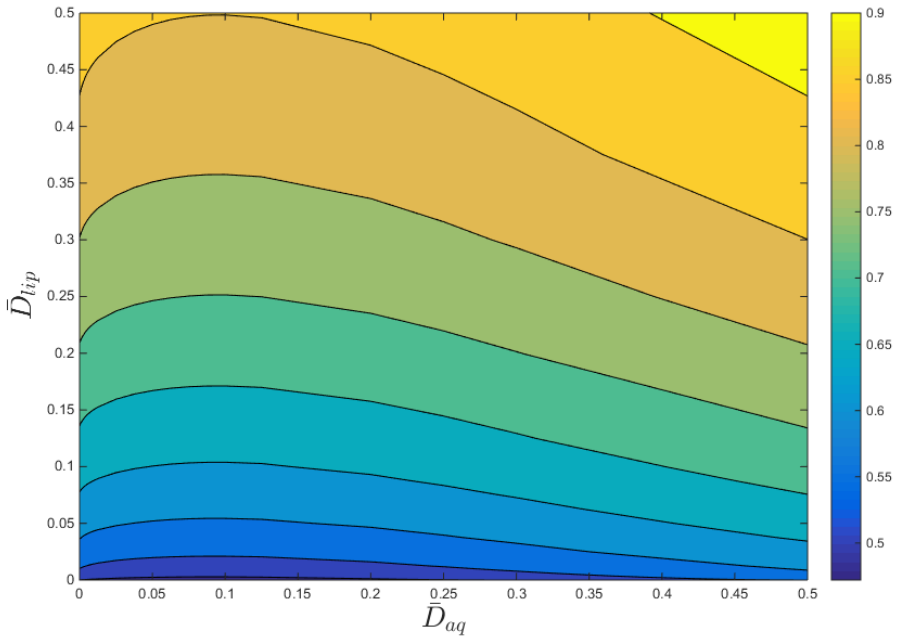

Figure 4-9: Dependence of amount of drug extracted on diffusion coefficient in aqueous and lipid domains for the nondimensional model. The graph shown is for the case $f_{aq} = 0.5$, $k_7 = 0.1$ ($C_0 = 1$, $Pl = 0.2$). The results for other values of k_7 and f_{aq} are qualitatively similar.

4.10 Conclusion

In this chapter (reverse) iontophoresis and the mechanisms involved have been described, with equivalence demonstrated between the Nernst-Planck equation and Faraday's law of electrolysis for electromigration. Models for drug delivery via iontophoresis are reviewed with a focus on the approach to modelling the SC structure. Accordingly we have created a 1D spatial model for the extraction of a reservoir in the SC via reverse iontophoresis. The model created for reverse iontophoresis builds on the model for reverse iontophoretic extraction by Paulley *et al.* [24] by incorporating SC structure and mechanisms identified in the literature on iontophoretic delivery. Our model considers a SC comprised of a lipid and an aqueous domain with diffusion in the lipid and electromigration, electroosmosis and diffusion in the aqueous domain, with partitioning between the two domains. This has not been done for reverse iontophoresis previously. Using the spatial aspect of the model we also incorporated the fact that the pathway of drug from plasma to the collection pad is through the stratum corneum. Our model is therefore able to capture the lag behaviour for the reservoir-free case which has not previously been achieved.

The results show that the distribution of the reservoir between the lipid and

aqueous domain and the rate of partitioning between the two has a potentially significant impact on the way that the reverse iontophoresis results are interpreted, especially if the parameter values are not known.

For a drug where the diffusion coefficient in the lipid/aqueous domain is on a comparable time scale to the extraction we expect that the distinction between drug extracted from the SC and from the plasma will be less well defined.

The number of samples and frequency of collection pad replacement could be optimised for the drug of interest by determining the lag time for the reservoir-free case to optimise the distinction between SC and plasma extraction. Ideally if lag time is not known the sample frequency should be as often as possible, however, as we are expecting only a small amount to be collected in each sample and this needs to reach a minimum value for quantification this may not be a practical solution in vivo. Sampling should also be continued until a steady extraction flux is obtained to maximise the chances of the reservoir being completely extracted and to be confident that the steady flux relates to the plasma concentration.

In this model we have assumed that the resistance, and therefore diffusion and mobility (which affects electromigration), remain constant in the SC over the period of reverse iontophoresis. It has, however, been shown that this is unlikely to be the case (Subsection 4.2.5). If resistance in the SC were to change during extraction, the reservoir may be over or under predicted by our model.

We have also made the assumption that the drug is 100% ionised in the SC. Ionisation and pH effects could be incorporated by following a similar procedure to Imanidis and Luetolf [120] who also consider that partitioning between lipid and aqueous compartments may be dependent on ionisation and pH.

We believe that the model for reverse iontophoresis presented here provides a convincing case for experimental work to be carried out to answer questions identified for furthering the understanding of the reverse iontophoresis process.

Chapter 5

Model Combination

5.1 Introduction

In this chapter we combine models for systemic drug concentration, reservoir formation and extraction from previous chapters to create an integrated model system. The model takes a prescribed dose regimen for a given drug over a set time period and predicts the resulting plasma concentration profile, the accumulation of that drug in the SC, and the reverse iontophoresis extraction fluxes. The objectives of this chapter are to bring together the work in previous chapters, to compare the predictions of the model system with data from the literature, to determine which factors from each model have the most significant impact on reverse iontophoresis readings, and what that impact is, and to explore the potential for reverse iontophoresis as a compliance monitoring technique.

We start with a brief review of the literature, with a focus on combination of transdermal delivery and PK models. The model system is adapted to lithium which exhibits straightforward physio-chemical properties so that model predictions can be compared with data from the literature. Using parameter estimates obtained for the lithium case we explore the more complex physio-chemical scenarios built up in previous chapters and look at their effects on the predicted reverse iontophoresis readings. Finally we explore the potential for reverse iontophoresis as a compliance monitoring technique.

5.2 Literature review

There are a small number of papers that combine transdermal delivery of a drug with the resulting systemic profile.

Reddy *et al.* [119] combined a number of passive transdermal delivery (TDD) models, developed in an earlier paper [136], with a one compartment systemic PK model to examine the effects of changing vehicle and blood concentrations and differences between the skin models chosen. In the first TDD model the skin is described as a single well mixed compartment. In this model vehicle skin and blood compartments are combined through a system of three ODEs, with linear first-order transfer between the vehicle and skin, and the skin and blood with a volume adjustment term for each. A constant boundary concentration is given for the vehicle-skin interface and a constant flux condition at the blood-skin interface. They conclude that, for short exposure times, the membrane model is most accurate. However, in circumstances where time taken for drug to absorb into skin is much shorter than exposure time, or when physical parameters are not exactly known, compartmental models provide acceptable predictions.

Nugroho *et al.* created a set of mathematical models for iontophoresis in vitro considering both the iontophoretic delivery and the resulting plasma profile [127]. They create four models: two models for drugs with one compartment elimination kinetics, and two models for drugs with two compartment elimination kinetics. The first model uses an ODE with a constant input rate from the skin and a first order elimination rate constant. The second model considers a time variant input which takes time dependent values of flux from the predicted clearance from skin in their 2004 paper [126], discussed in Chapter 4. In the third and fourth models an additional 'peripheral compartment' is added, into which drug reversibly distributes according to first order rate constants. Again constant and time dependent influx from the skin is considered. In both these cases the post-iontophoretic phase is explored by assuming that after the electric current is turned off, no further drug enters systemic circulation and so we have clearance only. In the two compartment model, drug continues to distribute into the peripheral compartment during the post iontophoresis phase and so elimination presents as a biexponential decay. In this paper they demonstrate the value of inclusion of a time varying input from the skin, which fits the iontophoresis and post iontophoresis data significantly better in both one and two compartment cases. This scenario is relevant to delivery where drug remains in the SC even after the device is removed but an equivalent for the RI case isn't obvious. As the models used are non-spatial, joining together of skin and plasma compartments is done using transfer rates between compartments.

A review paper by Grassi *et al.* considers mathematical modelling of simultaneous drug release and in vivo absorption [137]. Both passive and iontophoretic delivery are considered, with sink conditions used at the base of the skin for the passive case and flux matching on the stratum corneum/viable skin boundary for reverse iontophoresis to prevent drug accumulating there. Once the drug has entered the

body model from the skin it does not re-enter the skin.

5.3 Comparison of model predictions with lithium data

Given the lack of relevant data for our unknown mechanistic parameters, we exploit data collected on lithium extraction via reverse iontophoresis to provide parameter estimates to populate the models. Lithium is a useful drug in this context since it is small, positively charged, does not bind and is not metabolised (i.e. parameters are mostly known).

Detailed data for lithium monitoring via reverse iontophoresis is given in the paper by Leboulanger *et al.* [15], which provided motivation for the preliminary modelling work on reverse iontophoresis by Paulley *et al.* [24].

The study by Leboulanger *et al.* [15] involved 30 bipolar or schizo-affective patients, each of whom had been receiving chronic lithium therapy at doses of 12-36 mmol/day for no fewer than 3 weeks. Reverse iontophoresis was carried out on each patient for a period of 2 hours (four 30 minute intervals) using a collection pad of area $3.2 \pm 0.4 cm^2$ and a current of 0.8mA. A blood serum sample was taken for comparison at 90-100 min after initiation of reverse iontophoresis.

Blood samples showed that around 75% of the patients had serum lithium concentrations between 0.5-0.9mmol, which lie within the therapeutic range (Figure 5-1). Data in Figures 5-2 and 5-3 taken from Leboulanger *et al.* [15] show that extraction fluxes are greater within the first 30 minutes after which they reduce to align with plasma drug concentrations.

5.3.1 Assumptions and model adaptions

In order to model the plasma profile, reservoir formation, and extraction for lithium, we must make some adaptions to each of our three models. In the paper by Paulley *et al. [24]* the only mechanism used to describe reservoir formation is desquamation and the only mechanism for extraction is electromigration. We start by replicating this approach with our spatial models and compare the model predictions with data. We then reintroduce the mechanisms, where appropriate, from the full model to explore the impact on model predictions; diffusion in reservoir formation, diffusion and electroosmosis in extraction model and separation into lipid and aqueous domains in extraction.

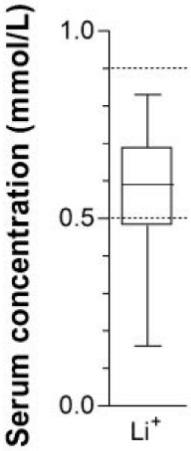

Figure 5-1: Taken from Leboulanger *et al.* [15]. Shows the serum concentrations of lithium for patients in the study. Note dotted lines indicate the 'normal' range.

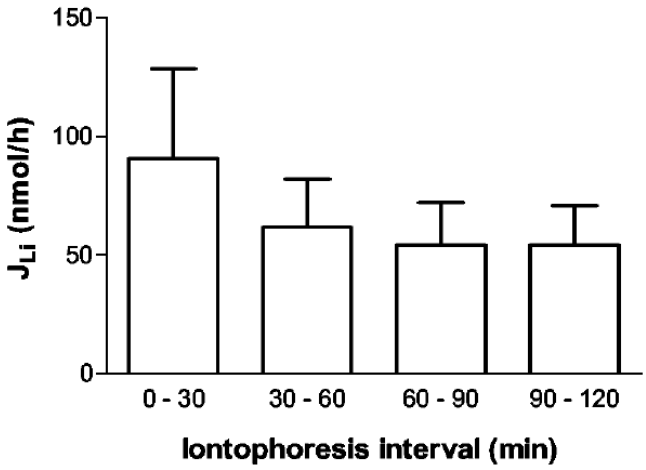

Figure 5-2: Taken from [15]. Shows extraction fluxes of lithium over the four 30 minute extraction periods.

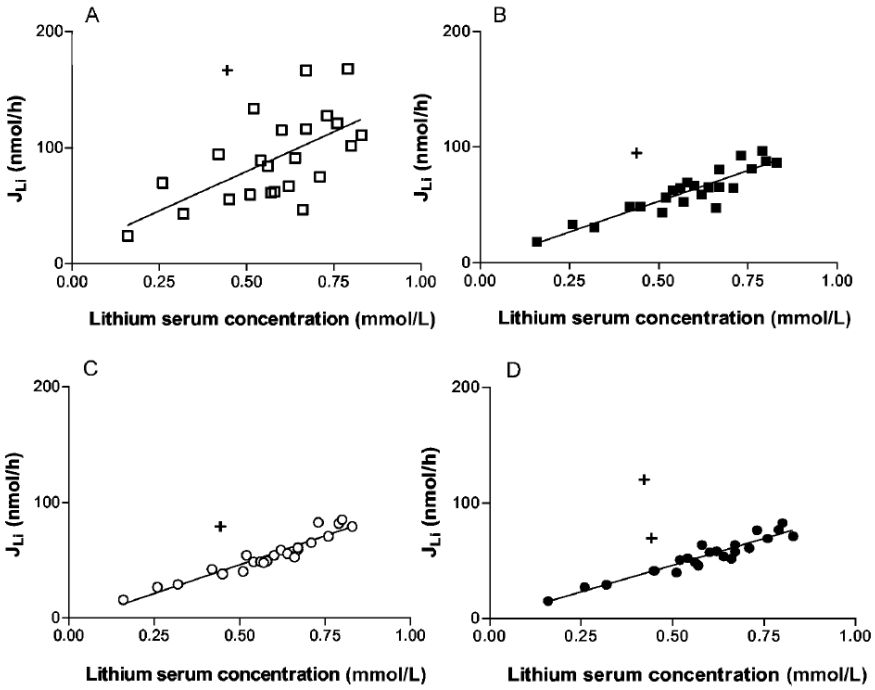

Figure 5-3: Taken from [15]. Figures A-D are plots of extraction flux data for iontophoresis extraction periods for each patient plotted against their plasma concentration. A: extraction period [0-30] minutes, B: extraction period [30-60] minutes, C: extraction period [60-90] minutes, and D: extraction period [90-120] minutes.

Model 1: Systemic Lithium

Lithium exhibits one compartment pharmacokinetics, therefore Model 1 will take the same form as the model from Paulley *et al.* [24]. For a daily oral dose of lithium the change in the plasma concentration of lithium over time is given by

$$\frac{dL_1}{dt} = -k_e L_1 + \sum \delta k e^{-kt} \tag{5.1}$$

where $L_1(t)$ is the lithium concentration in the plasma, δ is the dose, k_e is the excretion rate and k is the absorption rate.

Initial conditions: We start with a drug naive patient and 'administer' a daily dose of 24.3 mmol each day for 30 days to imitate the scenario in the study by Leboulanger *et al.*[15].

$$L_1(t = 0) = 0.$$

Model 2 : Reservoir Formation

We start with the simplest case and describe the formation of the reservoir in the SC by desquamation only. We consider the SC in one dimension with $x \in [0, L]$ where $x = 0$ is the base of the SC and $x = L$ is the skin surface. We therefore have

$$\frac{\partial L_2}{\partial t} = -v\frac{\partial L_2}{\partial x} \tag{5.2}$$

where $L_2(x, t)$ is the unbound lithium concentration in the SC ($nmol/\mu m$) directly beneath the collection pad and v is the velocity of desquamation ($\mu m/day$).

Boundary conditions: If we have plasma concentration as $L_1(mmolL^{-1}) = L_1(\mu molcm^{-3})$ and we assume that there is a smooth flat interface between the plasma and the SC at the base of the SC ($x = 0$) of area $3.2cm^2$, directly beneath the collection pad of the same area, then the concentration on that interface is given by

$$L_2(0, t) = L_1(t) \cdot 3.2 \cdot \alpha\frac{\mu mol}{cm} = L_1(t) \cdot 0.32 \cdot \alpha\frac{nmol}{\mu m}$$

where α is a dimensionless parameter which represents a combination of a partition coefficient and a correction factor to account for the assumption that plasma directly connects with SC at a smooth, flat interface.

Initial conditions: As we are considering an initially drug naive patient, at $t = 0$ we have initial condition

$$L_2(x, 0) = 0.$$

Model 3: Reverse Iontophoresis of Lithium

$L_2(x, t) = L_3(x, \tau)$ where $\tau = 0$ starts at $t = 30.5$ days. Since lithium is small and positively charged we assume that electromigration dominates the extraction flux and consider

$$\frac{\partial L_3}{\partial \tau} = -v_{em} \frac{\partial L_3}{\partial x} \tag{5.3}$$

where $L_3(x, \tau)$ is the concentration of lithium in the SC ($nmol/\mu m$) directly beneath the collection pad during extraction and v_{em}, the velocity due to electromigration, is given by

$$v_{em} = \frac{I \mu_{Li}}{F \sum C_i \left| z_i \right| \mu_i}$$

where parameter definitions and values are given in Table 5.1.

The same assumption is made here as in Chapter 4: concentration of lithium in SC is small compared to other ions present and so its contribution in the summation in the denominator is assumed to be negligible.

Note the time variable is denoted τ in this model, this is because $\tau = 0$ starts at $t = 30.5$ days, 12 hours after the dose on day 30, and time during extraction is measured in minutes, as this is an appropriate time scale for reverse iontophoresis.

The drug collected on the pad at $x = L$ is then given by

$$\frac{dL_{pad}}{d\tau} = \int_0^\tau v_{em} L_3 \big|_{x=L} \, d\tau$$

Parameter	Definition	Value	Reference
δ	Lithium dose	$24.3mmol$	[24, 138, 15]
k_e	Lithium excretion rate	$0.654day^{-1}$	[24, 138]
k	Lithium absorption rate	$4.62day^{-1}$	[24, 138]
L	SC thickness	$18.3\mu m$	[95]
v	Speed of desquaming skin	$1.307\mu mday^{-1}$	[52, 53]
I	Current density	$0.25mAcm^{-2}$	[15]
F	Faraday's constant	$96.487Cmmol^{-1}$	[15]
μ_{Na}	Aqueous mobility of sodium	$5.19 \times 10^{-4}cm^2s^{-1}v^{-1}$	[118]
μ_{Cl}	Aqueous mobility of chloride	$7.62 \times 10^{-4}cm^2s^{-1}v^{-1}$	[24]
μ_K	Aqueous mobility of potassium	$7.91 \times 10^{-4}cm^2s^{-1}v^{-1}$	[118]
C_{Na}	Concentration of Na in the SC	$32.7 \times 10^{-3}mmolcm^{-3}$	[139, 140]
C_{Cl}	Concentration of Cl in the SC	$61 \times 10^{-3}mmolcm^{-3}$	[139, 140]
C_K	Concentration of K in the SC	$91 \times 10^{-3}mmolcm^{-3}$	[139, 140]
μ_{Li}	Aqueous mobility of lithium	$4.01 \times 10^{-4}cm^2s^{-1}v^{-1}$	[118]
v_{em}	Velocity due to electromigration	$4.602\mu mmin^{-1}$	[125, 25, 19]

Table 5.1: Parameter estimates used for Lithium models

Boundary conditions: We assume plasma concentration remains unchanged during extraction and take the boundary condition at $x = 0$ as the plasma concentration 12 hours after the dose on day 30, adjusted for area, given by

$$L_3(0, \tau) = \bar{L_1}(t = 30.5) \cdot \alpha$$

where α=0.32.

Initial conditions: At the start of reverse iontophoresis we have a reservoir given by the Model 2 reservoir prediction at $t = 30.5$

$$L_3(x, \tau = 0) = L_2(x, t = 30.5)$$

5.3.1.1 Results and discussion

Model 1

The predicted plasma profile for a daily dose of lithium starting at $t = 0$ is given in Figure 5-4. This model has been replicated from [24] and the results obtained are identical to results given in that paper. The predicted plasma profile 'steady state' concentration is within the range specified in the paper by Leboulanger *et al.* [15].

Model 2

The predicted accumulation of lithium in the SC, scaled to the area of the collection pad, is given in Figure 5-5. In this case, movement into and through the SC was modelled by a constant advection rate representing desquamation. The value for partitioning of lithium from plasma into the SC is unknown. The area of the interface between plasma and stratum corneum beneath the collection pad was approximated to be $3.2cm^2$ (the same area as the interface between SC surface and the collection pad). In reality there is no such direct interface and even then it is unlikely to be smooth and flat. Therefore α is a combination of the unknown partition coefficient and an adjustment factor to account for this approximation. The value of α has been chosen so that the resulting reservoir size reflects that observed reservoir size from the data. This is a weakness in our model as exact reservoir size can't be determined from the data in Leboulanger *et al.* [15]. This identifies the need for further experimental work to determine the actual reservoir size (discussed in detail later). The prediction for the drug concentration in the SC given by Model 2 (equation (5.2)) qualitatively agrees with the model in Paulley *et al.* [24], increasing steadily before reaching a steady state value after 15-20 days. Taking reverse iontophoretic extraction at 30 days, therefore, should give the same predicted extraction as that for much longer term compliance.

Model 3

The predicted extraction of lithium is given as a continuous time profile in Figure 5-6(a) and the same results are presented as a cumulative extracted flux in 30 minute interval in Figure 5-6(b) for comparison with data given in [15] (shown in Figure 5-2). Comparing the predicted extraction in the final two intervals ([60-90], [90-120]) with the observed extraction for these intervals, good agreement is obtained. However the predicted initial extraction peak is too high and the equilibrium with plasma is reached too quickly: within the first interval rather than the observed [30-60] interval. In fact, on inspection of the continuous data the equilibrium with plasma is reached in about 4 minutes, suggesting that the model predicts that the reservoir is emptied too quickly.

The model for extraction (equation (5.3)) dictates that the time to empty the reservoir (when the whole reservoir is available) is determined by v_{em} and L. So we hypothesise that possible causes of the short lag time could be an an overestimate of the speed due to electromigration, v_{em}, or an underestimate of the path-length of extraction, L.

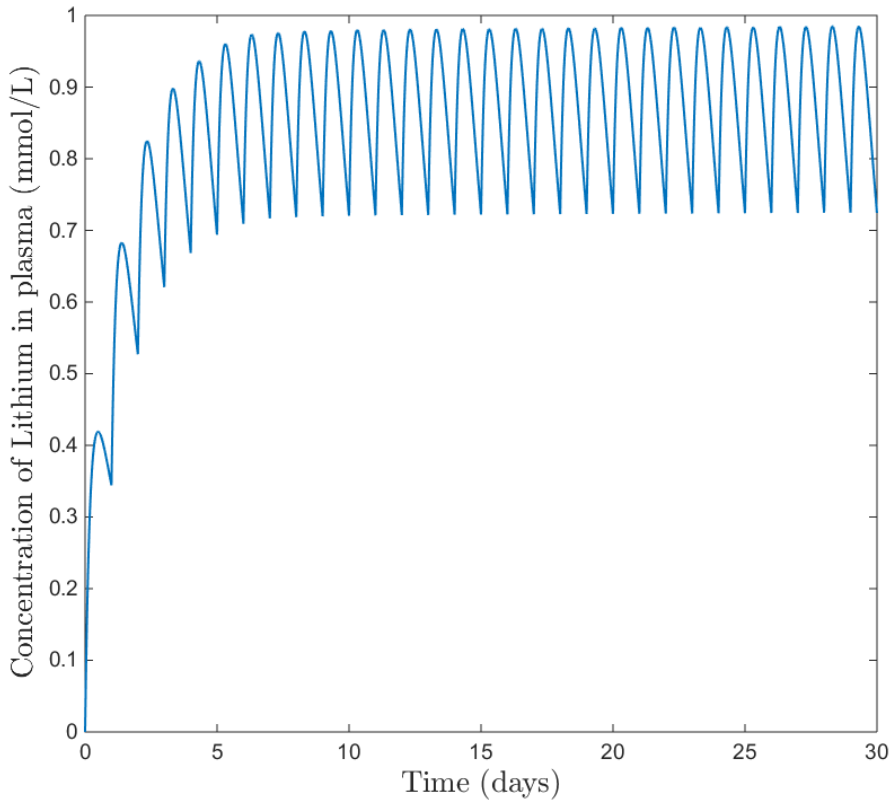

Figure 5-4: Predicted plasma concentration for a fully compliant patient on a daily dose of lithium described by equation (5.1).

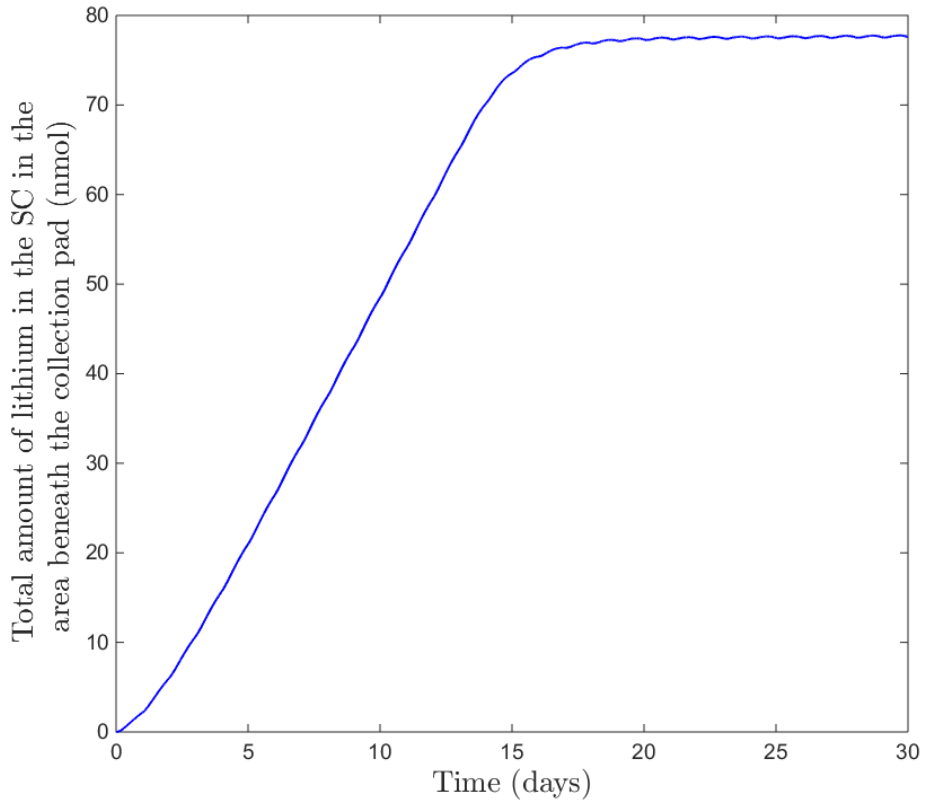

Figure 5-5: Predicted reservoir size over time in the SC directly beneath the collection pad (area $3.2cm^2$ as specified in Leboulanger *et al. [15]* experimental protocol) using equation (5.2).

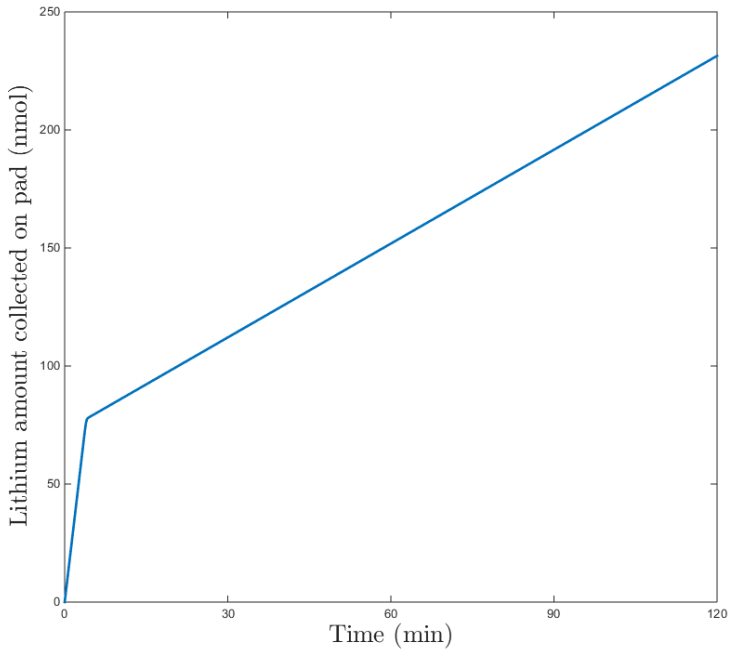

(a)

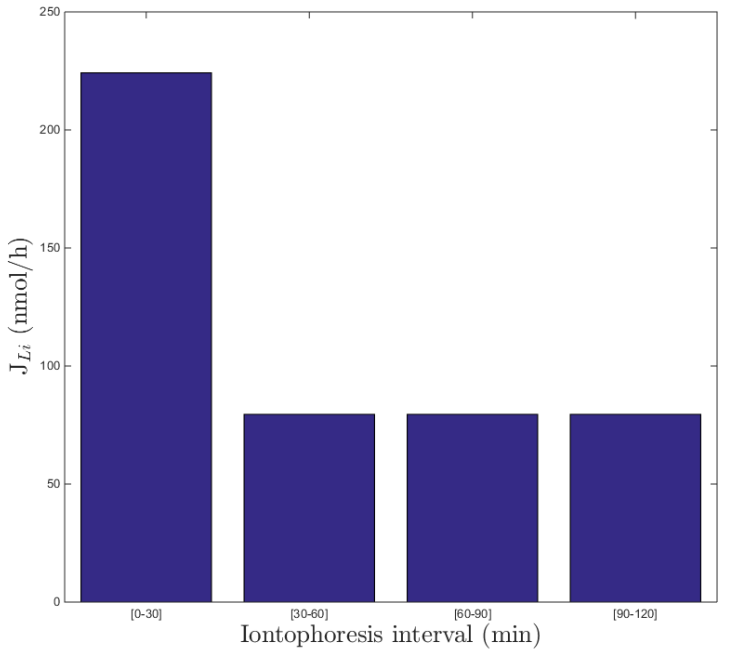

(b)

Figure 5-6: Extraction prediction for lithium presented as a continuous cumulative amount collected against time and cumulative extracted flux in each iontophoresis interval for comparison with data (Figure 5-2). Predictions as per equation (5.3) with $L = 18.3$, v_{em}= $4.602\mu\text{mmin}^{-1}$ Table 5.1.

5.3.1.2 Altering the advection value

Estimation of v_{em} from the literature is certainly subject to a range of parameter uncertainties and approximations. One option is to choose v_{em} to obtain a lag time as observed in [15]. If we assume that all reservoir of drug is immediately available for extraction, Figure 5-2 (from [15]) would suggest it takes between 30 and 60 minutes to cross the SC from the plasma. Taking the midpoint and keeping the path length unchanged would give

$$v_{em} = \frac{L}{45} = 0.407 \mu \text{mmin}^{-1}$$

which results in the model predictions shown in Figure 5-7, providing a good agreement with the lag time but a significant underestimate of plasma extraction in the intervals 60-90 min, 90-120 min.

5.3.1.3 Altering extraction path length

Alternatively the observed lag time could be increased by increasing the extraction path length. Reasonable agreement with extraction data (lag time within the 30-60 minute interval) is achieved with only a 10 fold increase in extraction path length, Figure 5-8, without altering the rate at which drug is extracted from the plasma in intervals 60-90 min, 90-120 min. This is done by increasing the extraction path length and redistributing the total reservoir, as predicted by Model 2, over this new space prior to extraction. An increase path length (i.e. tortuosity) of 10 fold does not seem unreasonable when considering the tortuosity of the intercellular route through the SC (as discussed in Chapter 3) has been shown to be as much as a 50 fold increase [86]. Whilst we interpret increased path length as introducing a more tortuous route through the SC; the route could alternatively include the subcutaneous tissues or lower layers of skin. To consider this would require model adaption including an intermediate compartment between plasma and SC which we don't consider here.

5.3.2 Potential for monitoring compliance

Using this model for lithium, with an increased path length during extraction, we explore detection of compliance via reverse iontophoresis. To do this we create the following four compliance scenarios

(a) Daily dose of 24.3mmol lithium for 30 days (fully compliant)

(b) Dose of 24.3mmol lithium every other day for 30 days

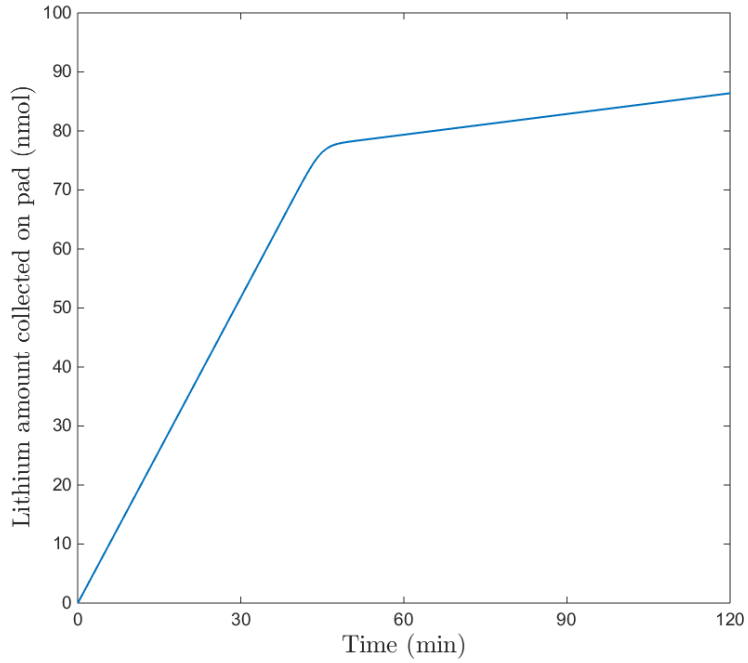

(a)

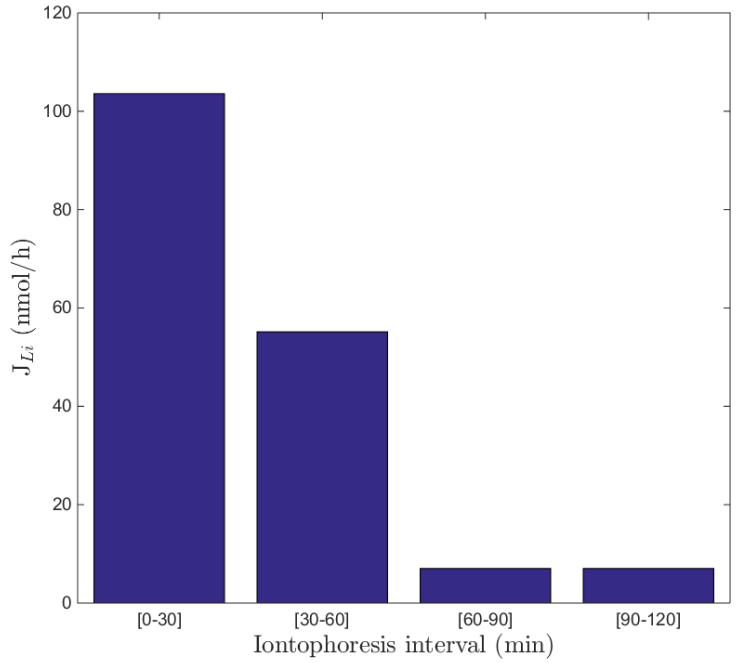

(b)

Figure 5-7: Extraction prediction for lithium presented as a continuous cumulative amount collected against time and cumulative extracted flux in each iontophoresis interval for comparison with data (Figure 5-2). Predictions using equation (5.3) with L=18.3, v_{em}= $L/45$ as discussed in section 5.3.1.2.

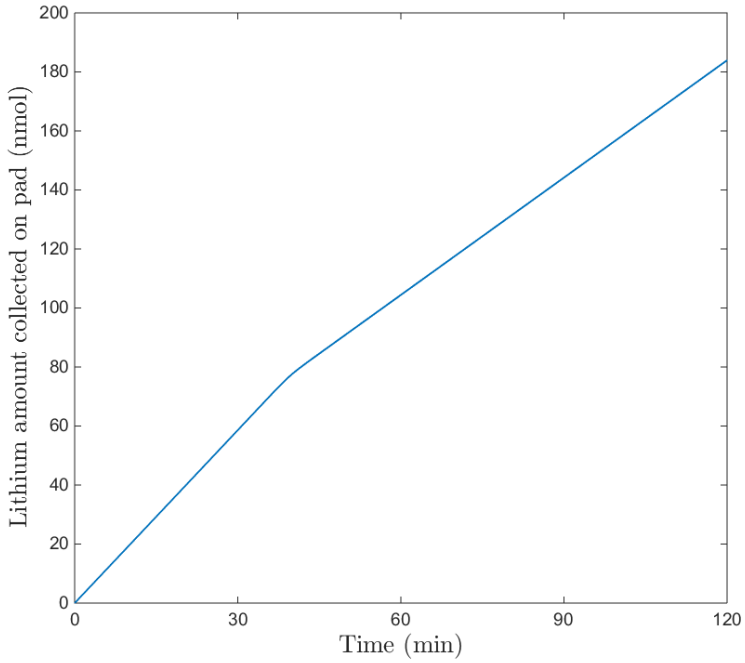

(a)

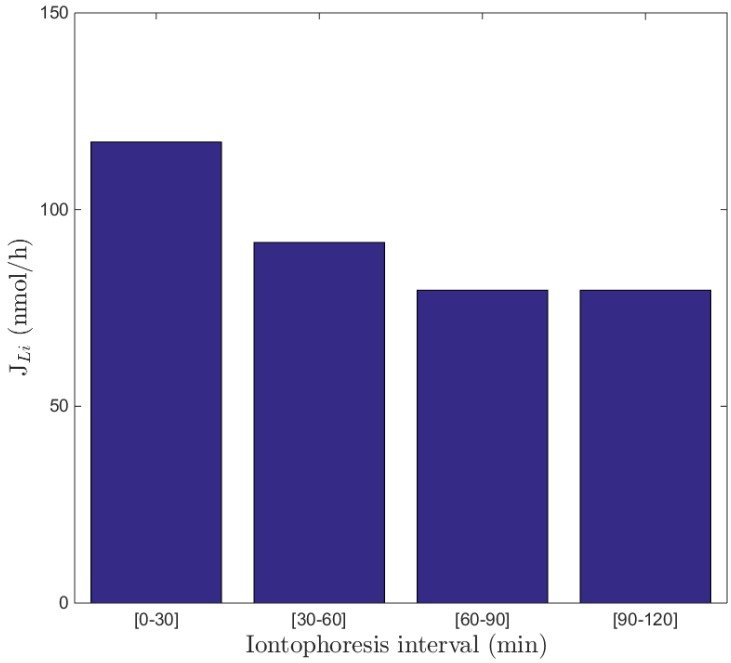

(b)

Figure 5-8: Extraction prediction for lithium presented as continuous cumulative amount collected against time and cumulative extracted flux in each iontophoresis interval for comparison with data (Figure 5-2). Predictions using equation (5.3) with L=183 as discussed in section 5.3.1.3 and v_{em}= 4.602 μmmin^{-1} (Table 5.1).

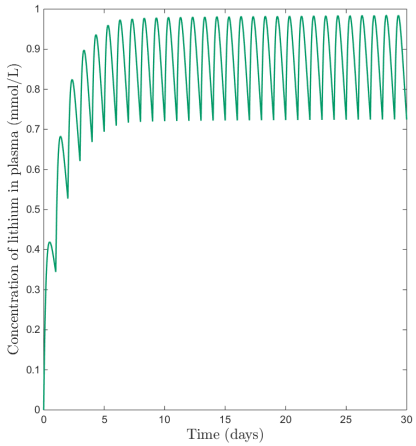

(a) Compliance scenario a

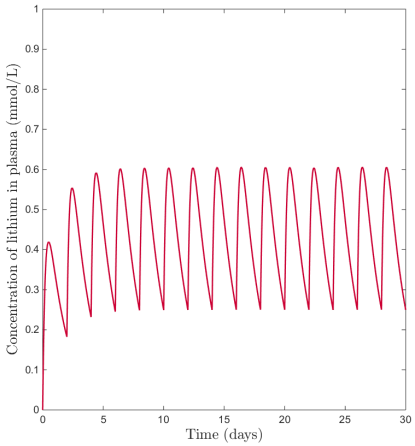

(b) Compliance scenario b

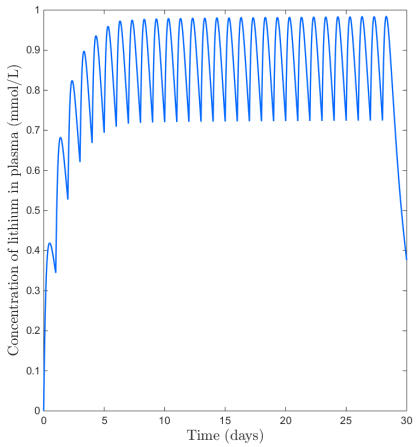

(c) Compliance scenario c

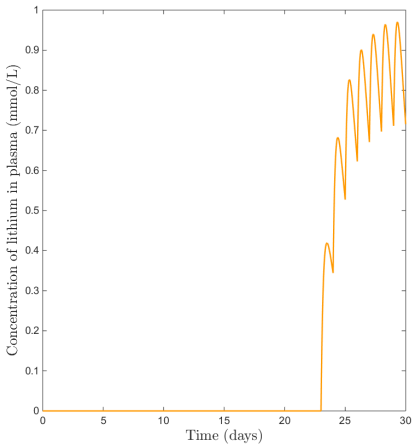

(d) Compliance scenario d

Figure 5-9: Plasma concentrations for compliance scenarios (a)-(d), as described in the text.

(c) Daily dose of 24.3mmol lithium every day for 29 days with a missed dose on day 30

(d) Daily dose of 24.3 mmol lithium on days 24- 30

Note that these scenarios have been selected as they are representative of traditional compliance monitoring via a blood sample at day 30, and should return similar compliance predictions for scenarios (a) and (d), and scenarios (b) and (c) despite significantly differing levels of compliance between them. The predicted plasma profiles for compliance scenarios (a)-(d) are given in Figure 5-9. Throughout this chapter plots relating to scenario (a) will be shown in green, (b) in dark pink, (c) in blue and (d) in yellow for ease of comparison.

The reservoirs corresponding to compliance scenarios (a)-(d) as predicted by

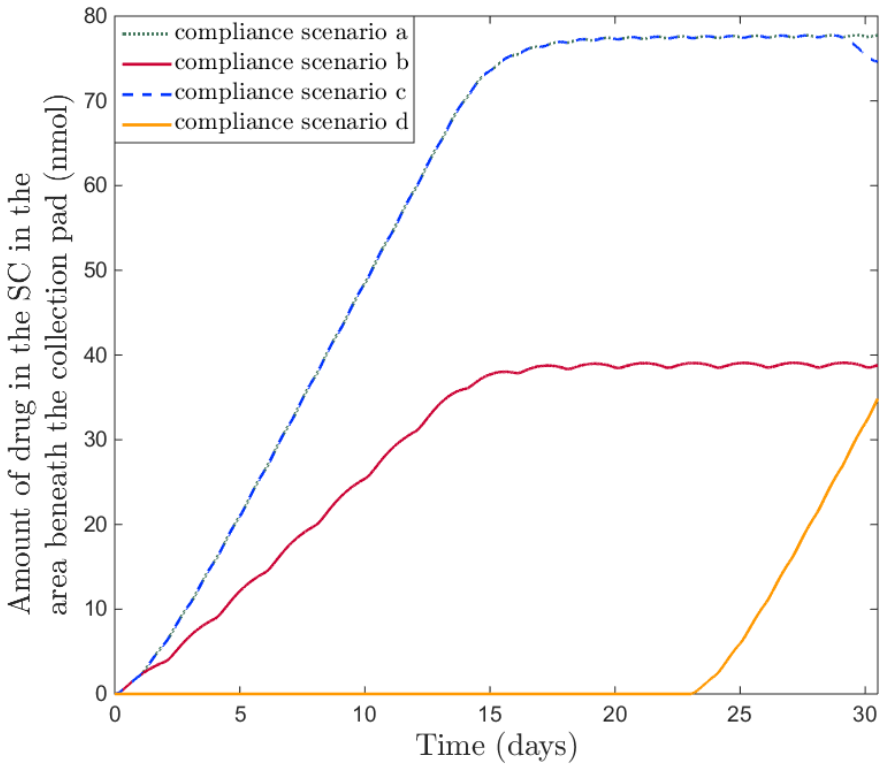

Figure 5-10: Predicted lithium reservoir in the case of no binding and no diffusion i.e. cell renewal only. Shown for the four compliance scenarios: (a) Compliant (daily dose for 30 days); (b) habitual non-compliance (dose every other day for 30 days); (c) missed dose on day 30; (d) doses start on day 24.

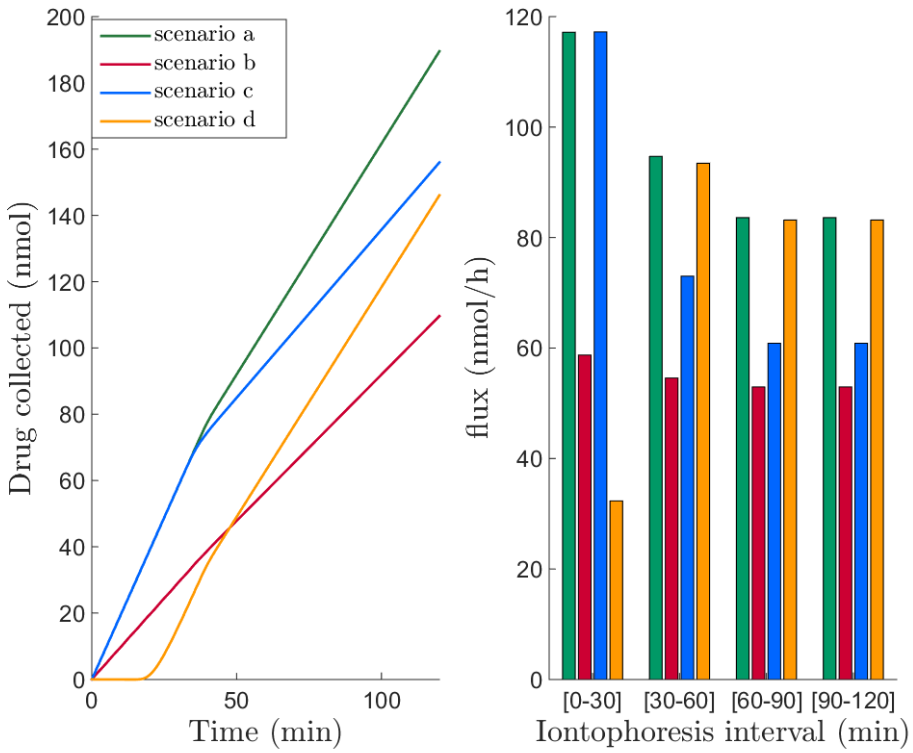

Figure 5-11: Predicted extraction for the lithium model for the four compliance scenarios: (a) Compliant (daily dose for 30 days); (b) habitual non-compliance (dose every other day for 30 days); (c) missed dose on day 30; and (d) doses start on day 24. (no diffusion). Path-length of extraction is adjusted as discussed in subsection 5.3.1.3 ($L = 183\mu m$).

equation (5.2) are given in Figure 5-10. Comparing these with the plasma concentrations at day 30 in Figure 5-9 we can see that although compliance scenarios a and d have the same plasma concentration, the reservoirs differ significantly. Again compliance scenarios b and c have similar plasma concentrations but, due to their compliance history, a different reservoir size.

The predicted extraction fluxes for all four compliance scenarios, via electromigration with an increased path length, are given in Figure 5-11. Scenarios a, b and c give a qualitatively similar profile (initial peak followed by lower extraction). To determine compliance from data like this would have to be comparative and sufficient data are needed to make accurate predictions. The extraction profile for scenario d gives an initially small extraction followed by a peak which then reduces. This is because dose was only administered in the last 7 days which means that the reservoir is located towards the base of the SC.

5.3.3 Inclusion of other model mechanisms for lithium

So far we have considered the simplest case scenario in each model. Now we reincorporate model mechanisms applicable to lithium in each model to inspect the impact of their inclusion.

5.3.3.1 Distribution of reservoir into lipid and aqueous domains

The predictions for extraction given in Figure 5-6 identifies a need for model adjustment. An alternative to the two suggested solutions (adjustment of v_{em} or L) is to reintroduce the division of the unbound reservoir into lipid and aqueous domains during extraction, as described in Chapter 4. As current passes through the aqueous domain it is from here that drug is extracted. Therefore introducing this division means that not all drug is available for immediate extraction and therefore a delay will be observed.

Reintroduction of this distribution for some arbitrary choice of unknown parameters k_7(=1.4) and f_{aq}(=0.11), gives the predicted extraction in Figure 5-12, it gives good qualitative and quantitative agreement with the data for path length $L = 18.3\mu m$ (stratum corneum thickness).

5.3.3.2 Diffusion in reservoir formation for lithium

Lithium is a small, mobile ion which means it has a large aqueous diffusion coefficient. Lithium also doesn't bind within the body and so it is likely that lithium will diffuse in the SC during reservoir formation. We therefore reintroduce

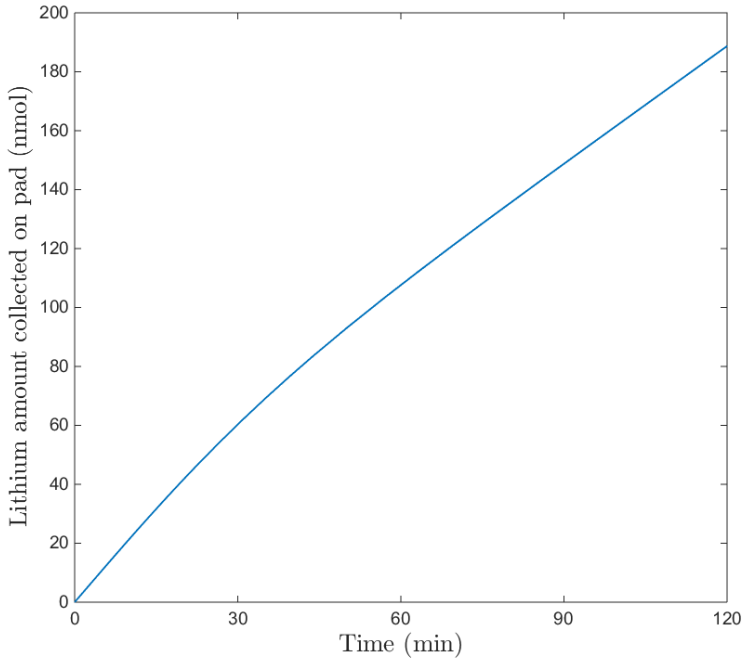

(a)

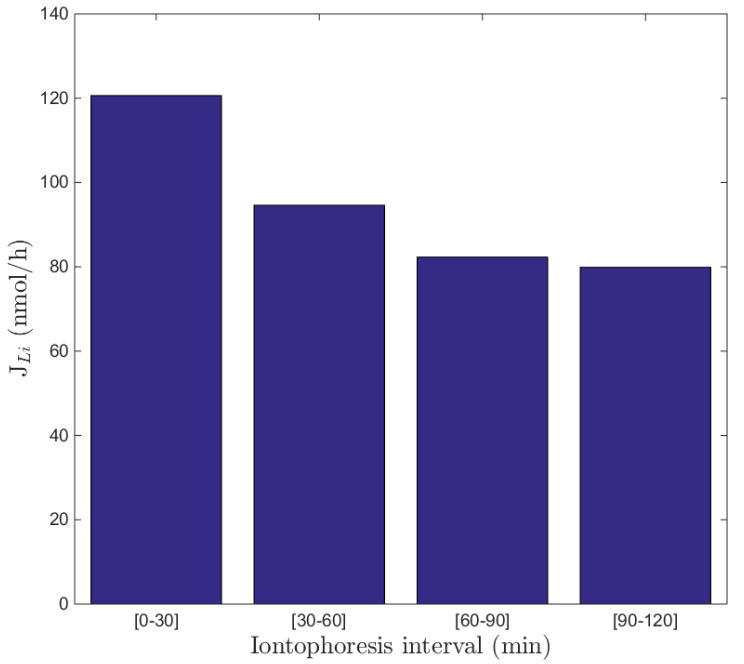

(b)

Figure 5-12: Extraction prediction for lithium presented as continuous cumulative amount collected against time and cumulative extracted flux in each iontophoresis interval for comparison with data (Figure 5-2). Predictions using model (5.3) with L=18.3, v_{em}=4.602 as given in Table 5.1. With division into lipid and aqueous compartments reintroduced for extraction with $f_{aq} = 0.11$, $k_7 = 1.4$

diffusion into the equation for reservoir formation of lithium. Model 2 is therefore given by

$$\frac{\partial L_2}{\partial t} = D\frac{\partial^2 L_2}{\partial x^2} - v\frac{\partial L_2}{\partial x}, \tag{5.4}$$

where D is the diffusion coefficient and v is the velocity of desquamation.

Figure 5-13 provides a comparison of the predicted formation of a lithium reservoir in the SC for different values of diffusion coefficient, D, and for the diffusion- free system. From this we can see that the reservoir formation with the theoretical lithium diffusion coefficient is much more sensitive to plasma concentration oscillations; the reservoir is quicker to fill and more sensitive to change. For small non-zero diffusion we actually see an increase in time to reach steady state, this is consistent with the findings in the Chapter 3 exploration (Figure 3-10). Provided sufficient time has passed, the diffusion free case essentially gives the average reservoir size. It is unlikely that this degree of fluctuation would be detectable, but as discussed in Chapter 3 it may have a more significant impact when considering non-compliance.

5.3.3.3 Electroosmosis and diffusion in reverse iontophoresis

If we now alter the extraction model to include electroosmosis and diffusion we have

$$\frac{\partial L_3}{\partial t} = D\frac{\partial^2 L_3}{\partial x^2} - v_{RI}\frac{\partial L_3}{\partial x}$$

where $v_{RI} = v_{em} + v_{eo}$

We introduce sink conditions on the boundary at $x = L$,

$$L_3(x = L, t) = 0,$$

The re-inclusion of electroosmosis in the extraction of lithium is mathematically the same as increasing the electromigration as these both make up the advection term for extraction. This results in a shorter lag time and increased plasma extraction.

Due to the sink conditions at the skin surface, the re inclusion of diffusion during extraction increases the speed at which lithium is transported across the SC, the result of including diffusion is therefore similar to increasing the advection .

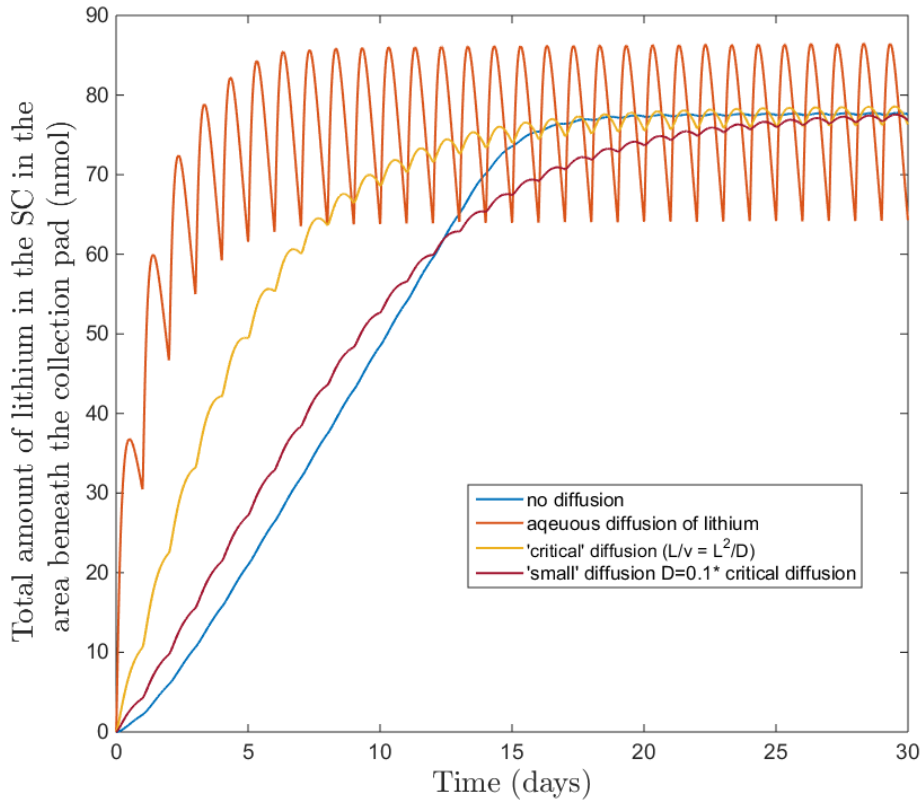

Figure 5-13: Reservoir size in the SC in the area directly beneath the collection pad predicted by equation (5.4) for different values of diffusion: (i) $D = 0$ (no diffusion, blue line); $D = 7588\mu m^2/day$ (aqueous diffusion coefficient of lithium, orange line); (ii) $D = \frac{1}{Lv}$ ('critical diffusion, yellow line); and (iii) $D = \frac{0.1}{Lv}$ (small diffusion, deep pink line).

5.4 Theoretical drug

The key parameters and mechanisms of interest identified in the previous chapters are binding and distribution of the reservoir between lipid and aqueous domains.

As mentioned previously, lithium does not bind. We therefore use a theoretical drug based on lithium data, with which we explore model mechanisms not applicable to lithium.

We are interested in the possibility of detecting non-compliance through reverse iontophoresis. We bring forward the four compliance scenarios and create reservoir and extraction predictions for various parameter sets to determine which, if any, drug properties allow for compliance to be clearly distinguished from the extraction predictions.

First we reintroduce binding in the SC and consider the reservoir formation in compliance scenarios a-d for a number of binding and diffusion values.

The reservoir formation model, as given in Chapter 3, is

$$\frac{\partial C_u}{\partial t} = D\frac{\partial^2 C_u}{\partial x^2} - v\frac{\partial C_u}{\partial x} + \mu C_b - \gamma C_u, \tag{5.5}$$

$$\frac{\partial C_b}{\partial t} = -v\frac{\partial C_b}{\partial x} - \mu C_b + \gamma C_u, \tag{5.6}$$

where $C_u(x,t)$ and $C_b(x,t)$ are the concentration in the SC ($mol/\mu m$) for unbound and bound forms of the theoretical drug, D is the diffusion coefficient, v is the speed of desquamation μ is the rate of unbinding and γ is the rate of binding.

As discovered in Chapter 3, the effects of binding during reservoir formation are intertwined with the effects of diffusion, as this is what differentiates movement of bound and unbound drug. We compare diffusion (of the magnitude predicted for lithium in water) and the diffusion-free case, and for each of these we consider $\gamma > \mu$ and $\gamma < \mu$.

This creates the four binding cases given in Table 5.2.

The resulting reservoir predictions for the binding sets 1-4 are given in Figures 5-14 to 5-17 respectively, for each compliance scenario (a)-(d). From comparison of these we can see that the ratio of bound to unbound drug in the reservoir is determined by the ratio of γ to μ. When considering bound and unbound drug, the magnitude of the unbound reservoir depends on the value of the diffusion coefficient chosen. A larger diffusion coefficient results in larger oscillations and larger reservoirs. This is because a large diffusion rate results in quick equilibration

Parameter set	D	γ	μ
Binding set 1	$7588\mu m^2 \text{day}^{-1\dagger}$	5day^{-1}	1day^{-1}
Binding set 2	$7588\mu m^2 \text{day}^{-1\dagger}$	1day^{-1}	5day^{-1}
Binding set 3	0	5day^{-1}	1day^{-1}
Binding set 4	0	1day^{-1}	5day^{-1}

Table 5.2: The four binding parameter sets used in Model 2 used with the L and v estimates given in table5.1. † theoretical diffusion coefficient calculated for lithium.

with plasma concentration and presence of binding acts as a 'storing mechanism,' so, as plasma concentration decreases (during daily fluctuations), drug which is 'stored' as bound drug doesn't diffuse to areas of low concentration. In Figures 5-14 and 5-15, at 12 hours after the day 30 dose, the predicted unbound reservoir size is similar for all four compliance scenarios with scenario b and c slightly lower than a and d. This is due to the high diffusion coefficient which means that reservoir size is quick to reflect plasma concentration change. In binding cases 3 and 4 shown in Figures 5-16 and 5-17 compliance could be easily distinguished with full knowledge of the reservoir size. Comparing Figures in 5-16 and 5-17 we see that a high rate of binding reduces the observable (unbound) reservoir.

5.4.1 Extraction

We wish to determine which parameter combination, if any, provide predictions for compliant and non-compliant patients that can be easily distinguished. This will help to identify potentially suitable drug candidates for this type of monitoring. For the extraction we consider the reservoir to be distributed between a lipid and aqueous domain and assume extraction is from the aqueous domain via electromigration, we therefore have the following equation for extraction

$$\frac{\partial C_{aq}}{\partial \tau} = -v_{em}\frac{\partial C_{aq}}{\partial x} - f(C_{aq}, C_{lip}), \tag{5.7a}$$

$$\frac{\partial C_{lip}}{\partial \tau} = f(C_{aq}, C_{lip}). \tag{5.7b}$$

where

$$f(C_{aq}, C_{lip}) = k_7(C_{aq} - f_{aq}(C_{lip} + C_{aq}))$$

with f_{aq} the fraction of drug in the aqueous domain at equilibrium and k_7 the rate at which drug moves between the lipid and aqueous domains.

The drug collected on the pad at $x = L$ is then given by

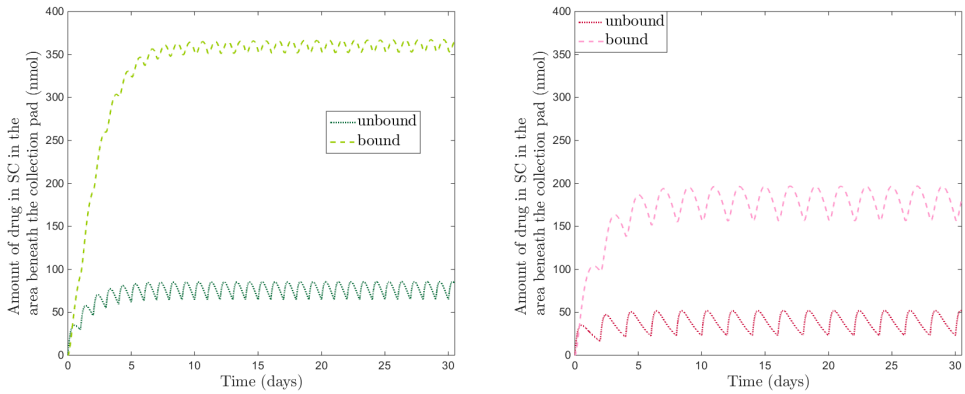

(a) Compliance scenario a

(b) Compliance scenario b

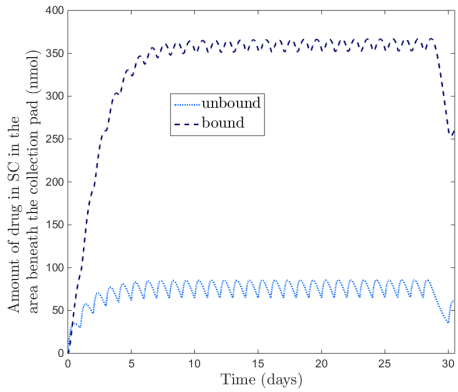

(c) Compliance scenario c

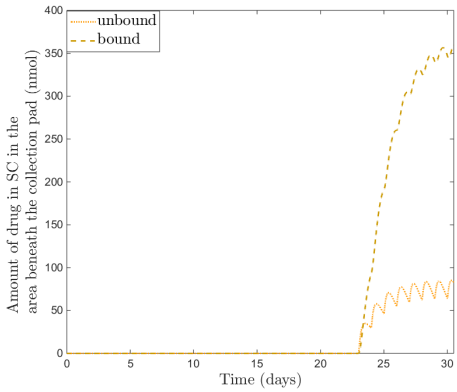

(d) Compliance scenario d

Figure 5-14: Predicted reservoir formation using binding parameter set 1, Table 5.2, presented for bound and unbound drug in each compliance scenario a-d as described in the text.

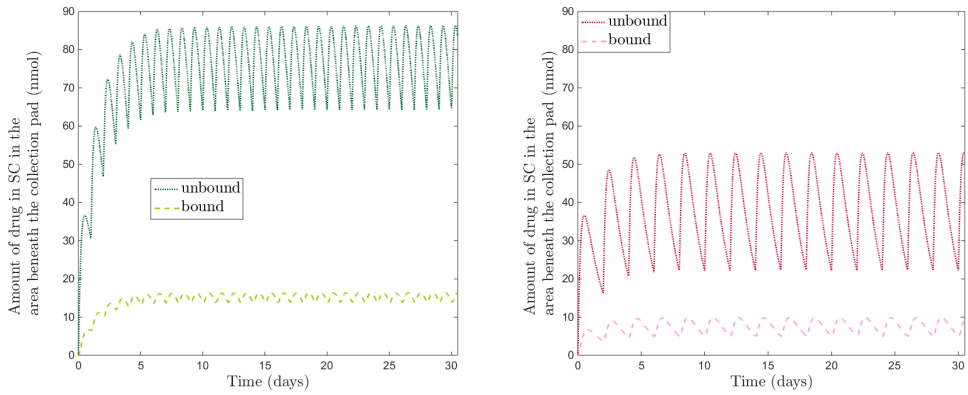

(a) Compliance scenario a

(b) Compliance scenario b

(c) Compliance scenario c

(d) Compliance scenario d

Figure 5-15: Predicted reservoir formation using binding parameter set 2, Table 5.2, presented for bound and unbound drug in each compliance scenario a-d as described in the text.

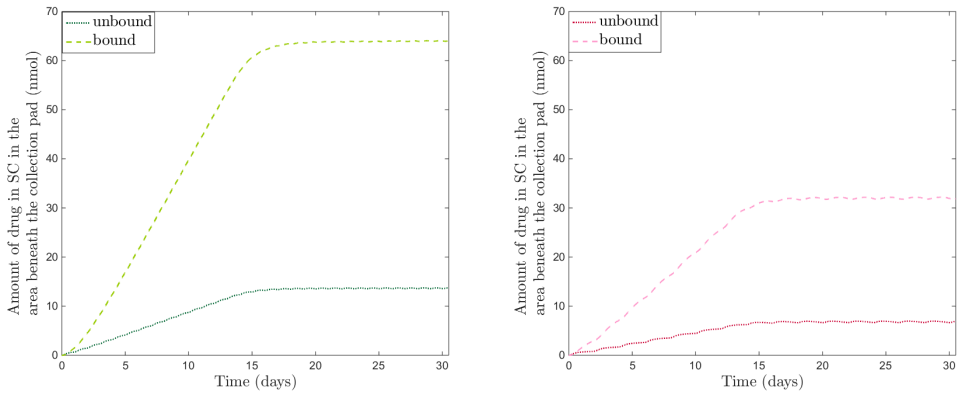

(a) Compliance scenario a

(b) Compliance scenario b

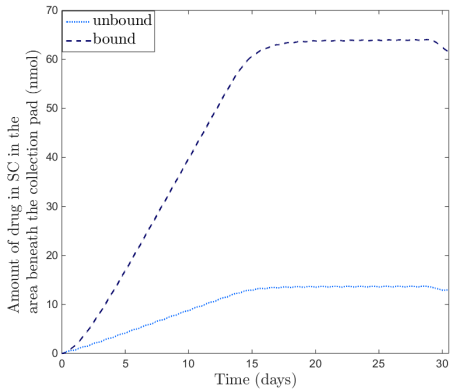

(c) Compliance scenario c

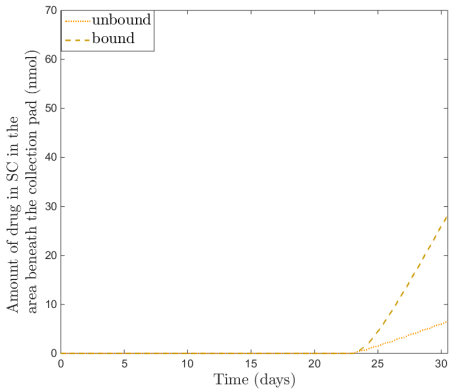

(d) Compliance scenario d

Figure 5-16: Predicted reservoir formation using binding parameter set 3, Table 5.2, presented for bound and unbound drug in each compliance scenario a-d as described in the text.

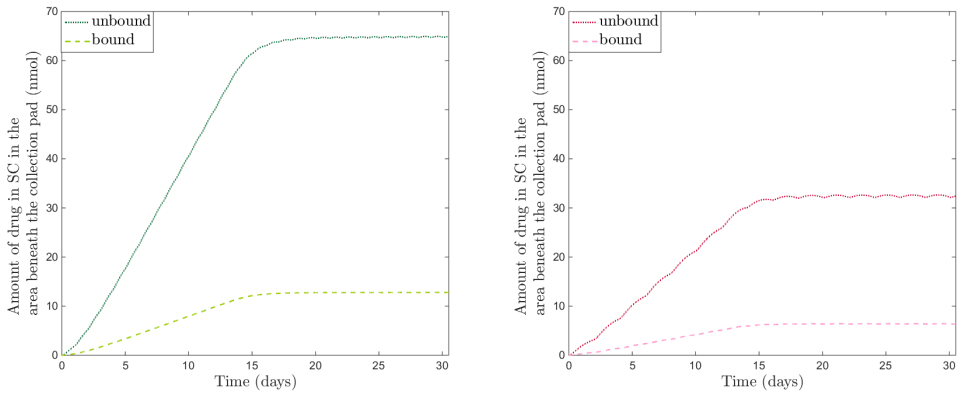

(a) Compliance scenario a

(b) Compliance scenario b

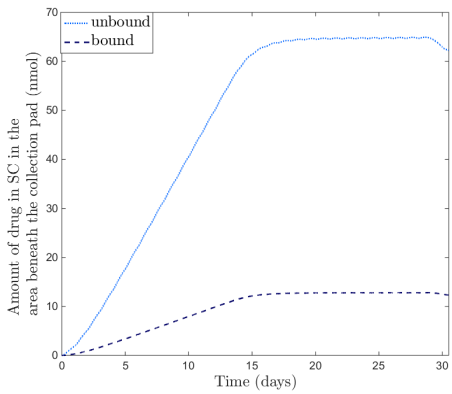

(c) Compliance scenario c

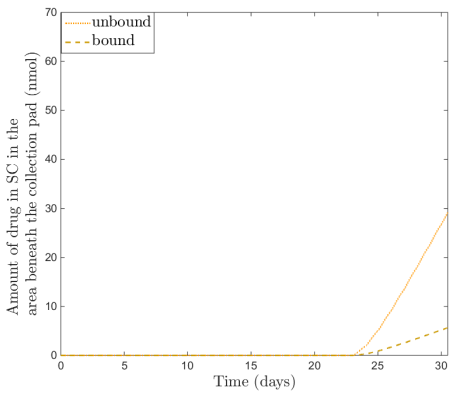

(d) Compliance scenario d

Figure 5-17: Predicted reservoir formation using binding parameter set 4, Table 5.2, presented for bound and unbound drug in each compliance scenario a-d as described in the text.

$$\frac{dC_{pad}}{d\tau} = \int_0^{\tau} J_{aq}|_{x=L}\, d\tau$$

where $J_{aq}|_{x=L}$ is the flux of ions from aqueous domain at $x = L$. As discussed previously, the location of the reservoir may significantly impact the way in which reservoir is extracted. We therefore consider two reservoir distributions; drug completely in the aqueous domain and drug distributed between aqueous and lipid domains with f_{aq}=0.1 (i.e. 10% of drug in aqueous domain at equilibrium). During extraction drug is removed from the aqueous domain and we assume that as this happens drug in the lipid domain will move into the aqueous domain in order to maintain f_{aq}. The rate at which this happens will affect the amount of drug available for extraction and the time in which it is extracted. We consider three values of k_7: 0.01, 0.1,1. Finally we construct initial conditions. Up until now we have assumed that drug in the reservoir is initially distributed between lipid and aqueous domains according to the value of f_{aq}. As described in Chapter 4 porous pathways 'open up' on application of a current. Therefore these porous pathways could be interpreted as a new space, initially containing no drug, which would mean that all drug is initially in the 'lipid' domain whilst maintaining that at equilibrium drug distributes between the domains according to f_{aq}. We therefore also explore both of these initial conditions in the following experiments.

Results have been presented in a series of 9 figures, each containing 6 sub figures.

Figures 5-18 - 5-20 take $f_{aq} = 1$, with reservoir initially in the lipid domain,

Figure 5-18: initial reservoir size determined using binding parameter set 1,

Figure 5-19: initial reservoir size determined using binding parameter set 3,

Figure 5-20: initial reservoir size determined using binding parameter set 4.

Results for the extraction of the reservoir resulting from binding parameter set 2 have been omitted as the unbound reservoir size for binding sets 1 and 2 were the same and so the same results were obtained.

The sub-figures show total collected and 30 minute cumulative extraction amounts in the four compliance scenarios taking three values for k_7, namely k_7=0.01,0.1 and 1.

This pattern is repeated with the next three figure sets. Figures 5-21 - 5-23 take f_{aq}=0.1, with reservoir initially in the lipid domain. Figure 5-24 - 5-26 take f_{aq}=0.1, with the reservoir initially distributed between the lipid and aqueous domain according to f_{aq}=0.1.

Effect of k_7 on predicted extraction From Figures 5-18 - 5-20 it is evident that for $f_{aq} = 1$, where drug is initially in the lipid, an increase in k_7 speeds up the availability of the reservoir and therefore a higher, earlier extraction of the reservoir is observed. However, when $f_{aq} = 0.1$, for both initial reservoir distributions, the opposite is observed as drug that is pulled through the SC from the plasma moves into the lipid domain and is not extracted. This unrealistic scenario is shown in Figures 5-21 - 5-26.

Effect of f_{aq} on predicted extraction For f_{aq}=0.1 (Figures 5-21 - 5-26) we notice a smaller extraction due to the reservoir of drug remaining in the lipid domain and in cases of high k_7 values, drug that is extracted from the plasma moving into lipid domains.

Effect of ICs on predicted extraction When drug is not initially in the pathway of extraction, a delay to extract the reservoir is observed dependent on k_7 and f_{aq}. Comparing Figures 5-21 with 5-24, 5-22 with 5-25, and 5-23 with 5-26 it can be seen that when some drug is initially in the pathway of extraction (IC distributed according to f_{aq}) that marginally more drug is extracted overall. It can also be seen that for small values of k_7 the difference between compliant and non-compliant extraction is more significant when the whole drug reservoir is initially in the lipid. However, as we have already mentioned, the results in Figures 5-21 - 5-26, wheref_{aq}=0.1, suggest that drug that is pulled through the SC from the plasma by reverse iontophoresis gets stuck in the SC. We do not believe this to be realistic and so any conclusions about initial conditions based on these results should be made cautiously.

Compliance The only parameter set in all of these graphs where different compliance scenarios gave distinct qualitative extractions is for parameter set: f_{aq}=1, k_7=1, binding parameter set 4: $D = 0, \gamma = 1, \mu = 5$, Figure 5-20, i.e. the scenario where drug is most available. This is because in all other cases the release/extraction of the reservoir is moderated by the release from the lipid domain and so differences in reservoir size are masked.

5.4.2 Optimal drug properties for extraction

The movement mechanism which dominates during reverse iontophoresis for a drug molecule is dependent on properties such as valency (charge), ionisation, size, and implicitly, on characteristics such as lipophilicity. It can be seen from transport number equations that species with larger valency are better charge carriers and so

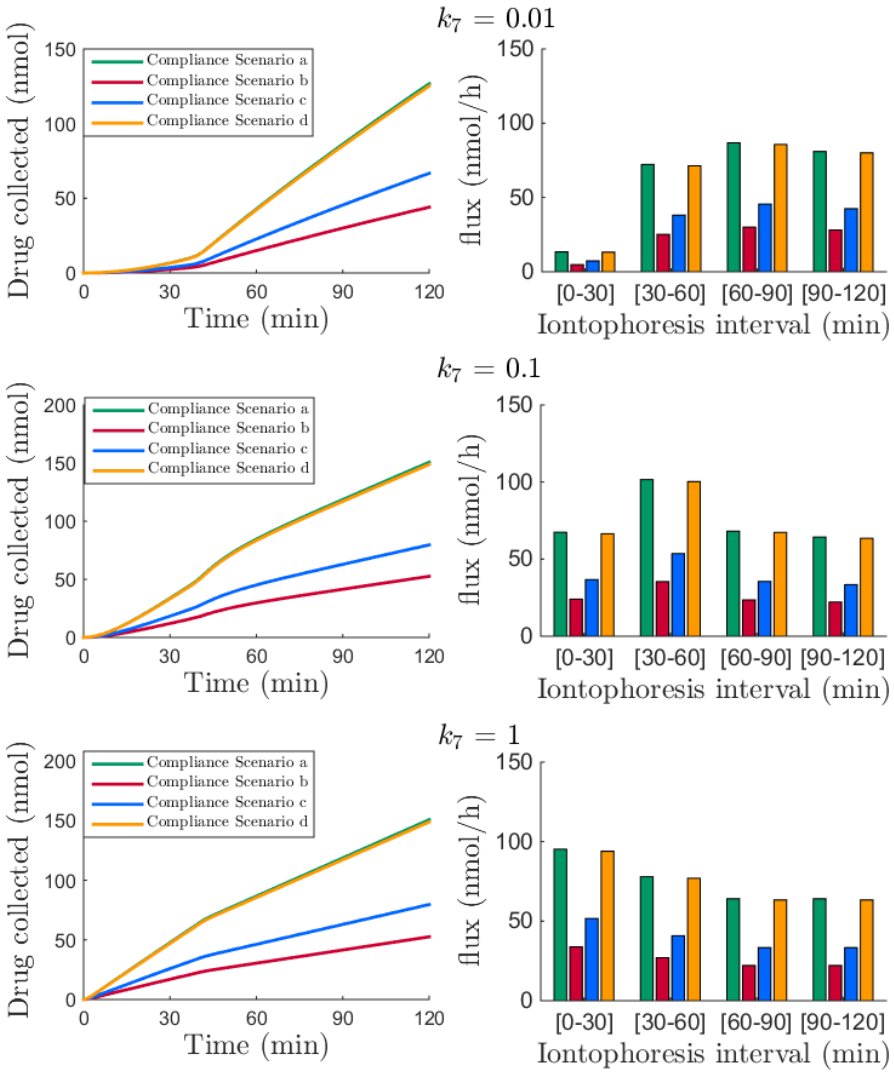

Figure 5-18: Extraction of reservoirs for compliance scenarios a-d as predicted by binding set 1 (Figure 5-14) with extraction parameters given by $f_{aq} = 1$, with whole reservoir initially in the lipid domain at the start of extraction shown for k_7=0.01,0.1 and 1

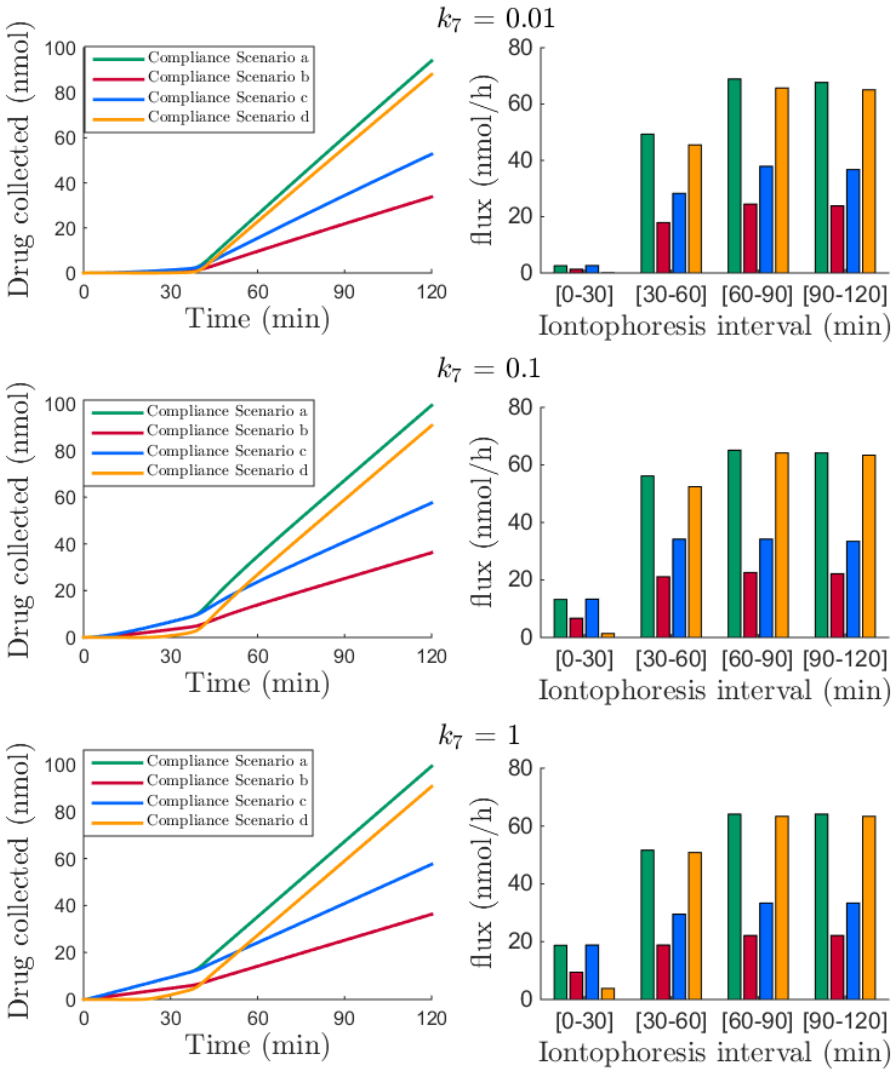

Figure 5-19: Extraction of reservoirs for compliance scenarios a-d as predicted by binding set 3 (Figure 5-16) with extraction parameters given by $f_{aq} = 1$, with whole reservoir initially in the lipid domain at the start of extraction shown for k_7=0.01,0.1 and 1

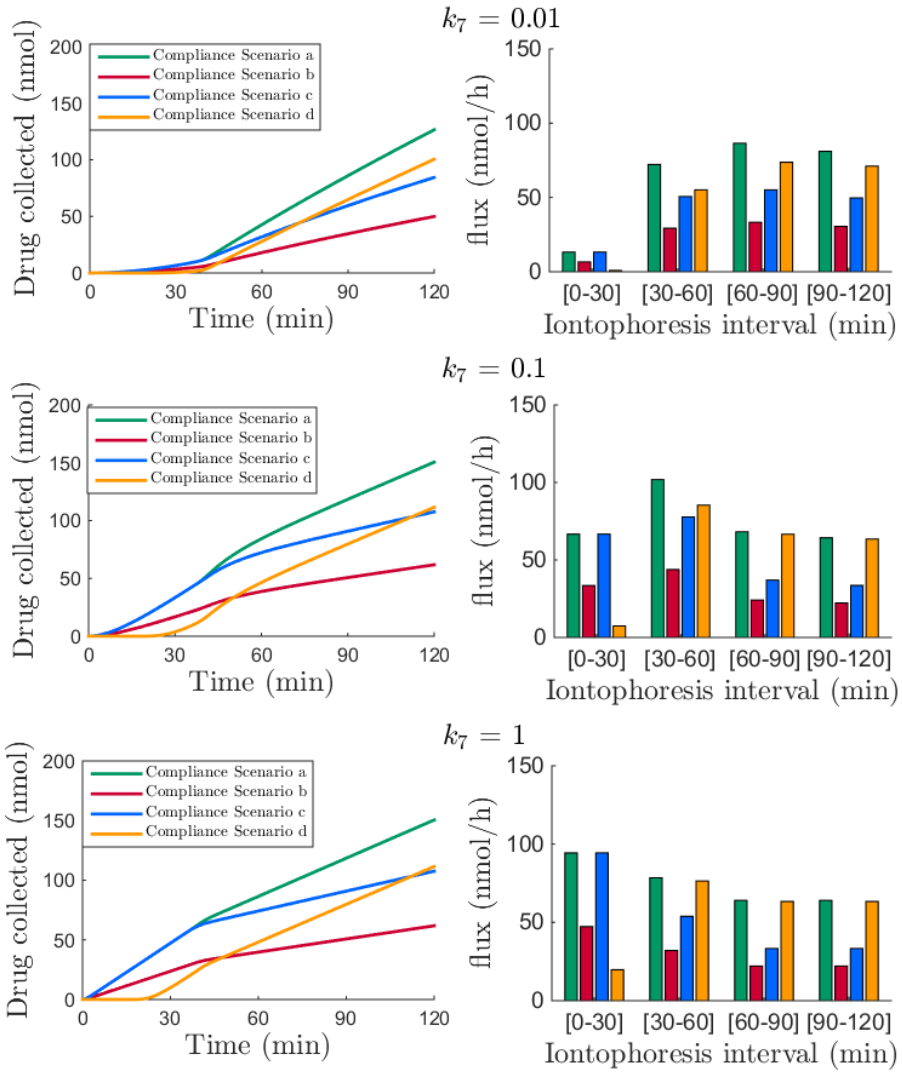

Figure 5-20: Extraction of reservoirs for compliance scenarios a-d as predicted by binding set 4 (Figure 5-17) with extraction parameters given by $f_{aq} = 1$, with whole reservoir initially in the lipid domain at the start of extraction shown for k_7=0.01,0.1 and 1

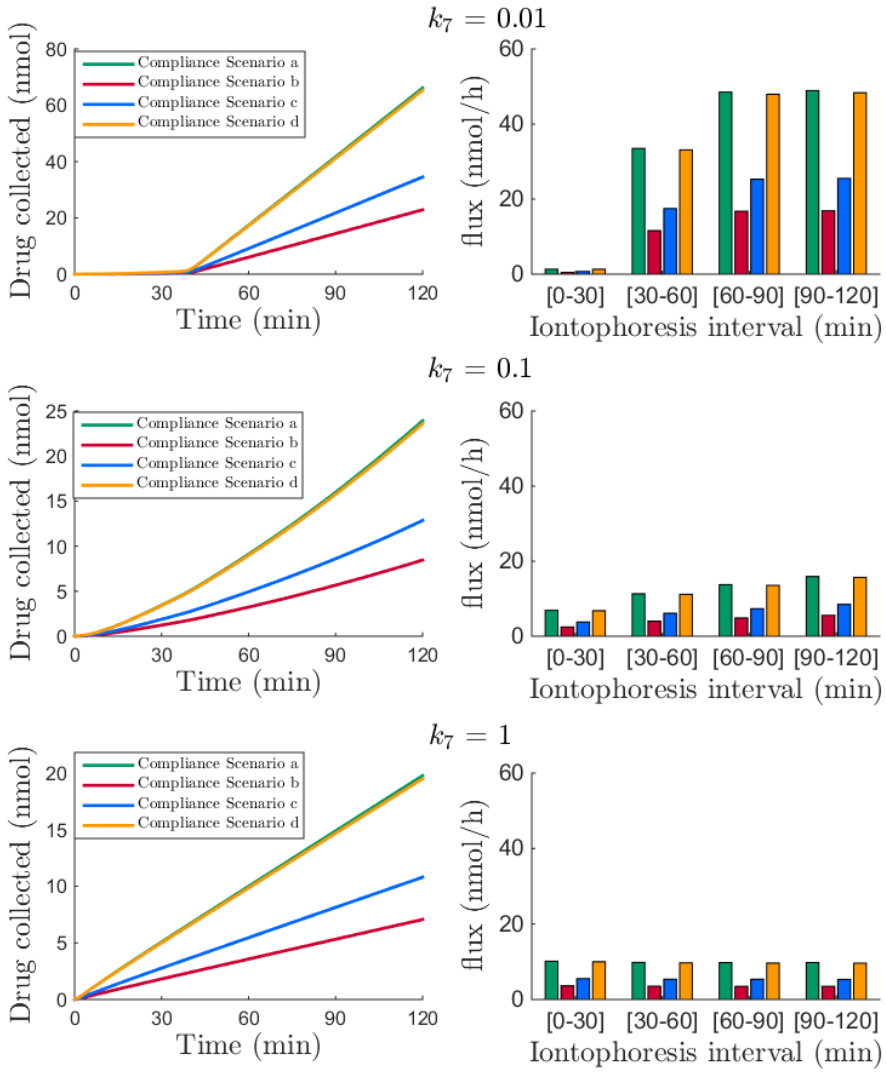

Figure 5-21: Extraction of reservoirs for compliance scenarios a-d as predicted by binding set 1 (Figure 5-14) with extraction parameters given by $f_{aq} = 0.1$, with whole reservoir initially in the lipid domain at the start of extraction shown for k_7=0.01,0.1 and 1

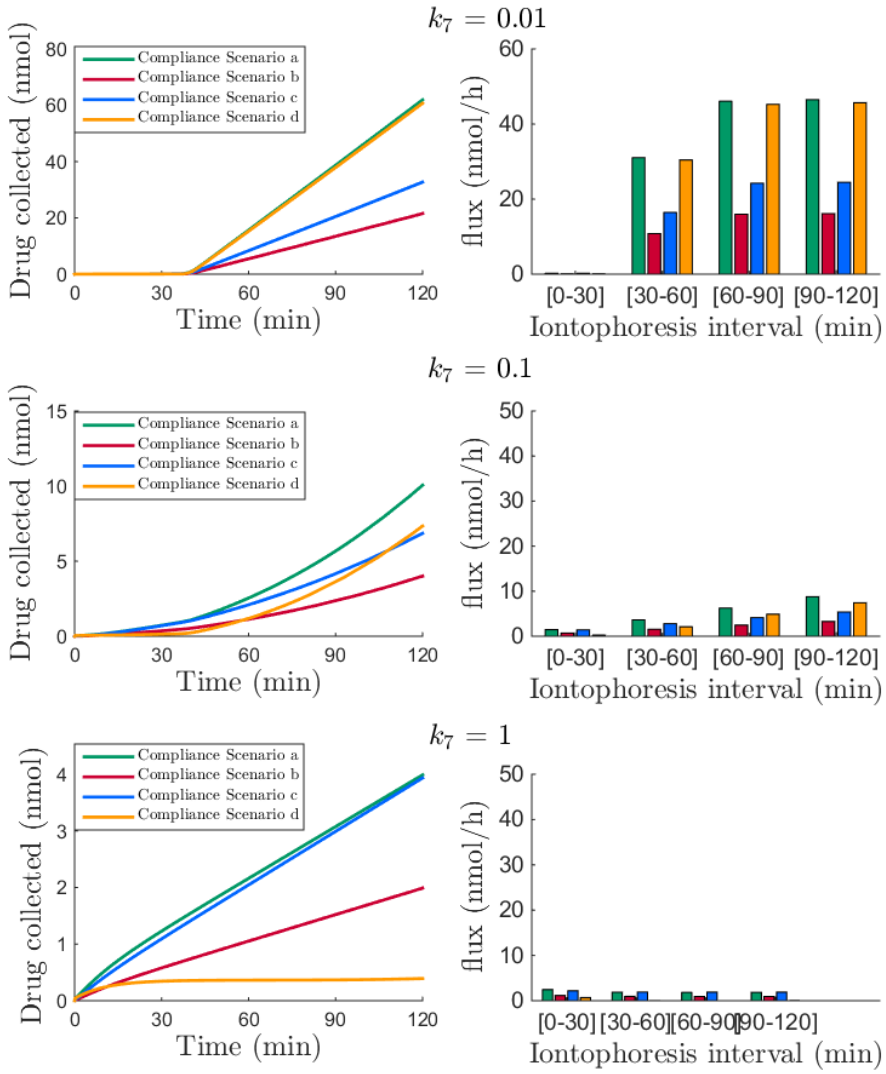

Figure 5-22: Extraction of reservoirs for compliance scenarios a-d as predicted by binding set 3 (Figure 5-16) with extraction parameters given by $f_{aq} = 0.1$, with whole reservoir initially in the lipid domain at the start of extraction shown for k_7=0.01,0.1 and 1

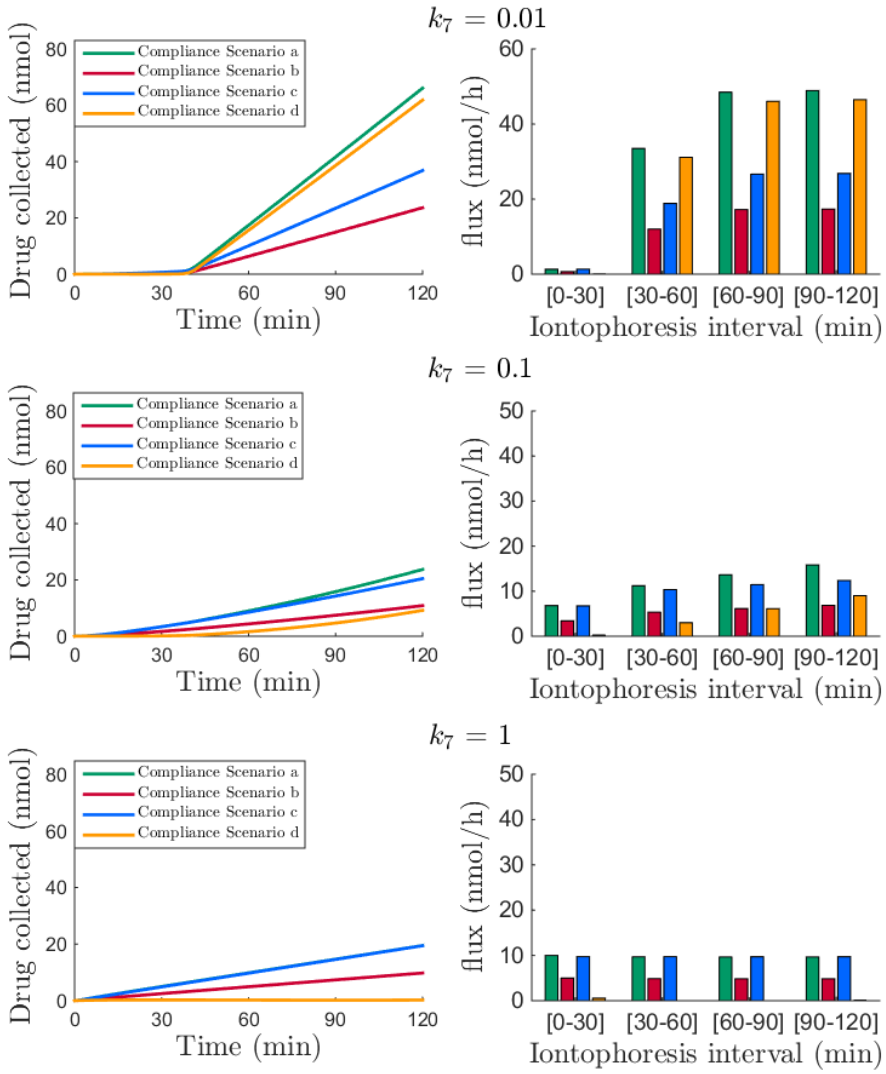

Figure 5-23: Extraction of reservoirs for compliance scenarios a-d as predicted by binding set 4 (Figure 5-17) with extraction parameters given by $f_{aq} = 0.1$, with whole reservoir initially in the lipid domain at the start of extraction shown for k_7=0.01,0.1 and 1

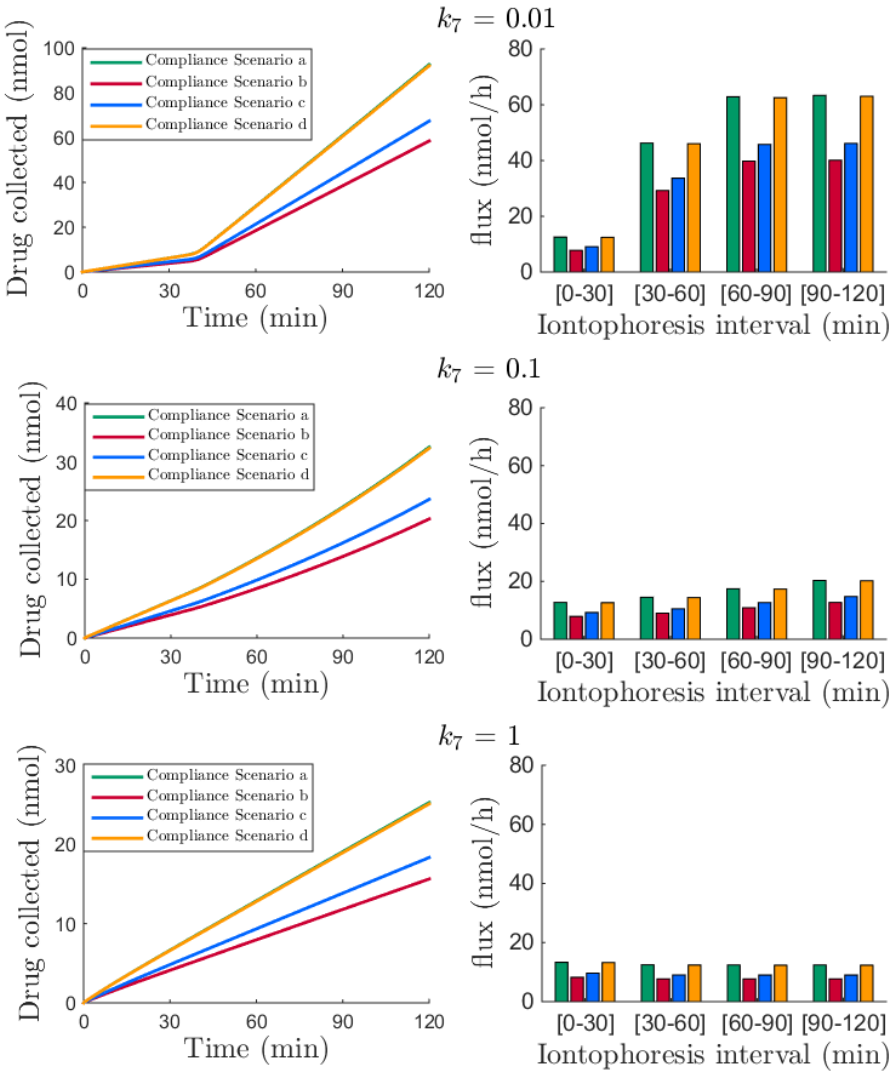

Figure 5-24: Extraction of reservoirs for compliance scenarios a-d as predicted by binding set 1 (Figure 5-14) with extraction parameters given by $f_{aq} = 0.1$, with the reservoir initially distributed between the lipid and aqueous domains according to f_{aq} at the start of extraction shown for k_7=0.01,0.1 and 1

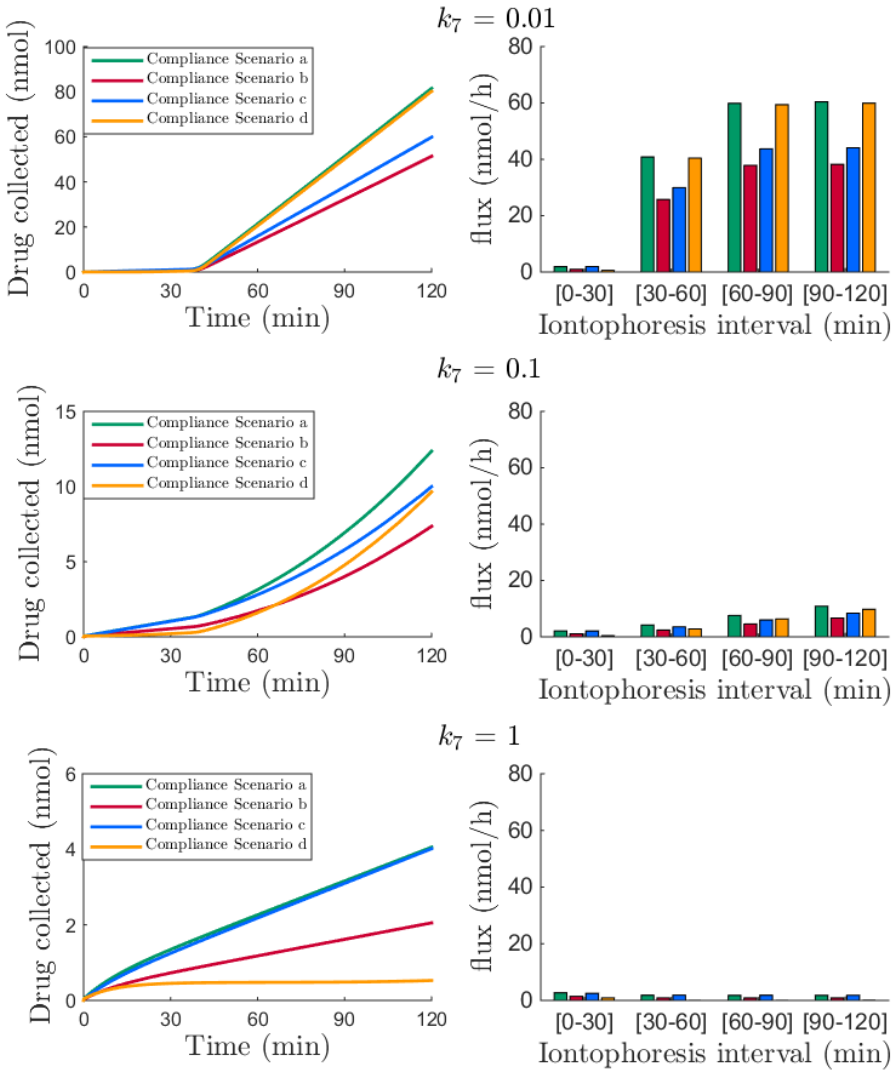

Figure 5-25: Extraction of reservoirs for compliance scenarios a-d as predicted by binding set 3 (Figure 5-16) with extraction parameters given by $f_{aq} = 0.1$, with the reservoir initially distributed between the lipid and aqueous domains according to f_{aq} at the start of extraction shown for k_7=0.01,0.1 and 1

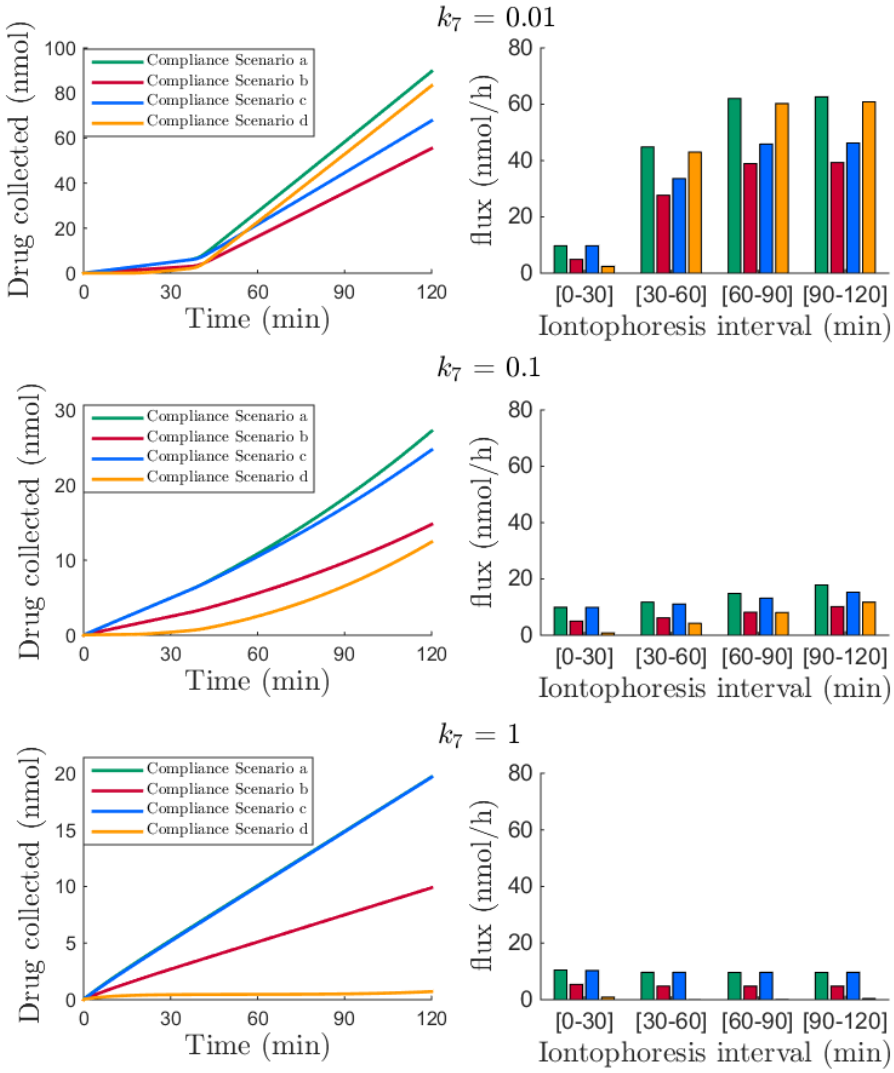

Figure 5-26: Extraction of reservoirs for compliance scenarios a-d as predicted by binding set 4 (Figure 5-17) with extraction parameters given by $f_{aq} = 0.1$, with the reservoir initially distributed between the lipid and aqueous domains according to f_{aq} at the start of extraction shown for k_7=0.01,0.1 and 1 . Note scenario (a) is overlayed by scenario (c) on the 5th graph.

have higher transport number, therefore presenting strong competition. However electromigratory flux is inversely proportional to valence and so optimal delivery is for a monovalent ion [104].

If we consider the equation for ion mobility

$$\mu_i = \frac{z_i e}{6\pi\eta r_i}$$

where η is the viscosity of the SC, r_i is the radius of the ion and z_i is the valency, it is clear to see that small ions are more mobile and are therefore expected to have a greater electromigratory flux. However, there is a link between diffusion coefficient and mobility of an ion,

$$D_i = \frac{\mu_i kT}{z_i e}.$$

We want our ion to be highly mobile during the extraction phase so that we have optimal electromigration. We have shown that diffusion of unbound drug during the reservoir formation is disadvantageous for compliance monitoring as we want a drug to enter the SC and stay put.

5.5 Conclusion and further work

In this chapter we have combined the work from the previous three chapters to create a full model; from drug administration to reservoir formation and extraction via reverse iontophoresis. We began by altering the model system for the case of lithium where reverse iontophoresis data is available for chronically dosed patients. Using parameter estimates from the literature our model gave reasonable agreement with the lithium data, however, without further adaption of the model, the true nature of the lag time was not captured. Three different solutions were explored: reduction of the velocity due to electromigration; increased tortuosity for extraction path length; and the division of the reservoir into a lipid and aqueous domain so that not all drug in the reservoir is immediately available for extraction. Any one or combination of these methods improves model fit but in order to determine the scenario which best reflects reality more data are needed; specifically continuous time data for reverse iontophoresis which would give an insight into the way in which a drug reservoir is drained from the SC.

We went on to investigate the inclusion of other model mechanisms in reservoir formation and extraction. We found that in order for a reservoir to contain the maximal information on drug history (14 days) that a small diffusion coefficient is needed. We also found that the presence of binding had potential to increase the

total (bound + unbound) reservoir but had only a small impact on the magnitude of unbound (extractable) reservoir if diffusion was present, consistent with the exploration in Chapter 3. The preference for a drug with small diffusion coefficient must be balanced with the demand for a highly mobile drug (i.e. high diffusion coefficient) for efficient extraction via reverse iontophoresis.

Two possibilities for the location of the reservoir prior to extraction were considered. The default assumption is that drug would be distributed between lipid and aqueous domains according to the equilibrium distribution (f_{aq}). However, it is thought that porous pathways open up on application of a current and so this scenario was recreated by reservoir being completely located in the lipid domain prior to extraction. On comparison with the default distribution we found that if drug does not start in the pathway of the drug that this leads to less drug collected overall. However, as we don't believe results offer realistic predictions for some of the parameter sets used, we restrain from concluding anything about the distribution prior to extraction.

The research in this chapter demonstrates the potential for drug presence in the skin to determine patient compliance to a drug regimen. However, more data are needed to determine extraction profiles which are realistic for an individual drug. Parameter estimates are difficult to obtain experimentally. Without accurate estimates of parameter values there is no way of knowing if the reservoir is completely emptied or not. Continuous time data could provide a much needed insight, as could a comparison between whole skin sampling (biopsy or tape stripping) and reverse iontophoretic extraction from the same patient. This is explored further in Chapter 6.

Chapter 6

Tape Stripping

6.1 Introduction

Although reverse iontophoresis is an established technique, there is not a great deal of usable (in vivo) data available in the literature to develop and validate mathematical models. As described in Chapter 5, in order to improve interpretation of experimental work in reverse iontophoresis a number of unknowns need to be determined. Much of this could come from more reverse iontophoresis data with different extraction time frames, but this does not guarantee determination of parameters or unknown factors, such as where in the SC the reservoir resides. In this chapter we explore alternative skin sampling techniques and investigate their potential for use in monitoring and to provide further insight into parameter values linked to reverse iontophoresis and reservoir formation.

6.2 Skin Analysis Techniques

Skin sampling provides potential for diagnosis of a number of local skin conditions (such as eczema, psoriasis and cancer) and of diseases associated with internal organs as well as detection of topical and systemic administered drugs [142]. There are a number of ways in which skin sampling can be carried out. These can be classified into three categories:

i) harvesting of epidermal constituents by minimally invasive methods, such as reverse iontophoresis, electroporation, ultrasound or suction blisters[143];

ii) direct collection of skin tissue by punch or shave biopsy, followed by liquification of the sample [144, 141]; and

iii) tape stripping.

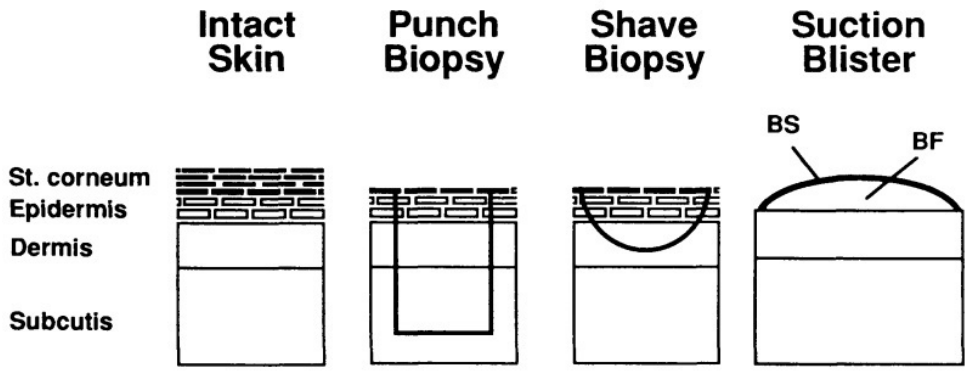

Figure 6-1: A schematic showing intact skin and three sampling techniques. BS, blister skin; BF, blister fluid. Taken from [141]

i) Such minimally invasive methods include reverse iontophoresis which has been the focus of much of this thesis. Electroporation uses pulses of high voltage to increase skin permeability by opening pores, which is sometimes done in conjunction with other transdermal delivery and sampling techniques including iontophoresis [145]. Ultrasound works in a similar way; low frequency ultrasound is used to produce micro-pores in the stratum corneum. In the suction blister technique, blisters are artificially induced causing the epidermis to detach from the underlying dermis. The induced blister then fills with fluid from the surrounding tissue which is extracted with a syringe for analysis (Figure 6-1).

ii) A punch biopsy is taken by rotating a circular blade into the skin to the depth of the sub-cutis to obtain a specimen which is lifted and cut from the site with scissors (Figure 6-1). A shave biopsy is usually taken using a scalpel and samples the skin to the depth of the dermis (Figure 6-1). Whilst these sampling techniques are valuable in disease diagnosis, the invasive nature of biopsies limits routine clinical adoption. Such skin sampling has been used post mortem in cases of overdose [146]. Post mortem data may prove valuable in determining the location and nature of a drug reservoir in the skin but previous drug history of the individual is unlikely to be known with any certainty.

iii) Tape stripping is comparatively quick and non-invasive. Though the practice of tape stripping has been criticised for lack of standardised protocol [142], it is the most practical way of collecting the whole reservoir ethically.

We therefore focus our efforts on verification of reverse iontophoresis via comparison with tape stripping.

6.3 Tape Stripping

One technique to take a sample from the SC is the use of appropriate adhesive tape to 'tape strip' an area. This involves sequentially applying pieces of tape to a chosen area of the skin and removing them to collect the surface layers of SC. The SC is then removed from the tape using a solvent and these SC samples can be tested for the presence of a given substance.

The amount of SC removed is typically determined by weighing the tape strips before and after the strip process. Using the area of the tape and taking the density of the SC as 1g/cm^3 [147] the depth of the sample can be determined. Alternative methods for determining depth of the SC removed, such as a colorimetric method, are also available but due to cost weighing is typically used [148].

To quantify the presence of a specific substance in the sample the SC must first be removed from the tape with a solvent. An appropriate assay is then carried out for the chosen drug. The limit of quantification for many of these tests, however, means that unless the concentration of drug present is sufficiently high the drug may go undetected.

We are interested in relating the observed reservoir from tape strips to the actual reservoir size in order to make inferences about systemic drug levels and therefore drug dosage. We therefore want to determine how large a reservoir must be before it is detectable and, if the selected drug is detected, how the amount of drug retrieved relates to the reservoir size.

Assuming all drug in the stratum corneum (bound and unbound in the lipid and aqueous domain) is collected on, and then removed from, tape during the tape stripping process then, for a reservoir with distribution in the SC given by

$$\underline{C} = C_u(x) + C_b(x),$$

we expect to retrieve

$$\int_{L-d}^{L} \underline{C} dx \cdot A \cdot m_r \tag{6.1}$$

where A is the area sampled, to a depth d, m_r is the molecular mass of the drug and $\underline{C}$ is the reservoir concentration profile for bound + unbound drug. Therefore, if we have a limit of quantification Q, in order to obtain a sufficient sample size for a drug to be detected we would need to strip an area of size

$$A_Q = \frac{Q}{\int_{L-d}^{L} \underline{C} dx \cdot m_r}. \tag{6.2}$$

We aim to discover if the values of unknown parameters such as f_{aq}, k_7, D, γ and μ could be determined through comparative tape stripping and reverse iontophoresis results, and if so, which experiments would need to be carried out.

To give an idea of the kind of insight that comparison with tape stripping could provide, we continue using the 'theoretical drug' discussed in Chapter 5. We continue to consider the binding parameter sets 1-4 for Model 2, Table 5.2.

For the iontophoretic extraction we consider two values of f_{aq} with drug initially distributed according to these values and with $k_7 = 0.1$.

For ethical reasons tape stripping is usually carried out until the trans-epidermal water loss (TEWL) reaches a critical value, at which point further tape stripping may cause pain and more permanent damage to the skin [149]. This is usually at about a depth of 75% of total SC depth. We assume that tape stripping achieves complete extraction of the SC reservoir to this depth. Results given are for a tape stripped area of $3.2cm^2$ so that the same area is sampled in both reverse iontophoresis and tape stripping. Of course in practice a larger area could be sampled to fulfil the requirement of equation (6.2) and then rescaled for comparison.

Fully compliant case:

We begin by considering the fully compliant case. Figures 6-2 - 6-5 show the results for binding parameter sets 1-4 respectively. The top sub-figure in each figure shows the spatial reservoir at $t = 30.5$days for bound and unbound drug in the SC for $x \in [0, L]$, where L is the skin surface. The second sub figure gives the predicted iontophoretic flux in each interval as would be observed experimentally. The final sub-figure compares the total extraction (approximated to be all drug extracted during the first hour) in each iontophoresis case and the extraction for tape stripping.

From these results it can be seen that for scenarios where there is more bound drug in the reservoir, tape stripping gives higher readings than both reverse iontophoresis extractions, Figure 6-2. However, where the reservoir is made up of mostly unbound drug, in the cases where f_{aq}=1, i.e. where all unbound drug is available for extraction, predicted extraction by reverse iontophoresis is higher than tape stripping. This could arise in two ways: as tape stripping only retrieves drug in the surface 75% of the SC, and the whole unbound reservoir is retrieved by reverse iontophoresis when $f_{aq} = 1$, then if the unbound reservoir is that much larger than the bound reservoir then the extraction via reverse iontophoresis will be higher. Alternatively, as the predicted extraction for reverse iontophoresis

includes all drug extracted within the first hour, after the first 30 minute interval, a significant amount of that is likely to come from the plasma.

We therefore construct the following dose regimen in which drug is administered for 23 days and then withdrawn for 7 days before extraction (on day 30). This allows a reservoir to build up in the SC in days 1-23 and drug to clear from the plasma in the last 7 days without depleting the reservoir completely. The plasma profile resulting from this dose regimen is given in Figure 6-6. Then for each binding parameter set 1-4, we give in Figures 6-7 - 6-10, the predicted spatial reservoir 30.5 days after the initial dose, along with the predicted reverse iontophoretic extraction for f_{aq}=0.1 and f_{aq}=1, and the predicted drug collected from tape stripping.

Most notable when considering the 7 day abstinence case, is the significant reduction in reservoir size for the binding parameter sets 1 and 2, with high diffusion in reservoir formation. In fact, the comparison of a fully compliant reading to a 7 day placebo reading would provide a good idea of how quickly the reservoir empties and therefore a measure of the potential for historic monitoring.

In Figure 6-8 (binding set 2) we again predict a higher reading for reverse iontophoresis (when f_{aq}=1) than for tape stripping. As there is no drug extracted from the plasma this result would indicate that, due to diffusion, the reservoir is fairly evenly distributed in the SC and that a significant portion of it is unbound and so the disparity comes from the fact that tape stripping only retrieves the surface 75%. Comparing Figure 6-7 with 6-8, and Figure 6-9 with 6-10 it can be seen that a bigger difference is observed between reverse iontophoresis and tape stripping when the reservoir is mostly bound.

Comparison of tape stripping and reverse iontophoresis can give an estimate of the percentage of the reservoir available for extraction by reverse iontophoresis. This dosing regimen described provides an opportunity to view the reservoir separately from the plasma. However, the experiments suggested by these numerical simulations may be difficult to recreate in vivo for ethical reasons. Moreover, the reservoir size is significantly reduced (especially when diffusion is present) and so may not be detectable with procedures currently available. An alternative solution would be to take the empty-reservoir extraction from a drug-naive patient after a single dose and compare to a full-reservoir (compliant) extraction of the same patient so that the drug concentration relating to reservoir size could be identified.

6.4 Conclusion

In this chapter we have provided comparative results for reverse iontophoresis and tape stripping of the reservoir for two dose regimens for a range of parameter sets for Models 2 and 3.

As both bound and unbound drug in the lipid and aqueous are collected via tape stripping, it may appear to be a preferable extraction technique to reverse iontophoresis. However, tape stripping can be a long, arduous procedure to prepare for and process, and the experience can be uncomfortable for the patient. It is therefore more likely that tape stripping could be used to provide a method to identify parameters relating to the iontophoretic extraction.

We conclude that comparative tape stripping could provide valuable insight into the nature of the reservoir; reverse iontophoresis is only able to extract drug that is unbound and in the pathway of the current, whereas tape stripping is able to extract the whole reservoir to a depth of 75% of the SC. We believe the most valuable data would be for a situation where reservoir extraction via reverse iontophoresis could be isolated from plasma extraction either by using the compliance scenario described (which risks reservoir being too small) or by taking the empty-reservoir extraction from a drug naive patient and comparing to a full-reservoir (compliant) extraction of the same patient so that drug relating to reservoir size could be identified.

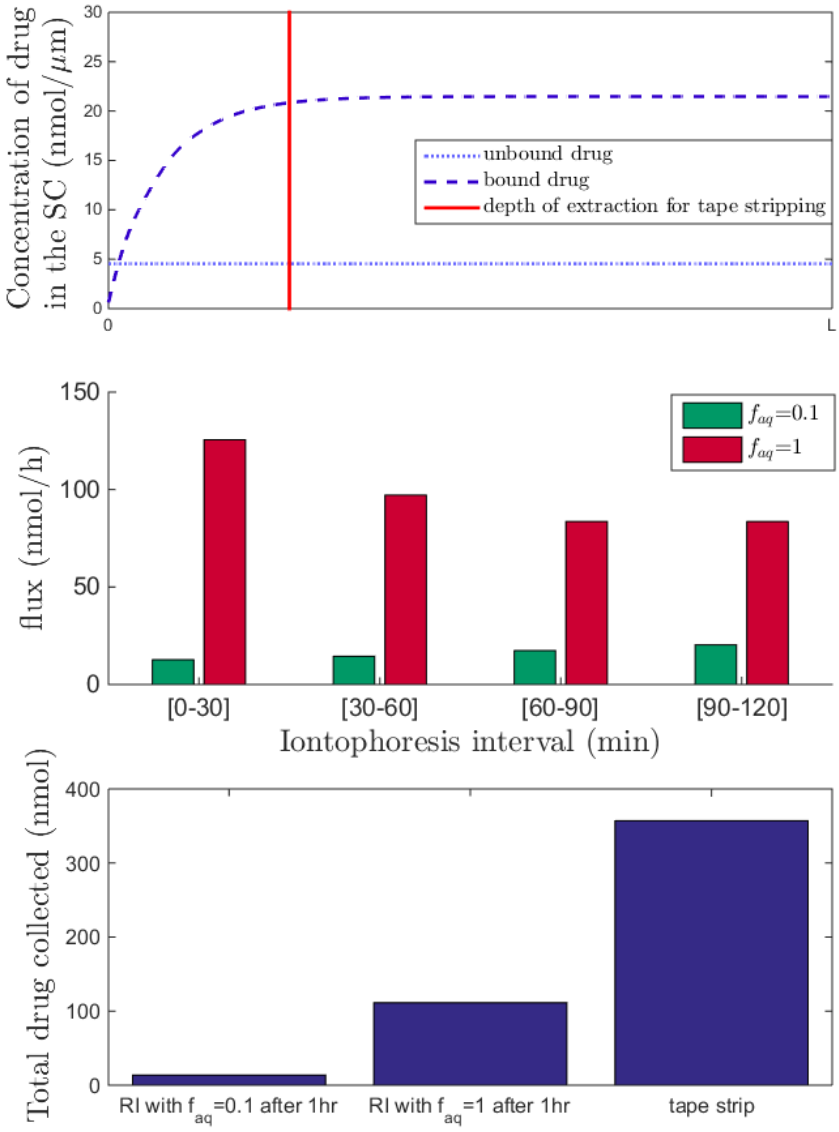

Figure 6-2: The predictions in this figure are for the fully compliant case using binding parameter set 1 for Model 2. (Top) the predicted spatial reservoir at $t = 30.5days$ for the fully compliant case with binding parameter set 1, where L is the skin surface. The vertical red line shows the depth of the tape stripping. (Middle) Predicted iontophoretic extraction flux in each interval for f_{aq}=0.1 and f_{aq}=1 with k_7=0.1 and drug distributed according to f_{aq} at the beginning of extraction. (Bottom) The extraction in the first hour of each iontophoresis case and total extraction via tape stripping.

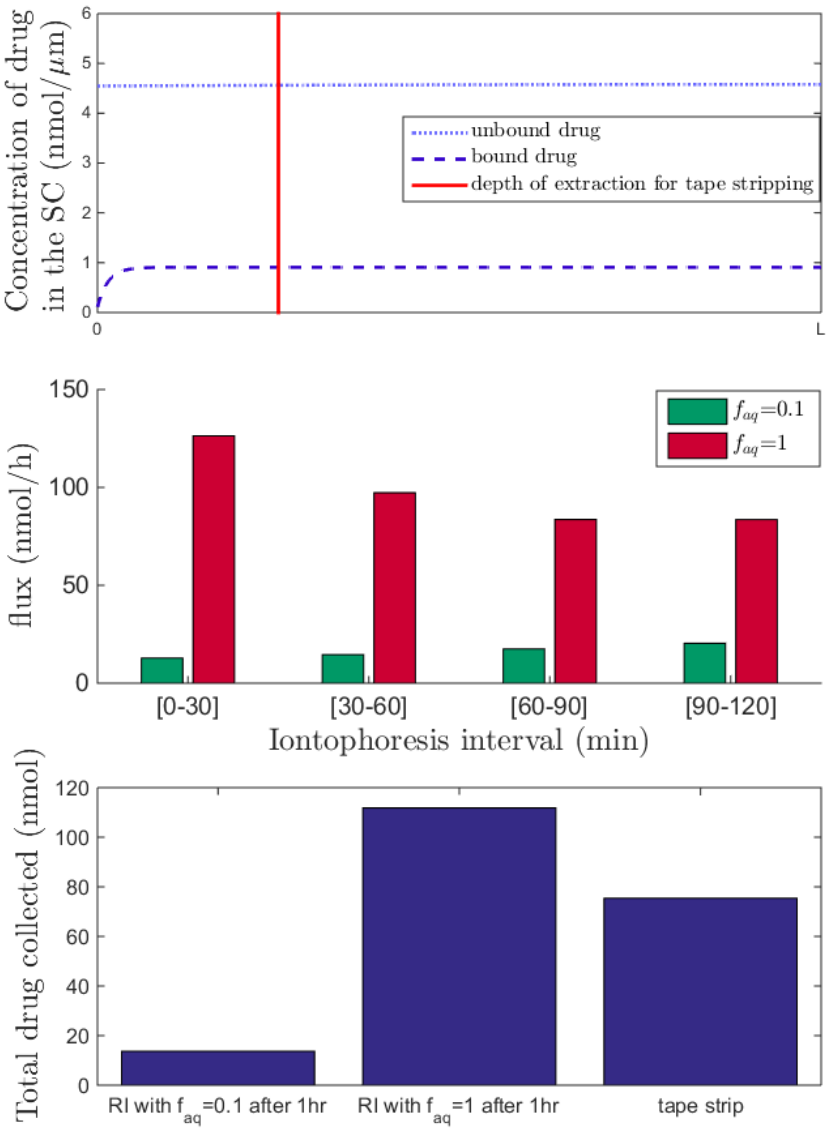

Figure 6-3: The predictions in this figure are for the fully compliant case using binding parameter set 2 for Model 2. (Top) the predicted spatial reservoir at $t = 30.5 days$ for the fully compliant case with binding parameter set 2, where L is the skin surface. The vertical red line shows the depth of the tape stripping. (Middle) Predicted iontophoretic extraction flux in each interval for f_{aq}=0.1 and f_{aq}=1 with k_7=0.1 and drug distributed according to f_{aq} at the beginning of extraction. (Bottom) The extraction in the first hour of each iontophoresis case and total extraction via tape stripping.

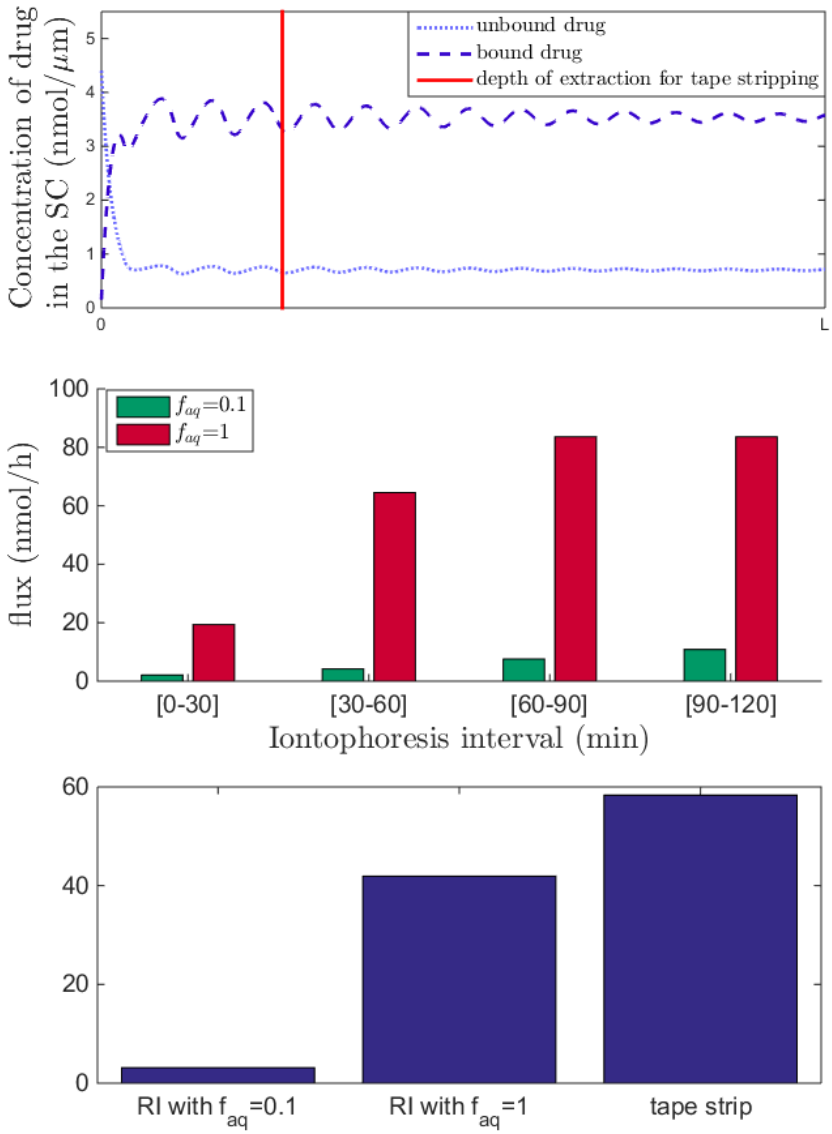

Figure 6-4: The predictions in this figure are for the fully compliant case using binding parameter set 3 for Model 2. (Top) the predicted spatial reservoir at $t = 30.5 days$ for the fully compliant case with binding parameter set 3, where L is the skin surface. The vertical red line shows the depth of the tape stripping. (Middle) Predicted iontophoretic extraction flux in each interval for f_{aq}=0.1 and f_{aq}=1 with k_7=0.1 and drug distributed according to f_{aq} at the beginning of extraction. (Bottom) The extraction in the first hour of each iontophoresis case and total extraction via tape stripping.

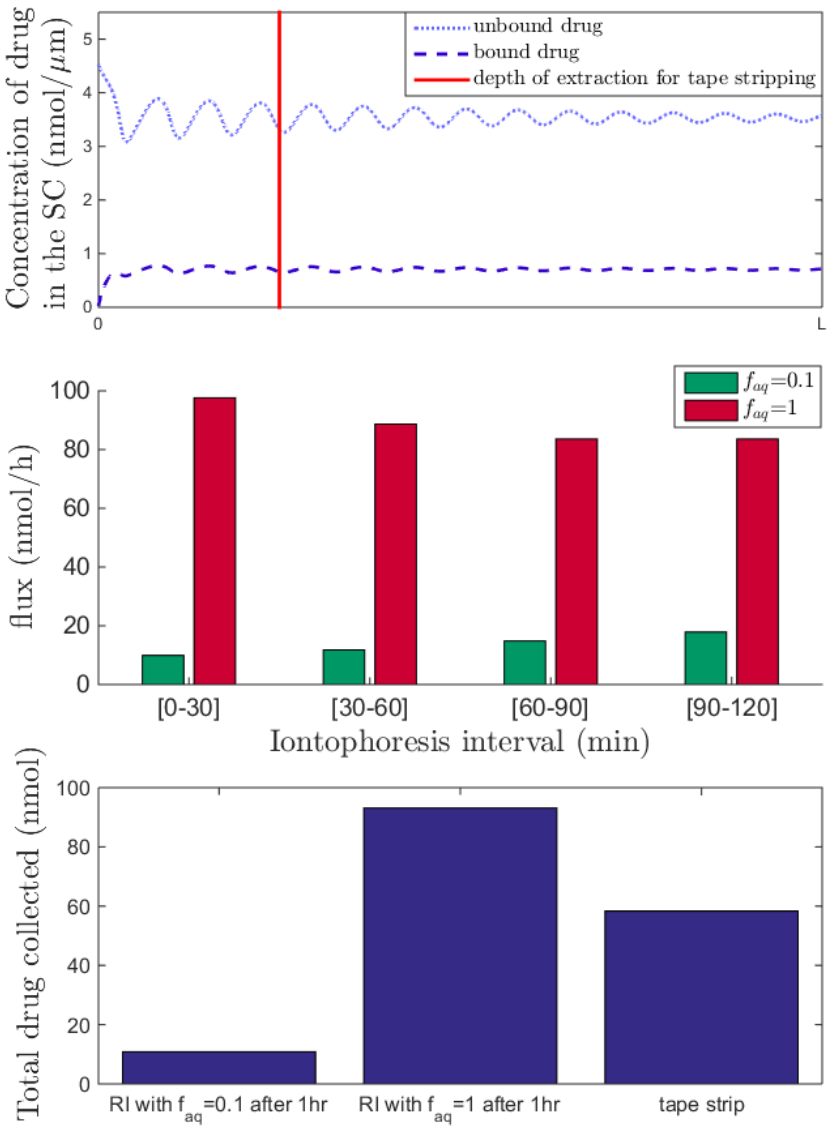

Figure 6-5: The predictions in this figure are for the fully compliant case using binding parameter set 4 for Model 2. (Top) the predicted spatial reservoir at $t = 30.5days$ for the fully compliant case with binding parameter set 4, where L is the skin surface. The vertical red line shows the depth of the tape stripping. (Middle) Predicted iontophoretic extraction flux in each interval for f_{aq}=0.1 and f_{aq}=1 with k_7=0.1 and drug distributed according to f_{aq} at the beginning of extraction. (Bottom) The extraction in the first hour of each iontophoresis case and total extraction via tape stripping.

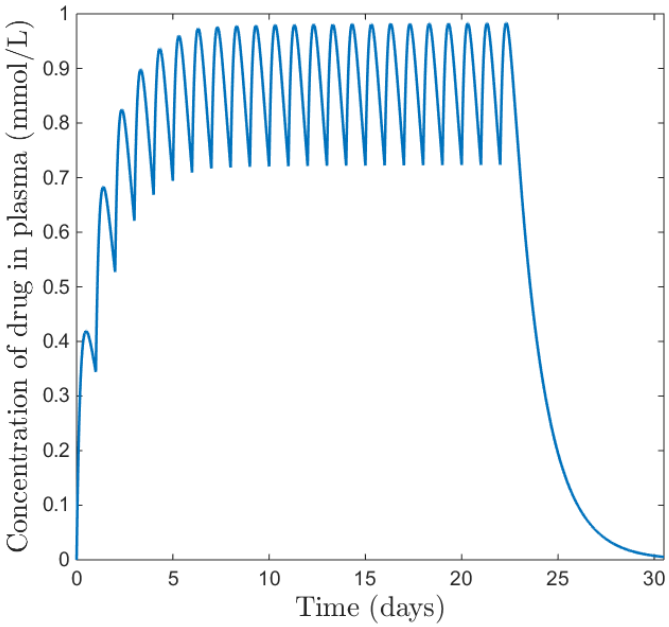

Figure 6-6: The predicted plasma profile for the drug regimen described, where drug is administered for days 1-23 and then a placebo dose is given in the remaining 7 days.

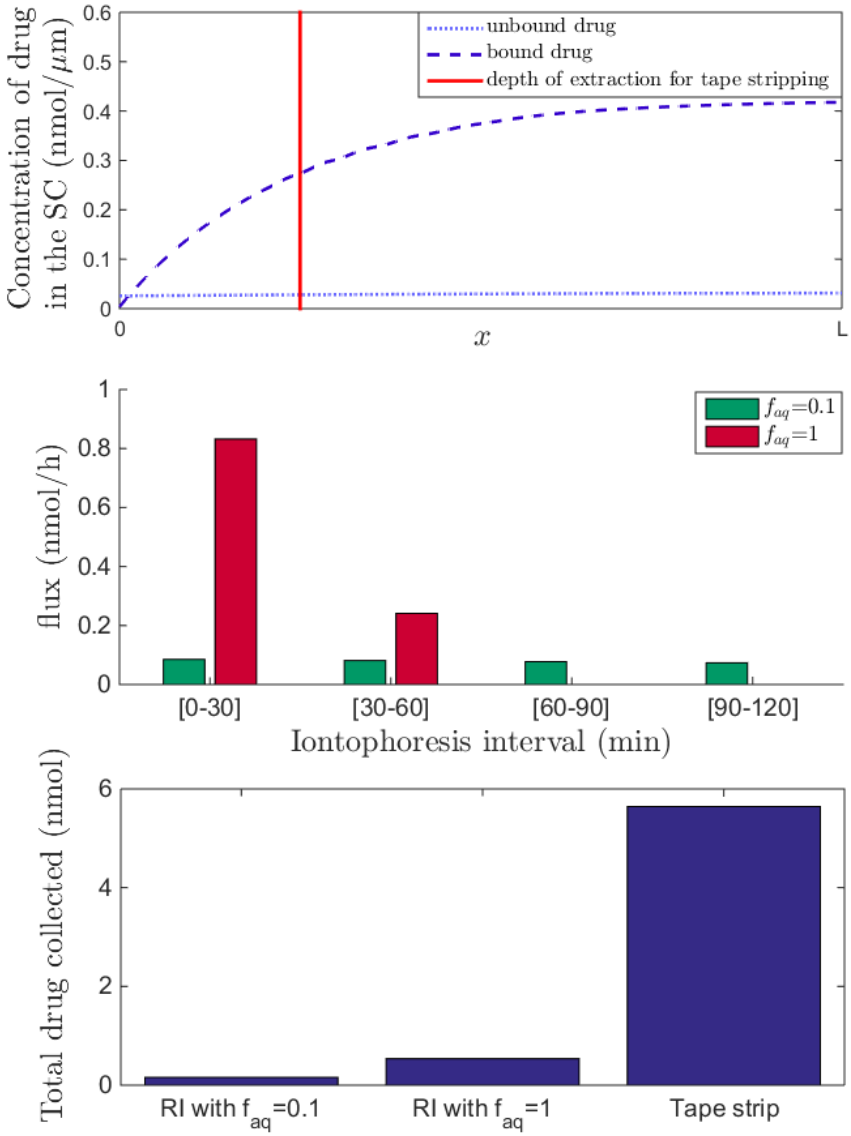

Figure 6-7: The predictions in this figure are for the drug regimen described, where drug is administered for days 1-23 and then a placebo dose is given in the remaining 7 days. Reservoir formation is predicted using binding parameter set 1 for Model 2. (Top) the predicted spatial reservoir at $t = 30.5 days$ for the fully compliant case with binding parameter set 1, where L is the skin surface. The vertical red line shows the depth of the tape stripping. (Middle) Predicted iontophoretic extraction flux in each interval for f_{aq}=0.1 and f_{aq}=1 with k_7=0.1 and drug distributed according to f_{aq} at the beginning of extraction. (Bottom) The extraction in the first hour of each iontophoresis case and total extraction via tape stripping.

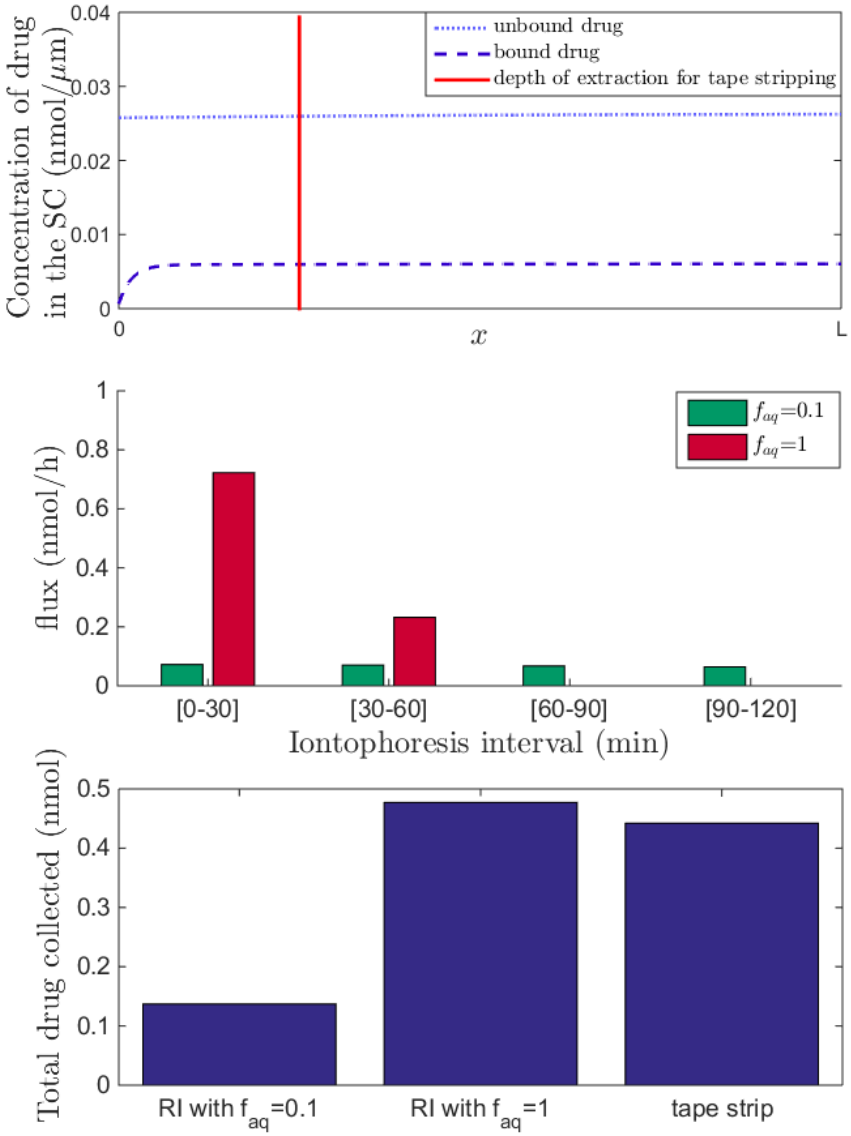

Figure 6-8: The predictions in this figure are for the drug regimen described, where drug is administered for days 1-23 and then a placebo dose is given in the remaining 7 days. Reservoir formation is predicted using binding parameter set 2 for Model 2. (Top) the predicted spatial reservoir at $t = 30.5 days$ for the fully compliant case with binding parameter set 2, where L is the skin surface. The vertical red line shows the depth of the tape stripping. (Middle) Predicted iontophoretic extraction flux in each interval for f_{aq}=0.1 and f_{aq}=1 with k_7=0.1 and drug distributed according to f_{aq} at the beginning of extraction. (Bottom) The extraction in the first hour of each iontophoresis case and total extraction via tape stripping.

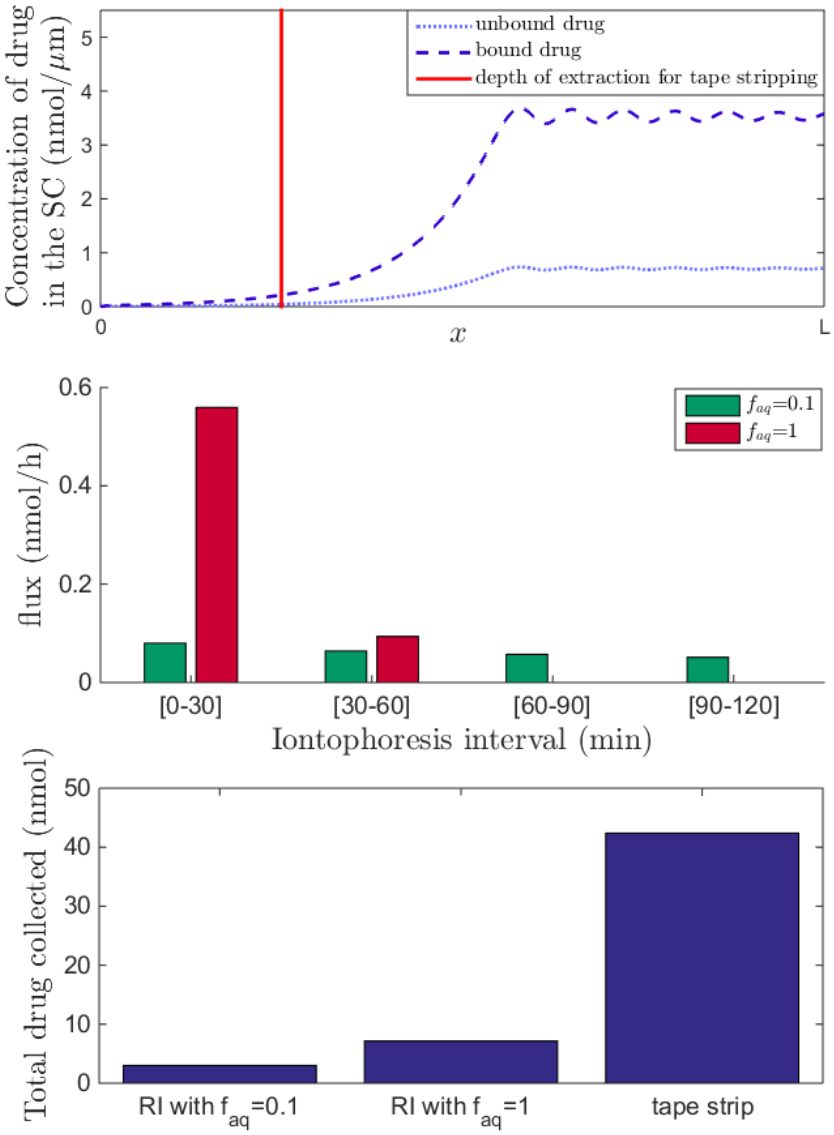

Figure 6-9: The predictions in this figure are for the drug regimen described, where drug is administered for days 1-23 and then a placebo dose is given in the remaining 7 days. Reservoir formation is predicted using binding parameter set 3 for Model 2. (Top) the predicted spatial reservoir at $t = 30.5 days$ for the fully compliant case with binding parameter set 3, where L is the skin surface. The vertical red line shows the depth of the tape stripping. (Middle) Predicted iontophoretic extraction flux in each interval for f_{aq}=0.1 and f_{aq}=1 with k_7=0.1 and drug distributed according to f_{aq} at the beginning of extraction. (Bottom) The extraction in the first hour of each iontophoresis case and total extraction via tape stripping.

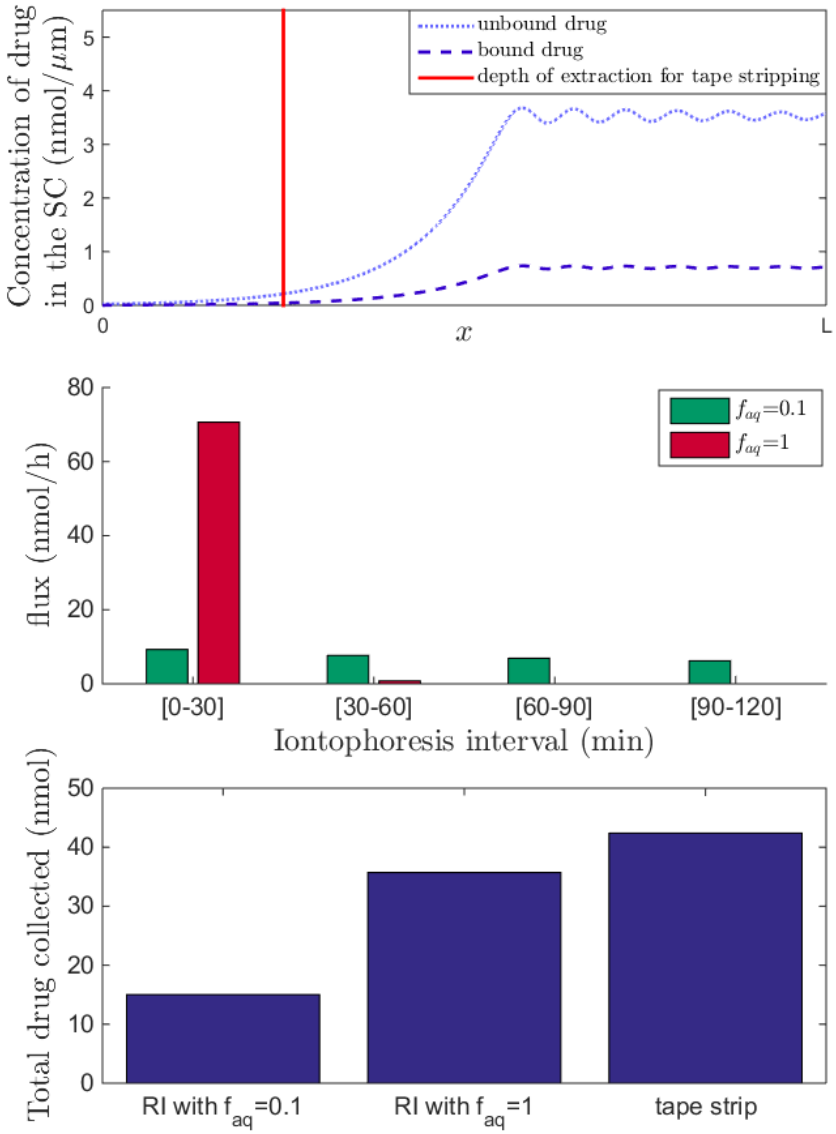

Figure 6-10: The predictions in this figure are for the drug regimen described, where drug is administered for days 1-23 and then a placebo dose is given in the remaining 7 days. Reservoir formation is predicted using binding parameter set 4 for Model 2. (Top) the predicted spatial reservoir at $t = 30.5 days$ for the fully compliant case with binding parameter set 4, where L is the skin surface. The vertical red line shows the depth of the tape stripping. (Middle) Predicted iontophoretic extraction flux in each interval for f_{aq}=0.1 and f_{aq}=1 with k_7=0.1 and drug distributed according to f_{aq} at the beginning of extraction. (Bottom) The extraction in the first hour of each iontophoresis case and total extraction via tape stripping.

Chapter 7

Conclusions

In Chapter 2, Model 1 was constructed using buprenorphine as a case study. A three compartment model of systemic drug concentration was developed comprising of three compartments; plasma, rapidly perfused tissues and slowly perfused tissues. The model acts as a structural example for the type of mechanistic, customisable-dose model that could be used with the full model system.

In Chapter 3 a full description of the skin structure and homoeostasis is provided and existing modelling approaches for passive transdermal delivery are reviewed. Building on these ideas we create a one dimensional spatial model of the SC which includes desquamation, binding and unbinding, and diffusion of the unbound drug in the SC. Results from the model exploration highlight the importance of binding within the SC as a mechanism for reservoir 'storage'. This supports other recent research in the literature which identifies binding as an important factor when considering passive movement across the SC [92]. The model lends itself well to the exploration of non-invasive extraction and drug monitoring techniques across the skin as it describes both total amount in the SC and also spatial distribution of drug in the SC. The first measure is relevant to extraction techniques such as reverse iontophoresis, whilst the second lends itself to the process of tape stripping.

In Chapter 4 a one dimensional SC model is created which divides the SC into a lipid and aqueous domain, as described by Imanidis and Luetolf in their iontophoretic delivery model [120]. All three mechanisms of movement; electromigration, electroosmosis and passive diffusion are considered for reverse iontophoretic transport, with electromigration assumed to provide the largest contribution based on research in the literature. Distribution of the reservoir between lipid and aqueous domains for reverse iontophoresis was shown to be an important factor for interpreting the results from iontophoresis, as drug in the lipid takes longer to be extracted as it must move into the aqueous domain first. One

of the key difficulties for modelling reverse iontophoresis is that exact lag time is unknown which means that drug that is extracted from the reservoir is not easily identified.

In Chapter 5 the work from the previous chapters is combined to provide a full model system describing drug administration to extraction. We created a simplified model for the drug lithium to compare to reverse iontophoresis data. A good fit is obtained after using any one of three model corrections: an adjustment to velocity associated with electromigration; an increased tortuosity of extraction path-length; or re-inclusion of the lipid aqueous domain division.

In Chapter 5, as in Chapter 3, it is shown that when the diffusion coefficient for reservoir formation is large, the historical nature of the reservoir is minimised. This is because diffusion causes the reservoir to quickly reach equilibrium with plasma concentrations. Therefore, when seeking a drug suited to skin monitoring, a drug with small diffusion coefficient is likely to be preferred. This has to be balanced with a requirement for high drug mobility, so that drug can be extracted via reverse iontophoresis. Analysis of the full model in Chapter 5 shows that diffusion has a much larger impact on reservoir size when drug is able to bind in the SC and that, whilst binding results in a larger overall reservoir size (bound + unbound), the size of the unbound reservoir is more influenced by the size of the diffusion coefficient.

Four compliance scenarios were chosen to see if skin monitoring could provide further compliance insight than blood sampling alone. The compliance scenarios were chosen so that pairs of different pairs of them would provide the same plasma concentration despite a difference in the number of doses taken. We found that distinction in extraction profiles between the various compliance scenarios was most clearly observed in the case where there was no diffusion during reservoir formation, the reservoir was mainly unbound, and mainly located in the aqueous domain. The research in Chapter 5 demonstrates the potential for drug presence in the skin to determine patient compliance to a drug regimen.

In Chapter 6 numerical simulations for tape stripping were presented for the fully compliant daily dose regimen and for a regimen which is devised to allow presence of a reservoir with near-zero plasma concentration, such that the reservoir is identifiable from RI predictions. Comparing the reverse iontophoresis reservoir with tape stripping predictions provides information about how much of the total reservoir is available for extraction i.e. how much of it is unbound and in the aqueous domain. As the tape stripping only takes the top 75% of the SC, using the drug regimen devised, the distribution of the reservoir across the depth of the SC could potentially be determined.

Further work

With additional availability of experimental data, the models can be further validated to establish their capabilities and limitations with increasing resolution. Specifically, the data required for the next stage of development should include (but is not limited to):

- continuous extraction data / shorter sampling intervals for reverse iontophoresis;
- estimates for binding within the stratum corneum (for the drug / drugs under scrutiny); and
- multiple sources of data from the same patient using alternative methods, i.e. tape stripping and reverse iontophoresis

The collection of new data opens up the possibility to investigate inter-patient variability, this is a necessary step in validating reverse iontophoresis as a historical drug monitoring technique.

The focus of the present study has been on lipophilic drugs. The reservoir formation model could be adapted for hydrophilic drugs by considering alternative routes through the stratum corneum. The transcellular pathway could be incorporated using a trapping and release method as used by Mollee and Bracken for an intercellular approximation [64], described in Chapter 3.

It is not fully understood where the drug in the SC resides as techniques involve breaking down the SC structure when sampling. However if this information becomes available in the future, stochastic cell based models may provide useful insight into reservoir formation.

The resistance of the SC changes on application of a current, this is thought to be caused by the opening of porous pathways. This was accounted for in part, in Chapter 5, by assuming that the drug reservoir is outside of the aqueous domain (porous pathway) prior to the start of reverse iontophoresis. As reservoir is mainly extracted during the first intervals of iontophoresis, the transient nature of resistance and therefore extraction in these early periods warrants further investigation.

It has been shown that ionisation and pH affects iontophoretic delivery for weak electrolytes. pH effects could be incorporated into the extraction model to identify further characteristics of a drug that would be well suited for compliance monitoring via the skin.

This thesis provides a novel mathematical framework from which the exploration of reverse iontophoresis as a monitoring method for patient compliance can be pursued.

References

[1] World Health Organization. Adherence to long-term therapy: Evidence for action. http://www.who.int/chp/knowledge/publications/adherence_introduction.pdf, 2003. Accessed 24/07/2015.

[2] A. Casati, D. Piontek, and T. Pfeiffer-Gerschel. Patterns of non-compliant buprenorphine, levomethadone and methadone use among opioid dependent persons in treatment. *Substance Abuse, Treatment, Prevention, and Policy*, 9(19), 2014.

[3] R. Düsing, K. Lottermoser, and T. Mengden. Compliance with drug therapy-new answers to an old question. *Nephrol. Dial. Transplant*, 16(7):1317–1321, 2001.

[4] S. Pichini, I. Altieri, P. Zuccaro, and R. Pacifici. Drug monitoring in nonconventional biological fluids and matrices. *Clinical Pharmacokinetics*, 30(3), 1996.

[5] J.T. Jones. Advances in drug testing for substance abuse alternative programs. *Journal of Nursing Regulation*, 6(4):62–67, JAN 2016.

[6] A. Palmeri, S. Pichini, R. Pacifici, P. Zuccaro, and A. Lopez. Drugs in nails: Physiology, pharmacokinetics and forensic toxicology. *Clinical Pharmacokinetics*, 38(2), 2000.

[7] T. Uematsu. Therapeutic drug monitoring in hair samples: Principles and practice. *Clinical Pharmacokinetics*, 25(2), 1993.

[8] M.S. Roberts, S.E. Cross, and Y.G. Anissimov. Factors affecting the formation of a skin reservoir for topically applied solutes. *Skin Pharmacology and Physiology*, 17:3–16, 2004.

[9] C.H. Vickers. Existence of reservoir in the stratum corneum: Experimental proof. *Archives of Dermatology*, 88(1):20–23, 1963.

[10] R.D. Carr and R.G. Wieland. Corticosteroid reservoir in the stratum corneum. *Archives of Dermatology*, 94(1):81–84, 1966.

[11] C.H. Vickers. Stratum corneum reservoir for drugs. *Advances in Biology of Skin*, 12:177–189, 1972.

[12] J.M. Nitsche and H.F. Frasch. Dynamics of diffusion with reversible binding in microscopically heterogeneous membranes: General theory and applications to dermal penetration. *Chemical Engineering Science*, 66(10):2019 – 2041, 2011.

[13] M.B. Reddy, R.H. Guy, and A.L. Bunge. Does epidermal turnover reduce percutaneous penetration? *Pharmaceutical Research*, 17(11):1414–1419, 2000.

[14] S. Seif and S. Hansen. Measuring the stratum corneum reservoir: Desorption kinetics from keratin. *Journal of Pharmaceutical Sciences*, 101:3718–3728, 2012.

[15] B. Leboulanger, J.M. Aubry, G. Bondolfi, R.H. Guy, and B.M. Delgado-Charro. Lithium monitoring by reverse iontophoresis in vivo. *Clinical Chemistry*, 50(11):2091–2100, 2004.

[16] V. Wascotte, M. B. Delgado-Charro, E. Rozet, P. Wallemacq, P. Hubert, R. H. Guy, and V. Préat. Monitoring of urea and potassium by reverse iontophoresis in vitro. *Pharmaceutical Research*, 24(6):1131–1137, 2007.

[17] L. M. Ebah, I. Read, A. Sayce, J. Morgan, C. Chaloner, P. Brenchley, and S. Mitra. Reverse iontophoresis of urea in health and chronic kidney disease: a potential diagnostic and monitoring tool? *European Journal of Clinical Investigation*, 42(8):840–847, 2012.

[18] G. Rao, R.H. Guy, P. Glikfeld, W.R. LaCourse, L. Leung, J. Tamada, R.O. Potts, and N. Azimi. Reverse iontophoresis: Noninvasive glucose monitoring in vivo in humans. *Pharmaceutical Research*, 12(12):1869–1873, 1995.

[19] B. Leboulanger, R.H. Guy, and M.B. Delgado-Charro. Reverse iontophoresis for non-invasive transdermal monitoring. *Physiological Measurement*, 25(3):R35–R50, 2004.

[20] M. J. Tierney, J.A. Tamada, R.O. Potts, R.C. Eastman, N.R. Ackerman, and S.J. Fermi. The glucowatch biographer: a frequent automatic and noninvasive glucose monitor. *Annals of Medicine*, 32(9):632–641, 2000.

[21] The Diabetes Research in Children Network (DirecNet) Study Group. Accuracy of the glucowatch g2 biographer and the continuous glucose monitoring system during hypoglycemia. experience of the diabetes research in children network (direcnet). *Diabetes Care*, 27(3):722–726, 2004.

[22] A Sieg, R.H. Guy, and M. B. Delgado-Charro. Reverse iontophoresis for noninvasive glucose monitoring: the internal standard concept. *Journal of Pharmaceutical Sciences*, 92(11):2295–2302, 2003.

[23] Christopher McCormick, David Heath, and Patricia Connolly. Towards blood free measurement of glucose and potassium in humans using reverse iontophoresis. *Sensors and Actuators B: Chemical*, 166-167:593–600, 5 2012.

[24] Y. Paulley, M.B. Delgado-Charro, and K.A.J. White. Modelling formation of a drug reservoir in the stratum corneum and its impact on drug monitoring using reverse iontophoresis . *Computational and Mathematical Methods in Medicine*, 11(4):353, 2010.

[25] B. Leboulanger, M. Fathi, R.H. Guy, and M. B. Delgado-Charro. Reverse iontophoresis as a noninvasive tool for lithium monitoring and pharmacokinetic profiling. *Pharmaceutical Research*, 21(7):1214–1222, 2004.

[26] J.G. Jones, K.A.J. White, and M.B. Delgado-Charro. A mechanistic approach to modelling the formation of a drug reservoir in the skin. *Mathematical Biosciences*, 281:36 – 45, 2016.

[27] A. Rostami-Hodjegan. Physiologically based pharmacokinetics joined with in vitro- in vivo extrapolation of ADME: A marriage under the arch of systems pharmacology. *Clinical Pharmacology and Therapeutics*, 92(1), 2012.

[28] L.K. Paalzow. Torsten Teorell, the father of pharmacokinetics. *Journal of Medical Sciences*, 100:41–46, 1995.

[29] L. Cucurull-Sanchez, K.G. Spink, and S.A. Moschos. Relevance of systems pharmacology in drug discovery. *Drug Discovery Today*, 17(1314):665 – 670, 2012.

[30] P. Zhao, L. Zhang, J.A. Grillo, Q. Liu, J.M. Bullock, Y.J. Moon, P. Song, S.S. Brar, R. Madabushi, T.C. Wu, B.P. Booth, N.A. Rahman, K.S. Reynolds, E. Gil Berglund, L.J. Lesko, and S.M. Huang. Applications of physiologically based pharmacokinetic (pbpk) modeling and simulation during regulatory review. *Clinical Pharmacology and Therapeutics*, 89(2):259–267, 2011.

[31] A. Elkader and B. Sproule. Buprenorphine clinical pharmacokinetics in the treatment of opioid dependence. *Clinical Pharmacokinetics*, 44:661–680, 2005.

[32] A. Avdeef, D.A. Barrett, P.N. Shaw, R.D. Knaggs, and S.S. Davis. Octanol-, chloroform-, and propylene glycol dipelargonat- water partitioning of morphine-6-glucuronide and other related opiates. *Journal of Medical Chemistry*, 39:4377–4381, 1996.

[33] G.A. McMillin, R. Davis, H. Carlisle, C. Clark, S.J. Marin, and D.E. Moody. Patterns of free (unconjugated) buprenorphine, norbuprenorphine, and their glucuronides in urine using liquid chromatography tandem mass spectrometry. *Journal of Analytical Toxicology*, 36:81–87, 2012.

[34] S.L. Kacinko, H.E. Jones, R.E. Johnson, R.E. Choo, M. Concheiro-Guisan, and M.A. Huestis. Urinary excretion of buprenorphine, norbuprenorphine, buprenorphine-glucuronide, and norbuprenorphine-glucuronide in pregnant women receiving buprenorphine maintenance treatment. *Clinical Chemistry*, 55(6):1177–1187, 2009.

[35] R.C. Heel, R.N. Brogden, T.M. Speight, and G.S. Avery. Buprenorphine: A review of its pharmacological properties and therapeutic efficacy. *Drugs*, 17(2):81–110, 1979.

[36] R. Likar. Transdermal buprenorphine in the management of persistent pain-safety aspects. *Theraputics and Clinical Risk Management*, 2, 2006.

[37] P.J. Robinson and S.I. Rapoport. Kinetics of protein binding determine rates of uptake of drugs by brain. *American Journal of Physiology*, pages 1213–1220, 1986.

[38] A. Iliadis and P. Macheras. *Modeling in Biopharmaceutics, Pharmacokinetics, and Pharmacodynamics: Homogeneous and Heterogeneous Approaches.* Springer Science and Business Media, Inc., New York, 2006.

[39] M.L. Jensen, D.J.R. Foster, R.N. Upton, K. Kristensen, S.H. Hansen, N-H. Jensen, B.N. Nielsen, U. Skram, H.H. Villesen, and L. Christrup. Population pharmacokinetics of buprenorphine following a two-stage intravenous infusion in healthy volunteers. *European Jounal of Clinical Pharmacology*, 63(12):1153–1159, Dec 2007.

[40] P. Poulin and S. Haddad. Advancing prediction of tissue distribution and volume of distribution of highly lipophilic compounds from a simplified tissue-composition-based model as a mechanistic animal alternative method. *Journal of Pharmaceutical Sciences*, 101(6):2250–2261, 2012.

[41] K. Kobayashi, T. Yamamoto, K. Chiba, M. Tani, N. Shimada, T. Ishizaki, and Y. Kuroiwa. Human buprenorphine N-dealkylation is catalyzed by cytochrome P450 3A4. *Drug Metabolism and Disposition*, 26(8):818–821, 1998.

[42] Z.E. Barter, J.E. Chowdry, J.R. Harlow, J.E. Snawder, J.C. Lipscomb, and A. Rostami-Hodjegan. Covariation of human microsomal protein per gram of liver with age: Absence of influence of operator and sample storage

may justify interlaboratory data pooling. *Drug Metabolism and Disposition*, 36(12):2405–2409, 2008.

[43] G.L. Kedderis and S.D. Held. Prediction of furan pharmacokinetics from hepatocyte studies: Comparison of bioactivation and hepatic dosimetry in rats, mice, and humans. *Toxicology and Applied Pharmacology*, 140(1):124 – 130, 1996.

[44] C. Iribarne, D. Picart, Y. Dreano, J-P. Bail, and F. Berthou. Involvement of cytochrome P450 3A4 in N-dealkylation of buprenorphine in human liver microsomes. *Life Sciences*, 60(22):1953–1964, 1997.

[45] J.J. Kuhlman, S. Lalani, J. Magluilo, B. Levine, W.D. Darwin, R.E. Johnson, and E.J. Cone. Human pharmacokinetics of intravenous, sublingual, and buccal buprenorphine. *Journal of Analytical Toxicology*, 20:369–378, 1996.

[46] A.R. Paradkar. *Biopharmaceutics & Pharmacokinetics*, chapter 3. Pragati Books, PUNE 411005, 2008.

[47] R.P. Nath, R.A. Upton, E.T. Everhart, P. Cheung, P. Shwonek, R.T. Jones, and J.E. Mendelson. Buprenorphine pharmacokinetics: Relative bioavailability of sublingual tablet and liquid formulations. *The Journal of Clinical Pharmacology*, 39:619–623, 1999.

[48] G. Sumithra, T. Tsang-Bin, and A. Cowan. Characterization of the pharmacokinetics of buprenorphine and norbuprenorphine in rats after intravenous bolus administration of buprenorphine. *European Journal of Pharmaceutical Sciences*, 15(3):287 – 293, 2002.

[49] A. Andaluz, X. Moll, R. Abellan, R. Ventura, M. Carbo, L. Fresno, and F. Garcia. Pharmacokinetics of buprenorphine after intravenous administration of clinical doses to dogs. *The Vetinary Journal*, 181:299–304, 2009.

[50] S. Yu, X. Zhang, Y. Sun, Y. Peng, J. Johnson, T. Mandrell, A.J. Shukla, and C.S. Laizure. Pharmacokinetics of buprenorphine after intravenous administration in the mouse. *Journal of the American Association for Laboratory Animal Science*, 45(3):12–16, 2006.

[51] S.T. Ho, J.J. Wang, W. Ho, and O.Y. Hu. Determination of buprenorphine by high-performance liquid chromatography with fluorescence detection: application to human and rabbit pharmacokinetic studies. *Journal of Chromatography*, 570:338–350, 1991.

[52] A.C. Williams. *Transdermal and Topical Drug Delivery*. Pharmaceutical Press, 2003.

[53] L.C.U. Junqueira, J. Carneiro, and R.O. Kelley. *Basic Histology*. Lange Medical Book. Appleton & Lange, 6th edition, 1989.

[54] S. Mitragotri, Y.G. Anissimov, A.L. Bunge, H.F. Frasch, R.H. Guy, J. Hadgraft, G.B. Kasting, M.E. Lane, and M.S. Roberts. Mathematical models of skin permeability: An overview. *International Journal of Pharmaceutics*, 418(1):115 – 129, 2011.

[55] B.W. Barry. Drug delivery routes in skin: a novel approach. *Advanced Drug Delivery Reviews*, 54, Supplement(0):S31 – S40, 2002.

[56] M.A. Bolzinger, S. Briancon, J. Pelletier, and Y. Chevalier. Penetration of drugs through skin, a complex rate-controlling membrane. *Current Opinion in Colloid and Interface Science*, 17(3):156–165, 2012.

[57] S. Mitragotri. Modeling skin permeability to hydrophilic and hydrophobic solutes based on four permeation pathways. *Journal of Controlled Release*, 86(1):69 – 92, 2003.

[58] E.A. Essa, M.C. Bonner, and B.W. Barry. Human skin sandwich for assessing shunt route penetration during passive and iontophoretic drug and liposome delivery. *Journal of Pharmacy and Pharmacology*, 54(11):1481–1490, 2002.

[59] G.K. Menon. New insights into skin structure: scratching the surface. *Advanced Drug Delivery Reviews*, 54, Supplement(0):S3 – S17, 2002.

[60] R.L. Bronaugh and H.I. Maibach, editors. *Percutaneous Absorption-Mechanisms- Methodology- Drug Delivery*. Marcel Dekker, Inc, 2nd edition, 1989.

[61] A.S. Michaels, S.K. Chandrasekaran, and J.E. Shaw. Drug permeation through human skin -theory and in vitro experimental measurement. *AICHE Journal*, 21(5):985–996, 1975.

[62] P.M. Elias, E.R. Cooper, A. Korc, and B.E. Brown. Percutaneous transport in relation to stratum corneum structure and lipid composition. *The Journal of Investigative Dermatology*, 76:297–301, 1981.

[63] E.L. Cussler, S.E. Hughs, W.J. Ward, and R. Aris. Barrier membranes. *Journal of Membrane Science*, 38(2):161–174, 1988.

[64] T.R. Mollee and A.J. Bracken. A model of solute transport through stratum corneum using solute capture and release. *Bulletin of Mathematical Biology*, 69:1887–1907, 2007.

[65] R. Lange-Lieckfeldt and G. Lee. Use of a model lipid matrix to demonstrate the dependence of the stratum corneum's barrier properties on its internal geometry. *Journal of Controlled Release*, 20:183–194, 1992.

[66] M. Rosen. *Delivery System Handbook for Personal Care and Cosmetic Products: Technology, Applications and Formulations.* Personal Care and Cosmetic Technology. Elsevier Science, 2005.

[67] E. Candi, R. Schmidt, and G. Melino. The cornified envelope: A model of cell death in the skin. *Nature Reviews*, 6:328–340, april 2005.

[68] C. Blanpain and E. Fuchs. Epidermal homeostasis: A balancing act of stem cells in the skin. *Nature Reviews*, 10:207–218, 2009.

[69] C.S. Potten, R. Schofield, and L.G. Lajtha. A comparison of cell replacement in bone marrow, testis and three regions of surface epithelium. *Biochemica et Biophysica Acta*, pages 281–299, 1979.

[70] S. Ghazizadeh and L.B. Taichman. Organization of stem cells and their progeny in human epidermis. *Journal of Investigative Dermatology*, 124:367–372, 2005.

[71] I.C. Mackenzie. Retroviral transduction of murine epidermal stem cells demonstrates clonal units of epiderma structure. *Journal of Investigative Dermatology*, 109:377–383, 1997.

[72] C. Potten and C. Booth. Keratinocyte stem cells: a commentary. *Journal of Investigative Dermatology*, 119:888–899, 2002.

[73] D.P. Doupe and P.H. Jones. Interfollicular epidermal homeostasis: dicing with differentiation. *Experimental dermatology*, 21:249–253, 2012.

[74] H. Honda, T. Morita, and A. Tanabe. Establishment of epidermal cell columns in mammalian skin: Computer simulation. *Journal of Theoretical Biology*, 81(4):745 – 759, 1979.

[75] M. Loeffler, C.S. Potten, and H.E. Wichmann. Epidermal cell proliferation: A comprehensive mathematical model of cell proliferation and migration in the basal layer predicts some unusual properties of epidermal stem cells. *in Virchows Archive. B, Cell pathology including molecular pathology*, pages 286–300, 1987.

[76] S. Nakaoka and K. Aihara. Mathematical study on kinetics of hematopoietic stem cells- theoretical conditions for successful transplantation. *Journal of Biological Dynamics*, 6(2):836–854, March 2012.

[77] S. Nakaoka and K. Aihara. Stochastic simulation of structured skin cell population dynamics. *Journal of Mathematical Biology*, pages 807–835, 2013.

[78] K.D. McCarley and A.L. Bunge. Pharmacokinetic models of dermal absorption. *Journal of Pharmaceutical Sciences*, 90(11):1699–1719, 2001.

[79] A. Bunge, R.H. Guy, and J. Hadgraft. The determination of a diffusional pathlength through the stratum corneum. *International Journal of Pharmaceutics*, 188:121–124, 1999.

[80] J. Hadgraft. Skin, the final frontier. *International Journal of Pharmaceutics*, 224(12):1 – 18, 2001.

[81] M.E. Johnson, D. Blankschtein, and R. Langer. Evaluation of solute permeation through the stratum corneum: Lateral bilayer diffusion as the primary transport mechanism. *Journal of Pharmaceutical Sciences*, 86(10):1162 – 1172, 1997.

[82] Y.G. Anissimov, O.G. Jepps, Y. Dancik, and M.S. Roberts. Mathematical and pharmacokinetic modelling of epidermal and dermal transport processes. *Advanced Drug Delivery Reviews*, 65(2):169 – 190, 2013.

[83] L. Simon. Repeated applications of a transdermal patch: Analytical solution and optimal control of the delivery rate. *Mathematical Biosciences*, 209:593–607, 2007.

[84] J. Siepmann and F. Siepmann. Mathematical modeling of drug delivery. *International Journal of Pharmaceutics*, 364(2):328 – 343, 2008. Future Perspectives in Pharmaceutics Contributions from Younger Scientists.

[85] L. Simon, K.S. Kwang, and K. Kanneganti. Effects of epidermal turnover on the dynamics of percutaneous drug absorption. *Mathematical Biosciences*, 229:16–21, 2011.

[86] A. Couto, R. Fernandes, M.N.S. Cordeiro, S.S. Reis, R.T. Ribeiro, and A.M. Pessoa. Dermic diffusion and stratum corneum: a state of the art review of mathematical models. *Journal of Controlled Release*, 177:74–83, 2014.

[87] Y.G. Anissimov and M.S. Roberts. Diffusion modeling of percutaneous absorption kinetics. 1. Effects of flow rate, receptor sampling rate, and viable epidermal resistance for a constant donor concentration. *Journal of Pharmaceutical Sciences*, 88(11):1201–1209, 1999.

[88] Y.G. Anissimov and M.S. Roberts. Diffusion modeling of percutaneous absorption kinetics: 2. finite vehicle volume and solvent deposited solids. *Journal of pharmaceutical Sciences*, 90(4):504–520, 2001.

[89] M. Heisig, R. Lieckfeldt, G. Wittum, G. Mazurkevich, and G. Lee. Non steady-state descriptions of drug permeation through stratum corneum. I. the biphasic brick-and-mortar model. *Pharmaceutical Research*, 13(3):421–426, 1996.

[90] H.F. Frasch and A.M. Barbero. Steady state flux and lag time in the stratum corneum lipid pathway: Results from finite element models. *Journal of Pharmaceutical Sciences*, 92(11):2196 – 2207, 2003.

[91] Y.G. Anissimov and M.S. Roberts. Diffusion modelling of percutaneouos absorption kinetics:4. effects of a slow equilibration process within stratum corneum on absorption and desorption kinetics. *Journal of Pharmaceutical Sciences*, 98:772–781, 2009.

[92] G. Pontrelli and F. de Monte. A two-phase two-layer model for transdermal drug delivery. *Mathematical Biosciences*, 257:96–103, 2014.

[93] H. Frederick Frasch, Ana M. Barbero, Justin M. Hettick, and Johannes M. Nitsche. Tissue binding affects the kinetics of theophylline diffusion through the stratum corneum barrier layer of skin. *Journal of Pharmaceutical Sciences*, 100(7):2989 – 2995, 2011.

[94] L.H. Jansen, M.T. Hojyotom, and A.M. Kligman. Improved fluorescence staining technique for estimating turnover of human stratum-corneum. *British Journal of Dermatology*, 90(1):9–12, 1974.

[95] J. Sandby-Moller, T. Poulsen, and H.C. Wulf. Epidermal thickness at different body sites: Relationship to age, gender, pigmentation, blood content, skin type and smoking habits. *Acta Dermato- Venereologica*, 83:410–413, 2003.

[96] S. Rotheberg, R.G. Crounse, and J.L. Lee. Glycine-C-14 incorporation into the proteins of normal stratum corneum and the abnormal stratum corneum of psoriasis. *Journal of Investigative Dermatology*, 37(6):497–505, 1961.

[97] G.D. Weinstei and E.J. Vanscott. Autoradiographic analysis of turnover times of normal and psoriatic epidermis. *Journal of Investigative Dermatology*, 45(4):257, 1965.

[98] E. Tesselaar and F. Sjoberg. Transdermal iontophoresis as an in-vivo technique for study in microvascular physiology. *Microvascular Research*, 81(1):88–96, 2011.

[99] E.R. Scott, A.I. Laplaza, H.S. White, and J.B. Phipps. Transport of ionic species in skin: Contribution of pores to the overal skin conductance. *Pharmaceutical Research*, 10(12):1699–1709, 1993.

[100] E.R. Scott, H.S. White, and J.B. Phipps. Direct imaging of ionic pathways in stratum corneum using scanning electrochemical microscopy. *Solid State Ionics*, pages 176–183, 1992.

[101] B.D. Bath, E.R. Scott, J.D. Phipps, and H.S. White. Scanning electrochemical microscopy of iontophoretic transport in hairless mouse skin. analysis of the relative contributions of diffusion, migration, and electroosmosis to transport in hair follicles. *Journal of Pharmaceutical Sciences*, 89(12), 2000.

[102] N.H. Bellantone, S. Rim, M.L. Francoeur, and B. Rasadi. Enhanced percutaneous absorption via iontophoresis I. evaluation of an in vitro system and transport of model compounds. *International of Journal of Pharmaceutics*, 30:63–72, 1986.

[103] R.R. Burnette. *Transdermal Drug Delivery*, chapter 11. Iontophoresis, pages 247–289. Marcel Dekker, Inc, 1989.

[104] J.B. Phipps, R.V. Padmanabhan, and G.A. Lattin. Iontophoretic delivery of model inorganic and drug ions. *American Pharmaceutical Association*, 78(5):365–369, 1988.

[105] R.R. Burnette and D. Marrero. Comparison between the iontophoretic and passive transport of thyrotropin–releasing-hormone across excised nude-mouse skin. *Journal of Pharmaceutical Sciences*, 75(8):738–743, 1986.

[106] R.R. Burnette and B. Ongpipattanakul. Characterization of the permselective properties of excised human skin during iontophoresis. *Journal of Pharmaceutical Sciences*, 86(10), 1987.

[107] L. Gangarosa, N. Park, C. Wiggins, and J. Hill. Increased penetration of non-electrolytes into mouse skin during iontophoretic water transport (iontohydrokinesis). *Journal of Pharmacology and Experimental Therapeutics*, 212:377–381, 1980.

[108] M. Pikal. The role of electroosmotic flow in transdermal iontophoresis. *Advanced Drug Delivery Reviews*, 46:281–305, 2001.

[109] R.H. Guy, M.B. Delgado-Charro, and Y.N. Kalia. Iontophoretic transport across the skin. *Skin Pharmacology Applied Skin Physiology*, 14 (suppl 1):35–40, 2001.

[110] M. Pikal. Transport mechanisms in iontophoresis. I. a theoretical model for the effect of electroosmotic flow on flux enhancement in transdermal iontophoresis. *Pharmaceutical Research*, 7(2):118–126, 1990.

[111] N. Lakshminarayanaiah. Transport phenomena in artificial membranes. *Chemical Reviews*, 65(5):491, 1965.

[112] Y Kobatake, M Yuasa, and H Fujita. Studies of membrane phenomena. 6. further study of volume flow. *Journal of Physical Chemistry*, 72(5):1752–&, 1968.

[113] P. Lai, Y.G. Anissimov, and M.S. Roberts. Lateral iontophoretic solute transport in skin. *Pharmaceutical Research*, 16(1):46–54, 1999.

[114] S. Ghosal. Fluid mechanics of electroosmotic flow and its effect on band broadening in capillary electrophoresis. *Electrophoresis*, 25:214–228, 2004.

[115] M. Pikal. The role of electroosmotic flow in transdermal iontophoresis. *Advanced Drug Delivery Reviews*, 9:201–237, 1992.

[116] M.S. Roberts, P.M. Lai, and Y.G. Anissimov. Epidermal iontophoresis: I. developement of the ionic mobility-pore model. *Pharmaceutical Research*, 15(10):1569–1578, 1998.

[117] M.J. Pikal and S. Shah. Transport mechanisms in iontophoresis. II. electroosmotic flow and transference number measurements for hairless mouse skin. *Pharmaceutical Research*, 7(3), 1990.

[118] C.A.M. Brett and A.M.O. Brett. *Electrochemistry Principles, Methods and Applications*. Oxford Science Publications, 1993.

[119] M.B. Reddy, K.D. McCarley, and A.L. Bunge. Pysiologically relevant one-compartment pharmacokinetic models for skin. 2.comparison of models when combined with a systemic pharmacokinetic model. *Journal of Pharmaceutical Sciences*, 87(482-490), 1998.

[120] G. Imanidis and P. Luetolf. An extended model based on the modified Nernst-Planck equation for describing transdermal iontophoresis of weak electrolytes. *Journal of Pharmaceutical Sciences*, 95(7):1434–1447, 2006.

[121] M.J. Pikal and S. Shah. Transport mechanisms in iontophoresis. III. an experimental study of the contributions of electroosmotic flow and permeability change in transport of low and high molecular weight solutes. *Pharmaceutical Research*, 7(3), 1990.

[122] P.W. Ledger. Skin biological issues in electrically enhanced transdermal delivery. *Advanced Drug Delivery Reviews*, 9(2-3):289–307, 1992.

[123] H.A. Abramson and M.H. Gorin. Skin reactions IX the electrophoretic demonstration of the patent pores of the living human skin; its relation to the charge of the skin. *Journal of Physical Chemistry*, 44(9):1094–1102, 1940.

[124] C. Kochhar and G. Imanidis. In vitro transdermal iontophoretic delivery of leuprolide under constant current application. *Journal of Controlled Release*, 98(1):25–35, July 23 2004.

[125] J.C. Keister and G.B. Kasting. Ionic mass transport through a homogeneous membrane in the presence of a uniform electric field. *Journal of Membrane Science*, 29:155–167, 1986.

[126] A.K. Nugroho, O. Della Pasqua, M. Danhof, and J.A. Bouwstra. Compartmental modeling of transdermal iontophoretic transport: I. in vitro model derivation and application. *Pharmaceutical Research*, 21(11):1974–1984, 2004.

[127] A.K. Nugroho, O. Della-Pasqua, M. Danhof, and J.A. Bouwstra. Compartmental modeling of transdermal iontophoretic transport II: In vivo model derivation and application. *Pharmaceutical Research*, 22(3):335–346, 2005.

[128] H. Ohman and A. Vahlquist. In vivo studies concerning a pH gradient in human stratum corneum and upper epidermis. *Acta Derm Venereol*, 74:375–379, 1994.

[129] N.O. Wesley and H. I. Maibach. Racial (ethnic) differences in skin properties - the objective data. *American Journal of Clinical Dermatology*, 4(12):843–860, 2003.

[130] E. Berardesca, F. Pirot, M. Singh, and H. Maibach. Differences in stratum corneum pH gradient when comparing white caucasian and black african-american skin. *British Journal of Dermatology*, 139(5):855–857, 1998.

[131] S.H. Youn, C. W. Choi, J.W. Choi, and S.W. Youn. The skin surface pH and its different influence on the development of acne lesion according to gender and age. *Skin Research and Technology*, 19(2):131–136, 2013.

[132] S. Schreml, M. Kemper, and C. Abels. Skin pH in the elderly and appropriate skin care. *EMJ Dermatology*, pages 86–94, 2014.

[133] G. Yosipovitch, G. L. Xiong, E. Haus, L. Sackett-Lundeen, I. Ashkenazi, and H. I. Maibach. Time-dependent variations of the skin barrier function in humans: Transepidermal water loss, stratum corneum hydration, skin surface ph, and skin temperature. *Journal of Investigative Dermatology*, 110:20–23, 1998.

[134] N.H. Yoshida and M.S. Roberts. Structure transport relationships in transdermal iontophoresis. *Advanced Drug Delivery Reviews*, 9(2-3):239–264, 1992.

[135] N.H. Yoshida and M.S. Roberts. Solute molecular size and transdermal iontophoresis across excised human skin. *Journal of Controlled Release*, 25(3):177–195, 1993.

[136] K.D. McCarley and A.L. Bunge. Pysiologically relevant one-compartment pharmacokinetic models for skin. 1. development of models. *Journal of Pharmaceutical Sciences*, 87(470-481), 1998.

[137] M. Grassi, G. Lamberti, S. Cascone, and G. Grassi. Mathematical modelling of simultaneous drug release and in vivo absorption. *International Journal of Pharmaceutics*, 418:130–141, 2011.

[138] D. P. Thornhill. Pharmacokinetics of ordinary and sustained-release lithium carbonate in manic patients after acute dosage. *European Journal of Clinical Pharmacology*, 14(4):267–271, 1978.

[139] T.G. Grundin, G. M. Roomans, B. Forslind, M. Lindberg, and Y. Werner. X-ray microanalysis of psoriatic skin. *The Journal of Investigative Dermatology*, 85(4):378–380, 1985.

[140] L. Franzen, J. Anderski, V. Planz, K. Kostka, and M. Windbergs. Combining confocal raman microscopy and freeze-drying for quantification of substance penetration into human skin. *Experimental dermatology*, 23:942–944, 2014.

[141] C. Surber, K. Wilhelm, D. Bermann, and H. I. Maibach. In vivo skin penetration of acitretin in volunteers using three sampling techniques. *Pharmaceutical Research*, 10(9):1291–1294, 1993.

[142] S. Paliwal, B. H. Hwang, K. Y. Tsai, and S. Mitragotri. Diagnostic opportunities based on skin biomarkers. *European Journal of Pharmaceutical Sciences*, 50(5):546 – 556, 2013.

[143] C. Y. Wang and H. I. Maibach. Why minimally invasive skin sampling techniques? a bright scientific future. *Cutaneous and Ocular Toxicology*, 30(1):1–6, 2011.

[144] C. Herkenne, I. Alberti, A. Naik, Y. N. Kalia, F. Mathy, V. Préat, and R. H. Guy. In vivo methods for the assessment of topical drug bioavailability. *Pharmaceutical Research*, 25(1):87, 2008.

[145] C. T. S. Ching, L.S. Fu, T.H. Hsu, and K.M. Chang. Use of electroporation and reverse iontophoresis for extraction of transdermal multibiomarkers. *International Journal of Nanomedicine*, 7:885–894, 2012.

[146] J.A. Levisky, D.L. Bowerman, W.W. Jenkins, and S.B. Karch. Drug deposition in adipose tissue and skin: evidence for an alternative source of positive sweat patch tests. *Forensic Science International*, 110:35–46, 2000.

[147] R.L. Anderson and J.M. Cassidy. Variations in physical dimensions and chemical composition of human stratum corneum. *Journal of Investigative Dermatology*, 61:30–32, 1973.

[148] F. Dreher, A. Arens, J.J. Hostynek, S. Mudumba, J. Ademola, and H.I. Maibach. Colometric method for quantifying human stratum corneum removed by adhesive-tape-stripping. *Acta Derma Venereol*, 78:186–189, 1998.

[149] S.J. Bashir, A Chew, A. Anigbogu, F. Dreher, and H.I. Maibach. Physical and physiological effects of stratum corneum tape stripping. *Skin Research and Toxicology*, 7:40–48, 2001.